

**THE PHYSIOLOGICAL ROLES OF E3 UBIQUITIN LIGASES OF THE N-END RULE  
PATHWAY**

by

**JEE YOUNG AN**

B.Sc., Life Science, Sogang University, 1998

M.Sc., Life Science, Sogang University, 2000

Submitted to the Graduate Faculty of  
School of Pharmacy in partial fulfillment  
of the requirements for the degree of  
Doctor of Philosophy

University of Pittsburgh

2008

UNIVERSITY OF PITTSBURGH

SCHOOL OF PHARMACY

This dissertation was presented

by

Jee Young An

It was defended on

November 20<sup>th</sup>, 2008

and approved by

Yong Jun Lee, PhD, Professor  
Department of Surgery, School of Medicine, University of Pittsburgh

Song Li, MD, PhD, Associate Professor  
Pharmaceutical Science, School of Pharmacy, University of Pittsburgh

Yong Wan, PhD, Associate Professor  
Department of Cell Biology & Physiology, School of Medicine, University of  
Pittsburgh

Wen Xie, MD, PhD, Associate Professor  
Pharmaceutical Science, School of Pharmacy, University of Pittsburgh

Dissertation Advisor: Yong Tae Kwon, PhD, Associate Professor  
Pharmaceutical Science, School of Pharmacy, University of Pittsburgh

Copyright © by Jee Young An

2008

# THE PHYSIOLOGICAL ROLES OF E3 UBIQUITIN LIGASES OF THE N-END

## RULE PATHWAY

Jee Young An, PhD

University of Pittsburgh, 2008

The ubiquitin (Ub)-dependent N-end rule relates the *in vivo* half-life of a protein to the identity of its N-terminal residue. A substrate with destabilizing N-terminal residue is recognized by a family of mammalian E3 ubiquitin ligases of the N-end rule pathway, including UBR1 and UBR2. However, little is known about their roles in biological processes. The aim of this dissertation is to understand the physiological functions and underlying molecular mechanisms of the E3 ubiquitin ligases in the N-end rule pathway. First, I find that UBR2, a recognition E3 component of the N-end rule pathway, localizes to the meiotic chromatin, where it mediates the transcriptional silencing through histone ubiquitylation in a spatiotemporal manner. UBR2-lacking spermatocytes show impaired global ubiquitylation, including ubiquitylation of histone H2A, a histone modification often associated with transcriptional inactivation. HR6B, an E2 conjugating enzyme of the N-end rule pathway, interacts with UBR2 as an E2-E3 complex and cooperatively mediate H2A monoubiquitylation *in vitro*. Impaired H2A ubiquitylation in UBR2-deficient spermatocytes correlates to defects in transcriptional silencing. Furthermore, I provide evidences that UBR2 is involved in DNA damage response (DDR) pathway through protein ubiquitylation presumably to maintain genome integrity. UBR2 is exclusively associated with non-heterochromatin throughout nucleus and responds to genotoxic stress via post-translational modification. Ubiquitylation induced by DNA damage are significantly impaired in UBR2-

deficient cells. *UBR2*<sup>-/-</sup> mouse embryonic fibroblasts (MEFs) show increased vulnerability to the genotoxic agents and abnormality of chromosomes. Moreover, I show that divergent and cooperative functions of the E3 ligases of N-end rule pathway. UBR1 and UBR2 are 46% identical, and appear to be indistinguishable in their recognition of N-degrons, yet show different physiological implications in mutant mice. *UBR1*<sup>-/-</sup>*UBR2*<sup>-/-</sup> embryos die at midgestation, with defects in neurogenesis and cardiovascular development. These defects include reduced proliferation as well as precocious migration and differentiation of neural progenitor cells. The expression of regulators such as D-type cyclins and Notch1 is also altered in *UBR1*<sup>-/-</sup>*UBR2*<sup>-/-</sup> embryos. Overall, my dissertation suggests that the E3 Ub-ligases of the N-end rule pathway are required in meiosis, DDR pathway, and embryogenesis.

## TABLE OF CONTENTS

PREFACE.....	XII
1.0 THE N-END RULE PATHWAY.....	1
2.0 THE ROLE OF UBR2 IN TRANSCRIPTIONAL SILENCING DURING MEIOSIS .....	5
2.1 SUMMARY .....	5
2.2 BACKGROUND .....	6
2.3 METHODS.....	8
2.3.1 <i>UBR2</i> <sup>-/-</sup> , <i>Brca1</i> <sup><math>\Delta</math>11/<math>\Delta</math>11</sup> <i>p53</i> <sup>+/-</sup> , and <i>SPO11</i> <sup>-/-</sup> Mice.....	8
2.3.2 Immunohistochemistry on germ cell spread .....	8
2.3.3 Fluorescence <i>in situ</i> hybridization (FISH).....	10
2.3.4 Microarray analysis.....	11
2.3.5 Northern blot and real-time RT-PCR analyses .....	11
2.3.6 Acid extraction of core histones and immunoblotting .....	12
2.3.7 Affinity-purification of chicken anti-mouse UBR2 IgY .....	13
2.3.8 Preparation of N-recognins.....	14
2.3.9 Interaction between endogenous UBR2 and RAD6.....	14
2.3.10 <i>In vitro</i> ubiquitylation assay .....	15
2.4 RESULTS .....	15

2.4.1	The localization of UBR2 during meiotic prophase .....	15
2.4.2	Impaired ubiquitylation in <i>UBR2</i> <sup>-/-</sup> spermatocytes .....	20
2.4.3	Impaired ubiquitylation of histone H2A in <i>UBR2</i> <sup>-/-</sup> spermatocytes.....	24
2.4.4	UBR2 and HR6B mediate H2A monoubiquitylation .....	25
2.4.5	Impaired MSCI in <i>UBR2</i> <sup>-/-</sup> spermatocytes .....	28
2.4.6	Co-localization of UBR2 with ATR/BRCA in MSCI .....	32
2.5	DISCUSSION.....	35
3.0	THE ROLE OF UBR2 IN DNA DAMAGE RESPONSE THROUGH HISTONE MODIFICATIONS .....	39
3.1	SUMMARY .....	39
3.2	BACKGROUND .....	40
3.3	METHODS.....	41
3.3.1	Immunofluorescence microscopy.....	41
3.3.2	Cell culture and Genotoxic stress.....	42
3.3.3	Fractionation of cell extracts and immunoblotting .....	42
3.3.4	RNA interference and real-time RT-PCR.....	43
3.3.5	<i>in vivo</i> ubiquitylation assay.....	43
3.3.6	Cell survivality by MTT assay.....	44
3.3.7	Metaphase chromosome spread from MEFs .....	44
3.4	RESULTS .....	45
3.4.1	Unresolved meiotic DSBs in <i>UBR2</i> -deficient spermatocytes.....	45
3.4.2	The recruitment of proteins in meiotic recombination .....	45
3.4.3	Intracellular localization of UBR2 in somatic cells .....	48

3.4.4	Upregulation of UBR2 signal upon DNA damage .....	50
3.4.5	Impaired ubiquitylation upon DNA damage in UBR2-deficient cells .....	51
3.4.6	Altered histone modification in UBR2-deficient cells .....	53
3.4.7	Genomic instability in UBR-deficient MEFs.....	56
3.5	DISCUSSION.....	58
4.0	THE ROLE OF UBR1 AND UBR2 IN THE NEUROGENESIS AND CARDIOVASCULAR DEVELOPMENT .....	62
4.1	SUMMARY .....	62
4.2	BACKGROUND .....	63
4.3	METHODS.....	64
4.3.1	<i>UBR1</i> <sup>-/-</sup> <i>UBR2</i> <sup>-/-</sup> mice .....	64
4.3.2	Histology and immunohistochemistry .....	65
4.3.3	Measurements of cell proliferation and death .....	65
4.3.4	Whole mount PECAM staining.....	67
4.3.5	Immunoblotting .....	67
4.4	RESULTS .....	67
4.4.1	Embryonic lethality of <i>UBR1</i> <sup>-/-</sup> <i>UBR2</i> <sup>-/-</sup> double mutant .....	67
4.4.2	Impaired Neurogenesis in Embryos Lacking UBR1 and UBR2 .....	71
4.4.3	Impaired cardiovascular development in mutant embryos.....	78
4.4.4	Molecular Analysis of Mouse Embryos Lacking UBR1 and UBR2.....	82
4.5	DISCUSSION.....	85
5.0	PERSPECTIVES .....	89
	BIBLIOGRAPHY .....	91

## LIST OF TABLES

Table 1. Antibodies used in immunohistochemistry.....	9
Table 2. Primers used in real-time RT-PCR.....	12
Table 3. Antibodies used in immunohistochemistry and immunoblotting.....	66

## LIST OF FIGURES

Figure 1. The hierachial structure of the mammalian N-end rule pathway. ....	2
Figure 2. Localization of UBR2 in spermatocytes during meiotic prophase.....	16
Figure 3. UBR2 localization on meiotic chromosomes. ....	17
Figure 4. Specificity of rabbit anti-mouse UBR2 antibody .....	18
Figure 5. Surge of UBR2 signal throughout nucleus after mid pachytene .....	19
Figure 6. Localization of polyubiquitin conjugates in control and <i>UBR2</i> <sup>-/-</sup> spermatocytes.....	21
Figure 7. Overall ubiquitylation in control and <i>UBR2</i> <sup>-/-</sup> spermatocytes. ....	22
Figure 8. UBR2 is required for ubiquitylation of histone H2A. ....	23
Figure 9. Ubiquitylation of H2A in control and <i>UBR2</i> <sup>-/-</sup> testis. ....	25
Figure 10. Interaction of UBR2 and HR6B in testis.....	26
Figure 11. <i>in vitro</i> ubiquitylation of histone H2A by UBR2-HR6B as an E3-E2 complex. ....	27
Figure 12. Defective MSCI in <i>UBR2</i> <sup>-/-</sup> spermatocytes. ....	28
Figure 13. Northern blot analysis of genes expression during spermatogenesis. ....	29
Figure 15. XY synapsis and sex body formation in control and <i>UBR2</i> <sup>-/-</sup> spermatocytes.....	31
Figure 16. Co-localization of UBR2 with BRCA1 and ATR on meiotic chromosomes.....	33
Figure 17. Mutual independent function betIen UBR2 and BRCA1/ATR.....	34
Figure 18. Defective resolution of meiotic DSBs in <i>UBR2</i> <sup>-/-</sup> spermatocytes.....	46
Figure 19. Recruitment of recombination proteins in control and <i>UBR2</i> <sup>-/-</sup> spermatocytes.....	48

Figure 20. Impaired crossover formation in <i>UBR2</i> <sup>-/-</sup> spermatocytes. ....	49
Figure 21. UBR2 localization in control and <i>SPO11</i> <sup>-/-</sup> spermatocytes. ....	50
Figure 22. Chromatin associated UBR2 localization in somatic cells.....	51
Figure 23. Post-translational modification of UBR2 upon DNA damage.....	52
Figure 24. The level of UBR2 mRNA in DDR .....	53
Figure 25. Impaired DDR-related ubiquitylation in UBR2-deficient cells.....	54
Figure 26. Altered histone modifications in UBR2-deficient cells.....	55
Figure 27. Genomic instability in UBR2 <sup>-/-</sup> MEFs. ....	57
Figure 28. Gross morphology of <i>UBR1</i> <sup>-/-</sup> <i>UBR2</i> <sup>-/-</sup> mouse embryos. ....	68
Figure 29. Abnormal development of the central nervous system in <i>UBR1</i> <sup>-/-</sup> <i>UBR2</i> <sup>-/-</sup> embryos	69
Figure 30. Abnormal development of the neural tube in <i>UBR1</i> <sup>-/-</sup> <i>UBR2</i> <sup>-/-</sup> embryos .....	70
Figure 31. Abnormal proliferation patterns in <i>UBR1</i> <sup>-/-</sup> <i>UBR2</i> <sup>-/-</sup> neural tubes.....	72
Figure 32. Active phase of cell cycle in neural tube of <i>UBR1</i> <sup>-/-</sup> <i>UBR2</i> <sup>-/-</sup> embryos .....	73
Figure 33. Increased apoptosis in <i>UBR1</i> <sup>-/-</sup> <i>UBR2</i> <sup>-/-</sup> neural precursors.....	75
Figure 34. Abnormal differentiation patterns of <i>UBR1</i> <sup>-/-</sup> <i>UBR2</i> <sup>-/-</sup> neural precursors. ....	77
Figure 35. Impaired cardiac development in <i>UBR1</i> <sup>-/-</sup> <i>UBR2</i> <sup>-/-</sup> embryos. ....	79
Figure 36. Impaired development of cardiac cells in <i>UBR1</i> <sup>-/-</sup> <i>UBR2</i> <sup>-/-</sup> embryos.....	80
Figure 37. Impaired vascular development in <i>UBR1</i> <sup>-/-</sup> <i>UBR2</i> <sup>-/-</sup> embryos.....	81
Figure 38. Immunoblot analysis of <i>UBR1</i> <sup>-/-</sup> <i>UBR2</i> <sup>-/-</sup> embryos. ....	83

## **PREFACE**

Dedicated to Eun Hee Kim, My Raison d'être

## 1.0 THE N-END RULE PATHWAY

A protein substrate of the ubiquitin (Ub)-proteasome system, which controls the levels of many intracellular proteins, is conjugated to Ub through the action of E1, E2 and E3 enzymes (Hershko et al., 2000; Pickart, 2004; Hochstrasser, 2006; Varshavsky, 2006). The substrate's degradation signal (degron) is recognized by E3 for ubiquitylation. An ubiquitylated protein bears a covalently linked poly-Ub chain and is degraded by the 26S proteasome (Pickart, 2004; Hochstrasser, 2006). An essential determinant of one class of degrons, called N-degrons, is a substrate's destabilizing N-terminal residue (Varshavsky, 1996; 2006). An N-degron contains two determinants: a destabilizing N-terminal residue and a sterically appropriate internal Lys residue(s), the latter being the site of formation of a substrate-linked poly-Ub chain (Bachmair and Varshavsky, 1989; Varshavsky, 1996; Suzuki and Varshavsky, 1999). The set of destabilizing residues in a given cell type yields a rule, called the N-end rule, which relates the *in vivo* half-life of a protein to the identity of its N-terminal residue. The N-end rule pathway is present in all eukaryotes examined, from mammals and plants to fungi and its Ub-independent version is also present in prokaryotes (Varshavsky, 1996). Proteins required for the mammalian N-end rule pathway have been identified and shown to have a hierarchic structure (Kwon et al., 1999a; Kwon et al., 1998; Kwon et al., 2000; Kwon et al., 2001; Kwon et al., 2002; Kwon et al., 2003; Tasaki et al., 2005; Tasaki and Kwon, 2007) (Fig. 1). In mammals, N-terminal asparagine (Asn) and glutamine (Gln) can function as tertiary destabilizing residues through their

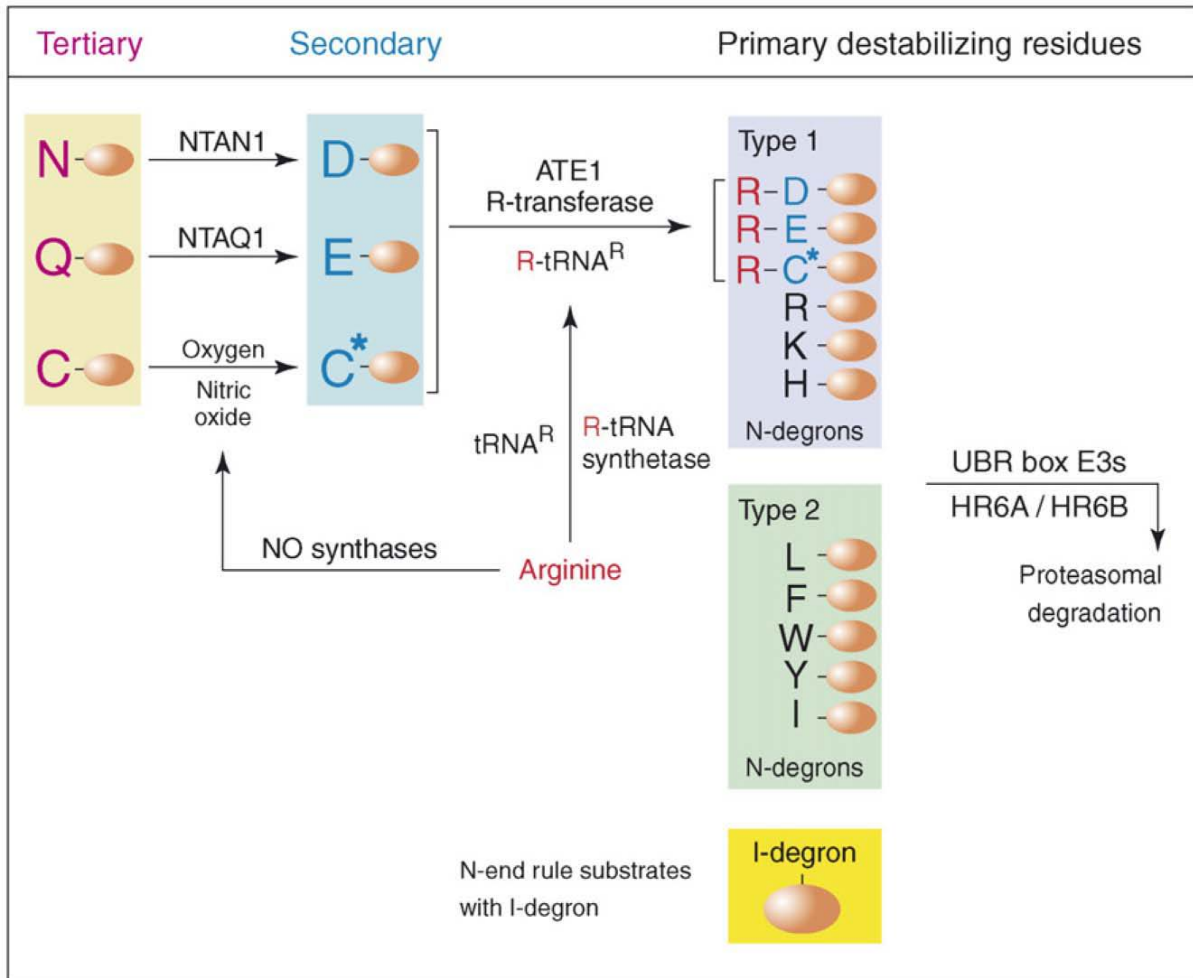


**Figure 1. The hierachial structure of the mammalian N-end rule pathway.**

The N-terminal amino acids are denoted as single-letter. The orange ovals indicate a substrate. The tertiary N-residues, Asn and Gln, are deamidated by NTAN1 and NTAQ1 which currently is a hypothetical enzyme, into the secondary N-residues Asp and Glu, respectively. The secondary N-residues C\* indicate an oxidized Cys, which can be structurally similar to Asp. The secondary N-residues are arginylated by ATE1 into the primary N-residues. Along with the substrate with internal degron (I-degron), substrates with type 1 or 2 primary N-residues are recognized by UBR box containing E3s and ubiquitinated by E3 associated with E2 such as HR6A or HR6B.

deamidation into the secondary destabilizing N-terminal residues aspartate (Asp) and glutamate (Glu), respectively, by N-terminal Asn-specific deamidase NTAN1 and a postulated deamidase termed NTAQ1 (Kwon et al., 2000) (Fig. 1). *NTAN1*<sup>-/-</sup> mice are alive but show abnormalities in certain aspects of learning, memory, and socially conditioned behavior (Kwon et al., 2001). The destabilizing activity of Asp and Glu requires their conjugation by *ATE1*-encoded isoforms of Arg-tRNA-protein transferase (Arg-transferase) to Arg, one of the primary destabilizing residues

(Kwon et al., 1999a; Kwon et al., 2002). In mammals, destabilizing N-terminal residues that function through their ATE1-dependent arginylation are not only Asp and Glu but also cysteine (Cys), which is a stabilizing (unarginylated) residue in *Saccharomyces cerevisiae* (Kwon et al., 2002). Arginylation of N-terminal Cys requires a prior oxidation of Cys into Cys sulfinate (CysO<sub>2</sub>H) or Cys sulfonate (CysO<sub>3</sub>H), which requires nitric oxide (NO) and oxygen gas (O<sub>2</sub>), suggesting that ATE1-dependent proteolysis may function as an *in vivo* sensor for NO and O<sub>2</sub> (Kwon et al., 2002; Hu et al., 2005; Lee et al., 2005). *ATE1*<sup>-/-</sup> mice die associated with various cardiovascular defects including ventricular hypoplasia, ventricular septal defect, and late angiogenesis (Kwon et al., 2002), indicating that ATE1-dependent arginylation is crucial for cardiovascular homeostasis and development.

N-terminal Arg together with other N-degrons are recognized by specific N-recognins for protein ubiquitylation (Fig. 1). The type 1 N-degrons are the basic N-terminal residues arginine (Arg), lysine (Lys), and histidine (His), while the type 2 N-degrons are the bulky hydrophobic N-terminal residues phenylalanine (Phe), leucine (Leu), tryptophan (Trp), tyrosine (Tyr), and isoleucine (Ile) (Bachmair et al., 1986; Kwon et al., 1998; Kwon et al., 1999b; Kwon et al., 2001; Kwon et al., 2003). A family of mammalian E3s termed UBR1 through UBR7 has been identified, which can potentially recognize N-degrons, perhaps through the conserved ~70 residue-Cys/His domain termed the UBR box motif (Tasaki et al., 2005). UBR box proteins are highly heterologous in sizes (50-570 kDa), sequences, and types of ubiquitylation domain (RING domain in UBR1, UBR2, and UBR3; HECT domain in UBR5; F-box in UBR6; PHD domain in UBR7). A distinctive set of UBR box proteins is present in all the examined eukaryotes, suggesting their essential and broad biological functions. Although the detailed biochemical properties of each UBR box proteins are to be further investigated, a set of UBR proteins (UBR1,

UBR2, UBR4, and UBR5) have been shown to bind to certain type 1 and/or type 2 N-degrons (Kwon et al., 2003; Tasaki et al., 2005). It is therefore increasingly clear that the mammalian N-end rule pathway is mediated by a complicated network of multiple E3s containing the UBR box motif, perhaps in a manner specific for substrates, cell and tissue types, and developmental stages.

## **2.0 THE ROLE OF UBR2 IN TRANSCRIPTIONAL SILENCING DURING MEIOSIS**

### **2.1 SUMMARY**

There is a general notion that ubiquitin plays an important role in epigenetic remodeling during meiosis, yet little is known about the pathways involved. UBR2 is a recognition E3 component of the N-end rule pathway, where Ub ligases recognize, for proteolytic polyubiquitylation, the N-termini of substrates as degrons. In this project, I show that UBR2 localizes to the meiotic chromatin, where it mediates protein ubiquitylation in a spatiotemporal manner during meiotic prophase. UBR2-lacking spermatocytes show significantly impaired global ubiquitylation of chromatin proteins, including monoubiquitylation of histone H2A, a histone modification found in various chromatin inactivation processes. UBR2 and HR6B form an E3-E2 complex and cooperatively mediate H2A monoubiquitylation *in vitro*. Impaired H2A ubiquitylation in UBR2-deficient spermatocytes correlates to defects in transcriptional silencing of genes linked to unsynapsed regions of the X and Y chromosomes. These results provide a convincing model where UBR2 accumulates on unpaired meiotic chromosomal axes to mediate transcriptional silencing through its non-proteolytic E3 activity for ubiquitylation of H2A, which requires the E2 enzyme HR6B of the N-end rule pathway. These results further suggest that UBR2-dependent H2A ubiquitylation and BRCA1-dependent H2AX phosphorylation represent two independent

pathways that together regulate chromatin inactivation and remodeling in germ cells and possibly in somatic cells as well.

## 2.2 BACKGROUND

Meiosis involves one of the most dramatic chromatin remodeling processes, including synapsis and transcriptional silencing. During the pachytene stage of meiosis when autosomal homologues have completed synapsis, the X and Y chromosomes are located into the nuclear periphery and form the sex- or XY-body, where they achieve partial synapsis only in the pseudoautosomal region (PAR). In the XY body, the transcription of genes linked to unsynapsed XY axes are silenced through a process called meiotic sex chromosome inactivation (MSCI) (Turner, 2007). Recent studies indicate that unpaired chromosomal regions are transcriptionally silenced during meiosis not only in the sex chromosomes but also in autosomal chromosomes, a mechanism called meiotic silencing of unsynapsed chromatin (MSUC) (Schimenti, 2005). MSUC is thought to be part of a checkpoint that maintains genome integrity by sensing unpaired chromosomal regions (Baarends et al., 2005; Schimenti, 2005; Turner et al., 2005). Meiotic chromatin silencing requires differential histone modifications, including ubiquitylation, phosphorylation, methylation and acetylation (de Napoles et al., 2004).

Although there is a general notion that Ub plays an important role in chromatin remodeling during meiosis, little is known about specific Ub pathways mediating ubiquitylation of chromatin-associated proteins. Monoubiquitylated histone H2A (uH2A), which occurs at lysine 119, comprises 5-15% of total H2A, representing the most abundant ubiquitylation substrate in mammals (Fang et al., 2004). Monoubiquitylated H2A is also the major Ub

conjugate in male meiosis, which accumulates in the XY body and the unsynapsed chromosomal regions undergoing meiotic chromatin inactivation (Baarends et al., 1999). In addition to meiotic chromatin inactivation, uH2A has been implicated in chromatin inactivation of somatic cells, including X inactivation of female somatic cells (de Napoles et al., 2004; Fang et al., 2004) and transcriptional silencing of Hox genes (Cao et al., 2005). Several studies showed that, in addition to H2A, histone H3 and testes-specific H3 are ubiquitylated during spermatogenesis, which becomes prominent in elongated spermatids (Chen et al., 1998). The mammalian genome is estimated to encode more than 500 Ub ligases (Ardley and Robinson, 2005), yet few are functionally implicated in meiotic prophase I. One such Ub ligase is UBR2. *UBR2*<sup>-/-</sup> male mice are infertile which was associated with arrest at meiotic prophase I and germ cell apoptosis, whereas *UBR2*<sup>-/-</sup> females are fertile but develop partial lethality throughout development (Kwon et al., 2003). Ub ligase Siah1 has also been implicated in meiosis. However, Siah1 is unlikely to be critical for meiotic chromatin remodeling, which occurs at zygotene, as mutant mice lacking this E3 are arrested at meiotic metaphase I (Dickins et al., 2002). Ubiquitylation by Ub ligase requires an Ub-conjugating enzyme. Amongst more than 50 E2 enzymes, HR6B, the homolog of *Saccharomyces cerevisiae* RAD6, appears to be the major meiotic E2 that has been shown to localize to meiotic chromatin and to be essential for transcriptional silencing of some genes linked to the sex chromosomes (Baarends et al., 2005; Baarends et al., 2007) (The mammalian genome encodes two HR6 isoforms, HR6A and HR6B, with 95% identity to each other, which I refer here as RAD6 when their biochemical properties cannot be distinguished). HR6B and its yeast homolog have been implicated as an E2 component of the N-end rule pathway (Dohmen et al., 1991; Kwon et al., 2001). In addition, *S. cerevisiae* RAD6 plays an important role in meiosis and ubiquitylation of histone H2B (Robzyk et al., 2000).

In this project, I characterize an Ub pathway that controls histone ubiquitylation during male meiosis. The results suggest a model where UBR2 accumulates on unpaired meiotic chromosomal axes to mediate transcriptional silencing through its non-proteolytic E3 activity for ubiquitylation of H2A, which requires the E2 enzyme HR6B of the N-end rule pathway. The results further suggest that UBR2-dependent H2A ubiquitylation and BRCA1-dependent H2AX phosphorylation represent two independent pathways that regulate chromatin inactivation and remodeling in germ cells and possibly in somatic cells as well.

## 2.3 METHODS

### 2.3.1 *UBR2*<sup>-/-</sup>, *Brcal* <sup>$\Delta 11/\Delta 11$</sup> *p53*<sup>+/-</sup>, and *SPO11*<sup>-/-</sup> Mice

*UBR2*<sup>-/-</sup> mice were produced by interbreeding *UBR2*<sup>+/-</sup> mice in 129SvImJ/C57BL/6 (Kwon et al., 2003). Surface-spread chromosomes from *Brcal* <sup>$\Delta 11/\Delta 11$</sup> *p53*<sup>+/-</sup> and *SPO11*<sup>-/-</sup> mice were previously described (Romanienko and Camerini-Otero, 2000; Xu et al., 2003).

### 2.3.2 Immunohistochemistry on germ cell spread

**Table 1. Antibodies used in immunohistochemistry**

Table Antibody	Species	Dilution	Reference
Anti-ATR	goat	1:100	SantaCruz, sc-1887
Anti-BRCA1	goat	1:100	SantaCruz, sc-1553
Anti-FANCD2	rabbit	1:500	NOVUS, NB100-182
Anti-H2A Ub	mouse	1:100	Upstate, 05-678
Anti-H2A.X gamma	mouse	1:12,000	Upstate, 05-636
Anti-MLH1	mouse	1:100	BD Pharmingen, 551091
Anti-RAD51	rabbit	1:200	SantaCruz, sc-8349
Anti-RPA	rabbit	1:100	Dr. Ingles, University of Toronto, Canada
Anti-SCP3	mouse	1:2000	Dr. Lee, Kobe University, Japan
Anti-SCP3	rabbit	1:750	Dr. Heyting, Wageningen University, Netherlands
Anti-FK1	mouse	1:2,500	Biomol, PW8805
Anti-FK2	mouse	1:500	Affinity research, PW8810
Anti-UBR2	rabbit	1:500	Kwon et al., 2003
Anti-mouse IgG Alexa Fluor® 488	goat	1:400	Molecular Probes, A11029
Anti-mouse IgG Cy3	goat	1:250	Jackson ImmunoResearch, 115-165-146
Anti-mouse IgM Cy3	goat	1:250	Jackson ImmunoResearch, 115-165-075
Anti-rabbit IgG Alexa Fluor® 488	goat	1:400	Molecular Probes, A11034
Anti-rabbit IgG Alexa Fluor® 555	goat	1:400	Molecular Probes, A21429
Anti-goat IgG Cy3	donkey	1:250	Jackson ImmunoResearch, 705-165-147

Surface-spread germ cells were prepared as previously described (Peters et al., 1997) with minor modification. Briefly, I harvested testes of different age and rinsed in phosphate-buffered saline (PBS). After removing tunica albuginea, seminiferous tubules were incubated in hypotonic buffer (30mM Tris, 50mM sucrose, 17mM trisodium citrate dehydrate, 5mM EDTA, 0.5 mM DTT, 0.5 mM PMSF, pH 8.2) for 1 h. Swollen tubules were finely minced by forceps and blade, resuspended in 100mM sucrose (pH 8.2) solution and kept in microtube until large clumps of tubules were sunk to the bottom. The suspension was evenly spread to the slides coated with fixing solution (1% paraformaldehyde, 0.15% Tx-100 in 10 mM sodium borate, pH 9.2). The slides were dried at least 2 h in a humidified chamber, washed for 2 min in 0.4% Photoflo twice,

briefly dried and stored at  $-80^{\circ}\text{C}$ . For immunostaining, I incubated slides in blocking solution (10% heat-inactivated goat or donkey serum, depend on secondary antibody, PBS with 0.1% Triton X-100) for 30 min. Primary antibodies were diluted in blocking solution and incubated with slides in a humidified chamber for 1h at room temperature or for O/N at  $4^{\circ}\text{C}$ . Then slides were washed 3 times in wash buffer (PBS with 0.1% Triton X-100) for 5 min each, incubated with secondary antibodies for 1h at RT, washed in wash buffer, and then mounted with media containing DAPI (Vector laboratories, Burlingame, CA). I captured the images using Nikon E600 Epifluorescent microscope and processed them using Adobe Phothoshop 7.0. Antibodies are listed in Table 1.

### **2.3.3 Fluorescence *in situ* hybridization (FISH)**

Chromosome painting was carried out using FITC-labeled Y probe and Cy3-labeled X probe (Cambio) according to manufacturer's instructions. Briefly, surface-spread slides were dehydrated by serial ethanol washing for 2 min each in 70% twice, 90% twice, and 5 min in 100% ethanol, followed by aging for 60 min at  $65^{\circ}\text{C}$ . Specimen were incubated in pre-warmed denaturation solution (0.6X SSC, 70% deionized formamide) for 2 min at  $65^{\circ}\text{C}$  and hybridized with X and Y probes in pre-warmed humidified chamber at  $37^{\circ}\text{C}$  for overnight. Next day, slides were washed twice for 5 min each in 1X SSC, stringency solution (0.5X SSC, 50% deionized formamide), and 1X SSC with all solutions at  $45^{\circ}\text{C}$ . Finally, they were incubated for 5 min three times in detergent solution (4X SSC, 0.05% Tlen-20) at  $45^{\circ}\text{C}$  and dried. For combined FISH with immunostaining, I post-fixed X-Y painted slides in 4% paraformaldehyde for 5 min at  $4^{\circ}\text{C}$

and rinsed them in PBS. Immunohistochemistry was performed as described (see METHOD 2.3.2).

#### **2.3.4 Microarray analysis**

Total RNA of each genotype was prepared from 2 individual testes of 16 days postpartum (d.p.p.) mice. Biotinylated cRNA was produced and hybridized on Affimetrix mouse genome 430A 2.0 arrays. Arrays were normalized to a trimmed mean signal level. To remove probe sets with low expression in testis, detection p-value greater than .04 in both genotypes were filtered. Probe sets with multiple chromosome location or without information were also eliminated. 14,705 probe sets were grouped by each chromosome and mean logarithmic ratio of expression level of *UBR2*<sup>-/-</sup> to wild type was calculated.

#### **2.3.5 Northern blot and real-time RT-PCR analyses**

For Northern analyses, 10 µg of total RNA from wild type, *UBR2*<sup>+/-</sup> and *UBR2*<sup>-/-</sup> testes of 6 week-old mice were electrophoresed and blotted to Nytran Plus membrane (Schleicher & Schuell). Probes of gene expressed in mouse testis were generated by RT-PCR and labeled with [ $\alpha$ -32P] dCTP (GE Healthcare) using DNA Labeling Beads (GE Healthcare). For hybridization, the membrane was incubated with the probe generated in the ExpressHyb solution (BD biosciences) at 68°C for 1 h. Then it was washed in 2X SSC, 0.05% SDS for 40 min at room temperature, followed by 0.1X SSC, 0.1% SDS for 40 min at 50°C. For real-time RT-PCR analyses of genes in X-Y chromosomes, I prepared total RNA from testis using RNeasy-mini kit (Qiagen) with on-column DNase digestion to prevent genomic DNA contamination. cDNA was

generated from 2  $\mu$ g of RNA using SuperScript III™ reverse transcriptase (Invitrogen). Real-time RT-PCR was carried out using Platinum®SYBR® Green (Invitrogen) in ABI 7300/7500 Real time PCR system. All samples were duplicated (or triplicated) and normalized by  $\beta$ -actin. Sequences of primers are listed in Table 2.

**Table 2. Primers used in real-time RT-PCR**

Gene	Forward	Reverse
Ube2a	5'-ATCCTAACGTCTATGCAGATGGT	5'-CGCTTTTCATATTCCCGCTTGTT
Mecp2	5'-ATGGTAGCTGGGATGTTAGGG	5'-TGAGCTTTCTGATGTTTCTGCTT
Ube1x	5'-TGAAGCAGACATAGACGAGAGC	5'-CAAGCCTGAGACAAGGACG
Hprt	5'-GTTAAGCAGTACAGCCCCAAA	5'-AGGGCATATCCAACAACAAACT
Hdac6	5'-ACAACCCAGTACATGAATGAAGG	5'-CCCCATGAGTGCATCTACCA
Pctk1	5'-TCCGCCGAGTCAGTTTGTC	5'-TCCGCCGAGTCAGTTTGTC
Rbmy	5'-TTCCTTACTTTCCGACGCCTT	5'-TGGTCTCTTCTTGCTACCACTTT

### 2.3.6 Acid extraction of core histones and immunoblotting

I harvested testes from 19 d.p.p. mice and removed tunica albuginea. Seminiferous tubules were lysed in 10X volume of NP-40 lysis buffer (150 mM NaCl, 50 mM Tris pH 8.0, 1% NP-40) with protease inhibitor mix (Sigma) by 15 times stroke with Dounce homogenizer on ice. Pellet was spun down at 12,000g for 10 min in cold room, followed by incubation with 0.5 ml of 0.2N H<sub>2</sub>SO<sub>4</sub> on ice for 30 min. After centrifugation at max speed (~16,000g) for 10 min at 4°C, proteins were precipitated by adding 0.5 ml of 50% TCA (25% of final concentration) to the supernatant and incubated on ice for 30 min. Core histones were pelleted at max speed for 10 min at 4°C, washed in 1 ml of ice-cold acetone for 30 min, and then dissolved in 100 mM Tris pH 7.5. Proteins were resolved by SDS-PAGE and subjected to Coomassie staining or

immunoblotting using antibodies for histone H2A (Cell Signaling), ubiquitylated histone H2A (uH2A) (Upstate), histone H2B (Cell Signaling), testis specific histone H2B (Abcam) and histone H3K4me2 (Abcam).

### **2.3.7 Affinity-purification of chicken anti-mouse UBR2 IgY**

I constructed a plasmid that the GST is fused with N-terminal 100 amino acid of UBR2 (GST-UBR2) and transformed it into *BL21* strain. GST-UBR2 proteins were prepared from 500 ml culture as previously described with some modifications (Frangioni and Neel, 1993). Briefly, cells were pelleted at 7,700g for 10 min at 4°C and resuspended in 25 ml of PBS containing protease inhibitors mix (Roche), and disrupted by sonication (Branson). Lysates were treated with the Triton X-100 to the final concentration of 1% and incubated for 30 min at 4°C, and centrifuged at 15,000g for 10 min at 4°C. Supernatant was filtered through 0.45 µm and incubated with glutathione sepharose 4B (GE healthcare) in accordance with manufacture's instruction. After washing the beads in PBS, GST-UBR2 was collected in elution buffer (10 mM reduced glutathione in 50 mM Tris pH 8.0). Proteins were concentrated using Centriplus® YM-10 (Millipore) according to manufacturer's instruction. 500 µg of protein was used for chicken anti-UBR2 IgY generation (Aves Labs). Affinity purification of UBR2 specific antibodies was carried out as previously described (Bar-Peled and Raikhel, 1996). Briefly, GST and GST-UBR2 were collected from 250 ml culture as abovementioned. Proteins were covalently cross-linked to the glutathione sepharose 4B by incubating in DMP solution (7.5 mg/ml dimethyl pimelimidate-HCl (Sigma) in 0.2M triethanolamine pH 8.3) for 30 min at room temperature. To terminate cross-linking reaction and remove non-covalently linked molecules, resins were washed in 0.2M

triethanolamine pH 8.6 and 0.1M glycine-HCl pH 2.5, followed by PBS. Cross-linked GST-resin was incubated with collected IgY, washed in PBS and centrifuged at 500g for 2 min at 4°C. The supernatant was applied to GST-UBR2-resin, incubated and washed in PBS. UBR2-specific antibodies were eluted in 0.1M glycine-HCl pH 2.5 and pH was adjusted to 7 with 2M Tris.

### **2.3.8 Preparation of N-recognins**

Affinity purified N-recognins were prepared from testes of rat (Pel-Freeze) and mouse. After homogenized in lysis buffer (10% glycerol, 75 mM NaCl, 0.1 mM EDTA, and 20 mM HEPES, pH7.9), lysate was centrifuged at 13,000 rpm for 1 h. NaCl was added to the supernatant to final concentration of 0.8 M. Biotin-labeled peptides (X- Ile-Phe-Ser-Thr-Ile-Glu-Gly-Arg-Thr-Tyr-Lys-Biotin, where X is Phe or Val) were synthesized and conjugated to Streptavidin Sepharose (GE healthcare). The Beads were incubated for overnight at 4°C in the lysate and washed in cold washing buffer (0.05% Tween 20, 0.8 M NaCl, and 20 mM HEPES, pH 7.9) 5 times. Proteins were eluted with washing buffer containing 10 mM Trp-Ala dipeptide and dialyzed in dialysis buffer (0.1 M NaCl, and 10 mM HEPES, pH7.9). Dialyzed proteins were concentrated using Amicon Ultra (Millipore). N-recognins were quantified by silver staining.

### **2.3.9 Interaction between endogenous UBR2 and RAD6.**

Affinity-purified proteins containing ~500 ng endogenous UBR2 were mixed with 1 µg chicken anti-UBR2 antibody or IgY for overnight. A protein sample eluted from Val-peptide was used as a control. UBR2 immunoprecipitates were subjected to immunoblotting with an antibody recognizing both HR6B and HR6A (Cell Signaling).

### **2.3.10 *In vitro* ubiquitylation assay**

*In vitro* ubiquitylation assay was carried out using Ubiquitylation kit (Biomol) in accordance with manufacturer's protocol. Total 20  $\mu$ l of reaction including 0.1  $\mu$ M human recombinant E1 (Biomol), 50 ng human recombinant HR6B (Biomol), 100 ng purified N-recognins, 1  $\mu$ g recombinant histone H2A (New England Biolabs), 1  $\mu$ g HA-tagged ubiquitin (Boston Biochem) and 5 mM Mg-ATP was incubated for 90 min at 37°. E2-E3 complex was purified from testes of wild type and *UBR2*<sup>-/-</sup> mice and used in reactions without human recombinant HR6B. Proteins were separated by SDS-PAGE and subjected to immunoblotting using antibodies for HA (Sigma), UBR2 (5-1) (Kwon et al., 2003) and uH2A (Upstate).

## **2.4 RESULTS**

### **2.4.1 The localization of UBR2 during meiotic prophase**

UBR2 mRNA was mainly expressed in spermatocytes as shown by in situ hybridization (Kwon et al., 2003). To investigate the role of UBR2 in meiosis further, I performed immunofluorescence analysis on meiotic surface-spread nuclei using the UBR2 (3-1) antibody which recognizes 51-63 residues of mouse UBR2 (Kwon et al., 2003). To determine the detailed stages of meiotic prophase, I co-immunostained the nuclei with an antibody recognizing SCP3, a component of the axial elements (AEs) of the synaptonemal complex (SCs) which is a meiosis-specific protein complex required for pairing between homologous chromosomes.

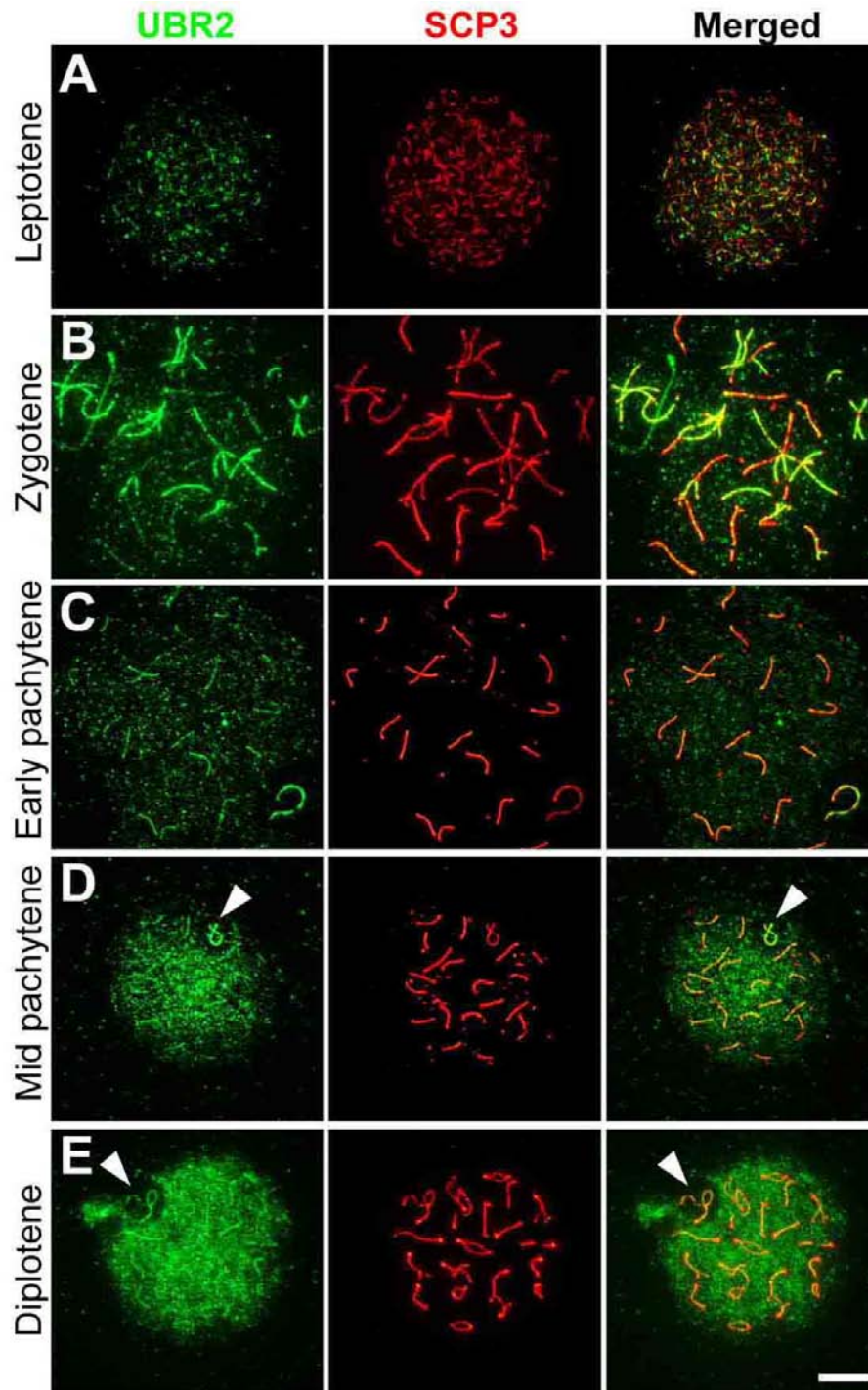


**Figure 2. Localization of UBR2 in spermatocytes during meiotic prophase.**

(A) At leptotene, UBR2 staining (green) appears as foci in the chromatin and as segment-like staining along the newly emerging axial elements. SCP3 (red) was co-stained to monitor meiotic sub-stages. (B) At zygotene, UBR2 staining is enriched on unsynapsed axial regions (arrowhead). (C) At early pachytene, UBR2 staining gradually disappears from the axes that have achieved synapsis and is enriched on the unpaired axes of the X and Y chromosomes. (D, E) At mid-pachytene, the number of UBR2 foci surge throughout the entire chromatin, except for the XY chromatin (arrowhead). Scale bar: 10  $\mu$ m

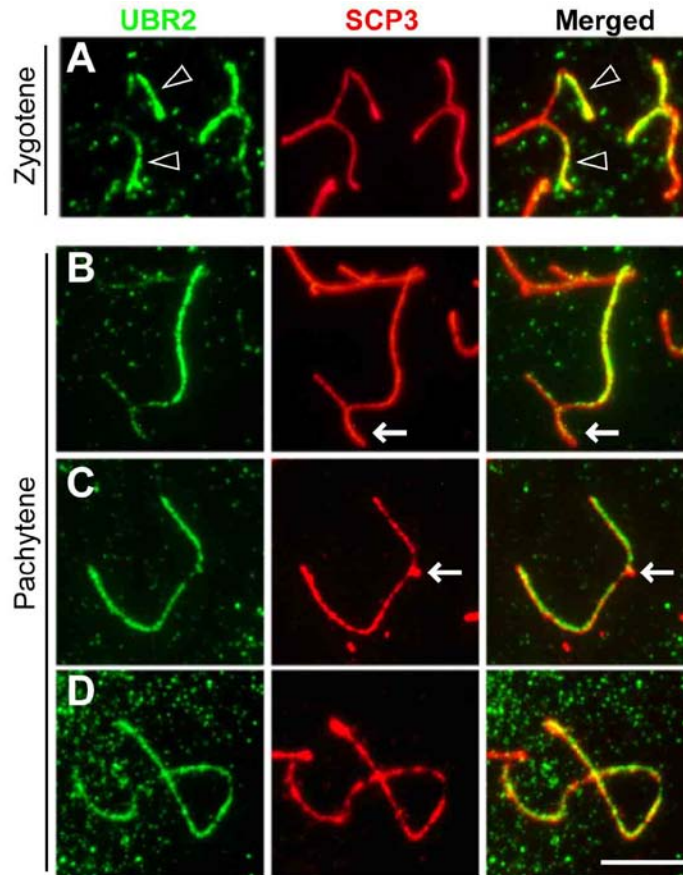


**Figure 3. UBR2 localization on meiotic chromosomes.**

(A) UBR2 staining is enriched on unsynapsed axial regions (arrowhead) of autosomes in zygotene. (B-D) UBR2 localization on unsynapsed axial regions of the sex chromosomes during early pachytene (B), mid-pachytene (C) and late pachytene (D). Arrow, PAR. Scale bar: 5  $\mu$ m

Two distinctive patterns of UBR2 localization were observed during meiotic prophase. One is on autosomal chromatin throughout nucleus and the other on the AEs of homologous chromosome. UBR2 foci on autosomal chromatin were first detected in leptotene nuclei (Fig. 2A). These foci were maintained the expression level until early-pachytene, and then showed a dramatic increase throughout nucleus from mid-pachytene onward (Fig. 2D, E). It was noticeable that the foci were excluded from sex chromatin even after dramatic increase of expression (Fig. 2C-E, 3B-D). In addition to the localization on autosomal chromatin, UBR2 expression was also detected on AEs from leptotene when SCs began to emerge (Fig. 2A).

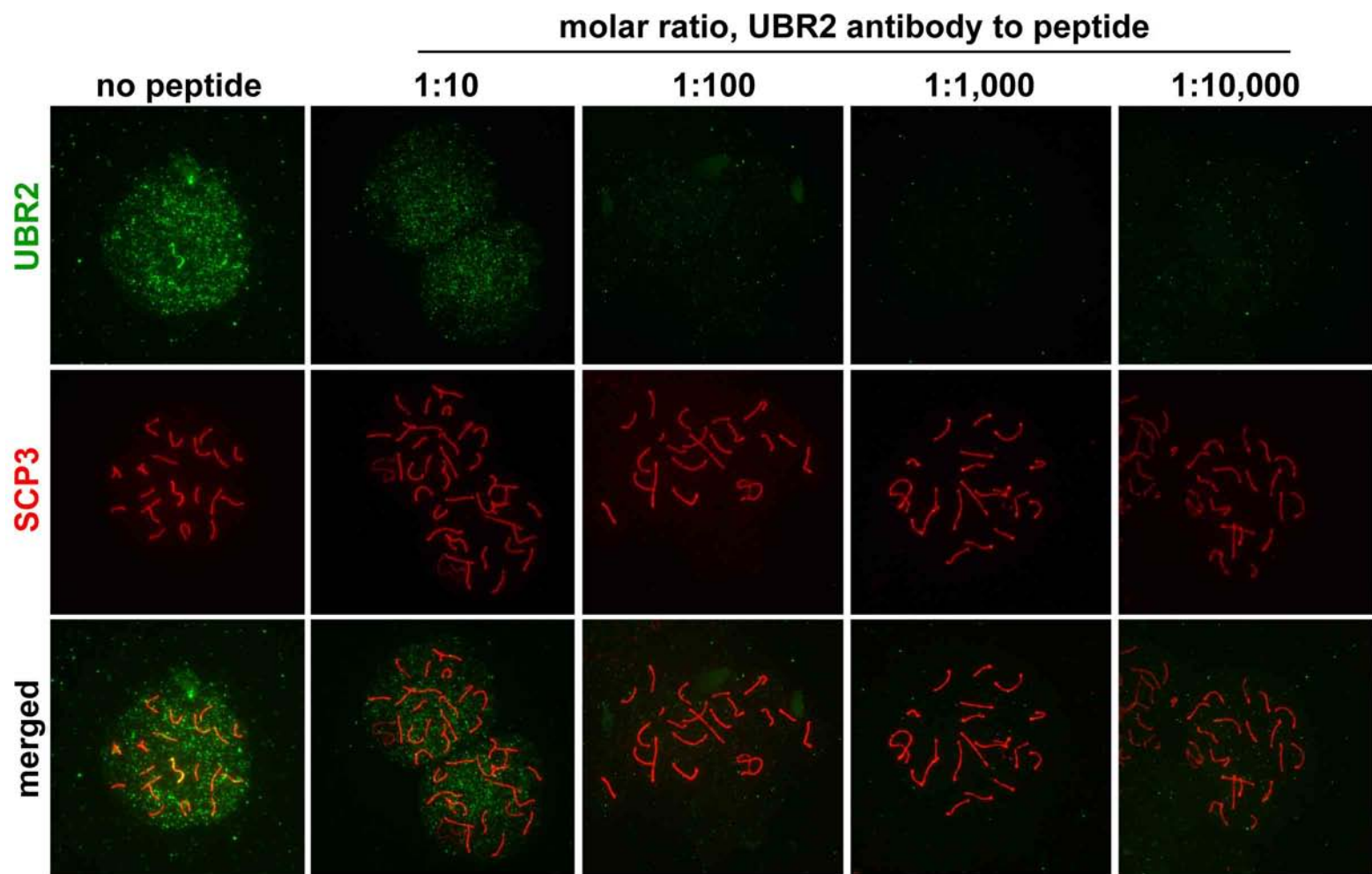


**Figure 4. Specificity of rabbit anti-mouse UBR2 antibody**

UBR2 antibody was incubated with increasing concentration of peptide which had been used for raising antibody. UBR2 signal was disappearing proportionally with the increase of peptide concentration.

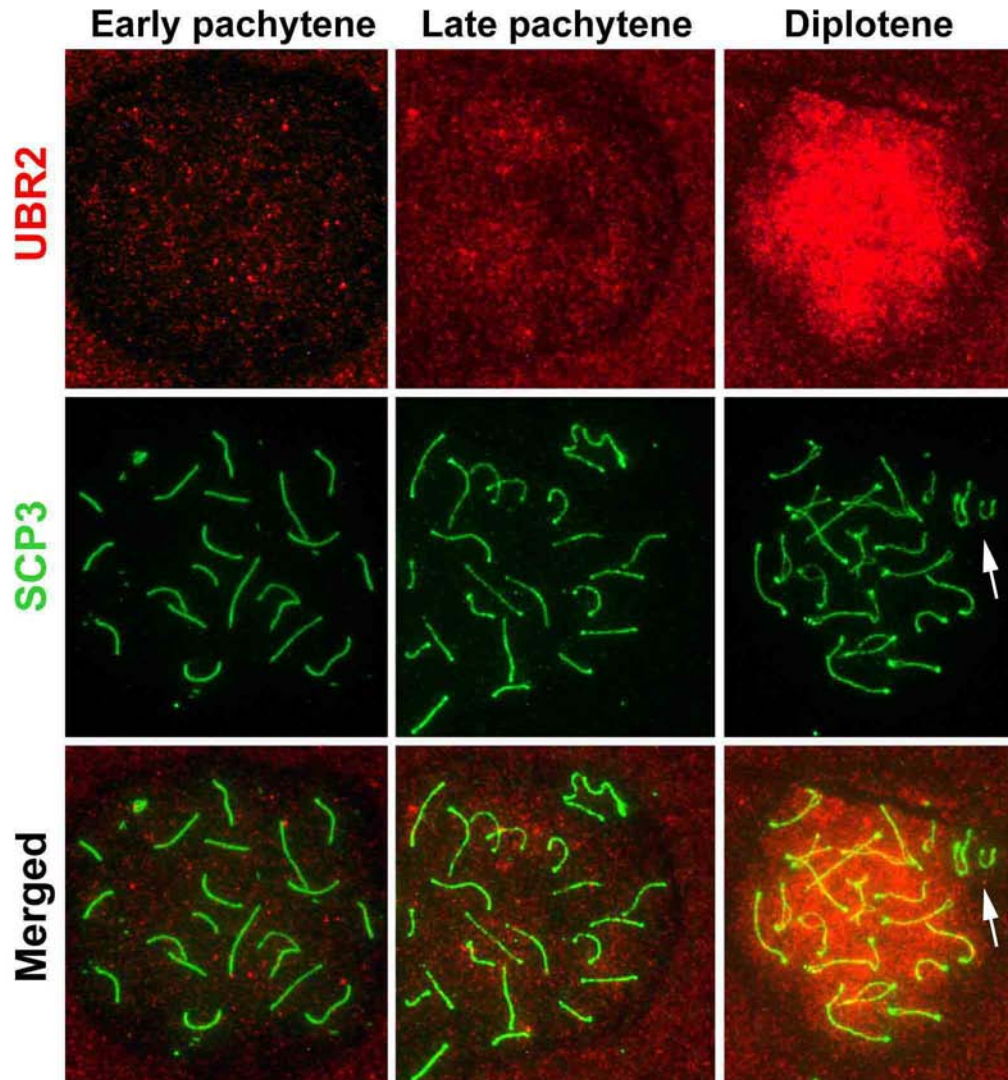


**Figure 5. Surge of UBR2 signal throughout nucleus after mid pachytene**

UBR2 signal (red) was detected using guinea pig anti-mouse UBR2 antibody recognizing 51-63 residues. The region covering sex chromosomes (arrows) is devoid of UBR2 signal at diplotene spermatocytes as previously reported (see Fig. 2).

In zygotene nuclei where homologous chromosomes begin to pair, UBR2 localization was enriched on unsynapsed AEs (Fig. 2B, 3A). Enriched UBR2 signal on unsynapsed AEs disappeared at pachytene where pairing of autosomal homologous chromosomes are completed, but still maintained on AEs of XY chromosome (Fig. 2C, 3B-D). The signal reside along AEs of sex chromosome were weak in pseudoautosomal region (PAR, Fig. 3B, C) where sex chromosomes are partially synapsed. To exclude the remote possibility that observed UBR2

signal was the result of non-specific binding of antibody, I incubated the antibodies for UBR2 and SCP3 with increasing concentration of peptides (51-63) which had been used to raise UBR2 antibody. As the concentration of peptides was increased, the level of UBR2 signal was decreased reciprocally without discernable change of SCP signal (Fig. 4). Guinea pig anti-mouse UBR2 antibody was generated using same peptides (51-63) to confirm UBR2 signal furthermore. Immunostaining using this antibody showed the consistent results that UBR2 signal on chromatin surged throughout the whole nucleus excluding sex body after mid pachytene (Fig. 5 and Fig. 2D, E). These distinctive localizations of UBR2 suggest that UBR2 has multiple functions during meiotic prophase.

#### **2.4.2 Impaired ubiquitylation in *UBR2*<sup>-/-</sup> spermatocytes**

Little is known about the global patterns of polyubiquitylation and monoubiquitylation of chromatin-associated proteins during meiosis. To test the possibility that UBR2 mediates (nonproteolytic) ubiquitylation of chromatin proteins during meiosis, I determined the spatiotemporal distribution of Ub conjugates on meiotic chromosomes from control and *UBR2*<sup>-/-</sup> spermatocytes. Polyubiquitylation was analyzed using FK1 antibody specific for polyubiquitin conjugates (Fig. 6A-C), and monoubiquitylation was deduced by subtracting FK1 (polyubiquitin) signals from FK2 signals representing both polyubiquitin and monoubiquitin conjugates (Fig. 7A-C) (Fujimuro et al., 1994). Polyubiquitylation signals were not detected during leptotene through late zygotene (Fig. 6A) and first appeared along the XY axes at early pachytene (Fig. 6B). During mid-pachytene through diplotene, intense polyubiquitin staining accumulated throughout the entire chromatin, with the highest level in the XY chromatin domain (Fig. 6C, and data not shown). Thus, it is likely that global polyubiquitylation of chromatin proteins plays

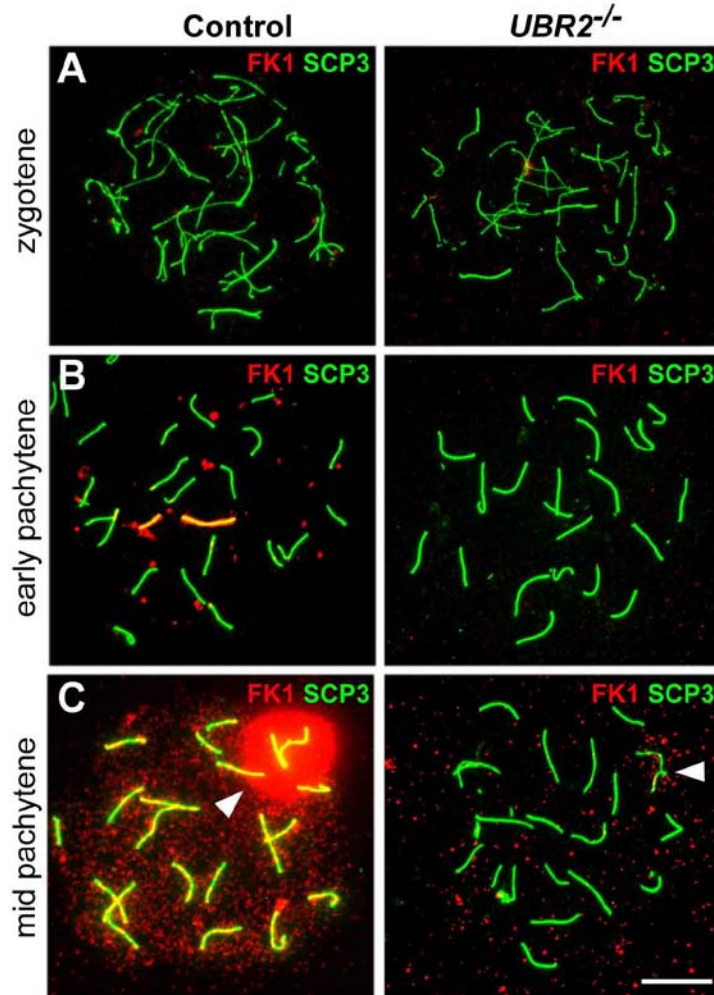


**Figure 6. Localization of polyubiquitin conjugates in control and *UBR2*<sup>-/-</sup> spermatocytes.**

Chromosomal distribution of polyubiquitin conjugates in control and *UBR2*<sup>-/-</sup> spermatocytes at zygotene (A), early pachytene (B) and mid-pachytene (C), as determined by immunostaining with FK1 (red) and SCP3 (green) antibodies. Arrowhead, XY chromatin. Scale bar: 10  $\mu$ m

a role in postsynaptic processes, possibly for proteolysis via the 26S proteasome. Moreover, comparison of the spatiotemporal staining patterns of FK1 and FK2 signals led us to deduce that monoubiquitylation-specific staining accumulates on unsynapsed axes of homologous chromosomes as early as late-zygotene (Fig. 7A). Another monoubiquitylation-specific signal was detected in the XY chromatin at early pachytene when FK1 and FK2 signals were respectively detected on the XY axes and the entire XY body (Fig. 7B). From mid-pachytene

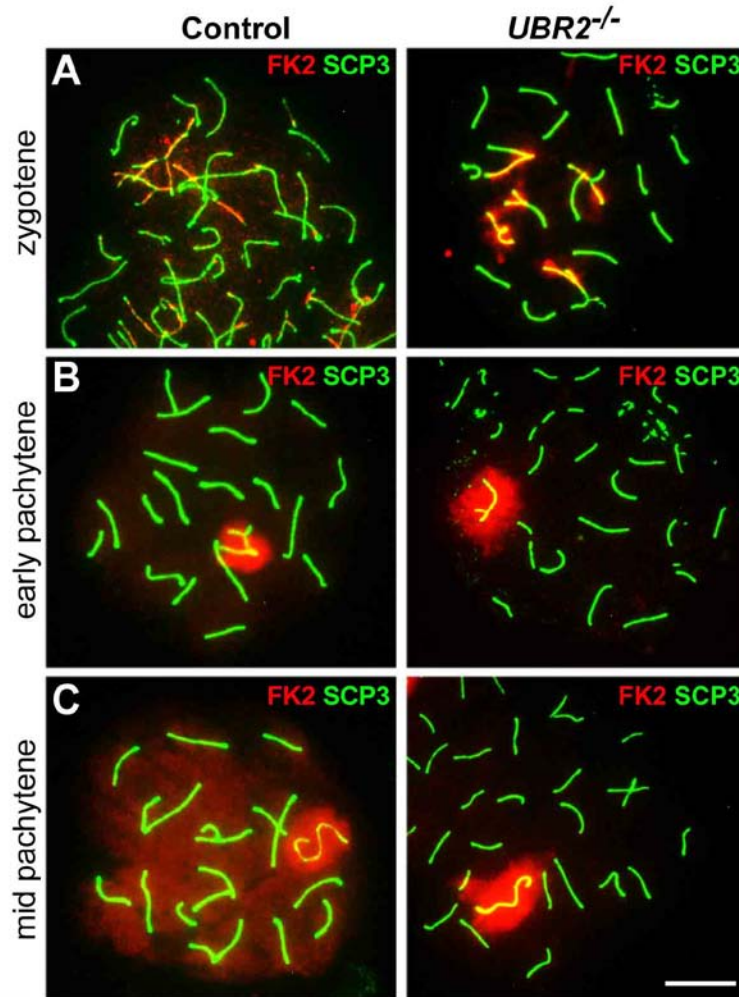


**Figure 7. Overall ubiquitylation in control and *UBR2*<sup>-/-</sup> spermatocytes.**

Chromosomal distribution of polyubiquitin- and monoubiquitin conjugates in control and *UBR2*<sup>-/-</sup> spermatocytes at zygotene (A), early pachytene (B) and mid-pachytene (C), as determined by immunostaining with FK2 (red) and SCP3 (green) antibodies. Scale bar: 10  $\mu$ m

through diplotene, both antibodies commonly showed strong signals throughout the entire chromatin, prominently in the XY body (Fig. 7C). Thus, monoubiquitylation and polyubiquitylation of chromatin proteins occur in meiosis, with dynamic changes as germ cells develop.

Next, I compared polyubiquitylation and monoubiquitylation signals on spread chromosomes from control and *UBR2*<sup>-/-</sup> spermatocytes. The FK1 (polyubiquitylation) signals on

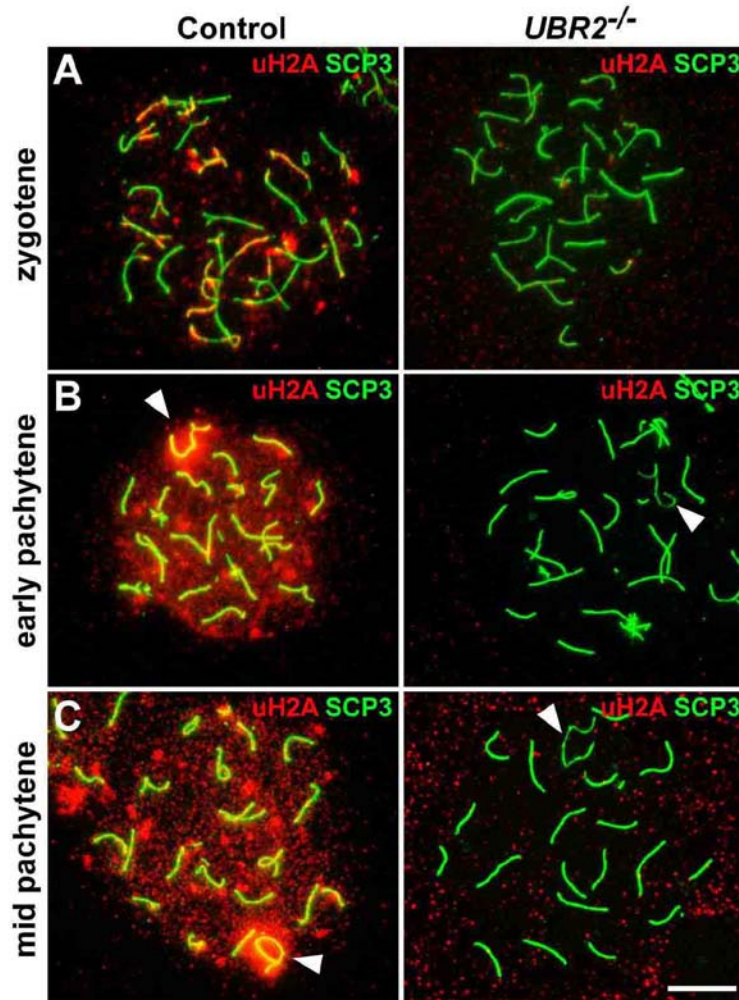


**Figure 8. UBR2 is required for ubiquitylation of histone H2A.**

Immunostaining of uH2A (red) on meiotic chromosomes from control and *UBR2*<sup>-/-</sup> spermatocytes at zygotene (A), early pachytene (B), and mid pachytene (C). The X and Y chromosomes are indicated by arrowheads. Scale bar: 10  $\mu$ m

the XY axes at early pachytene were found to be abolished in *UBR2*<sup>-/-</sup> spermatocytes. Moreover, by mid-pachytene, the global ubiquitylation signals on the autosomal chromosomes were profoundly diminished in *UBR2*<sup>-/-</sup> cells (Fig. 6C, 7C). These data together demonstrate that UBR2 is the major Ub ligase required, directly or indirectly, for global polyubiquitylation of chromatin-associated proteins during meiosis.

### 2.4.3 Impaired ubiquitylation of histone H2A in *UBR2*<sup>-/-</sup> spermatocytes

Chromatin remodeling during meiosis involves the functions of proteins that are recruited to and dissociated from the chromatin which, in turn, is associated with various proteinaceous complexes, such as nucleosomes and synaptonemal complexes. However, it has been rarely reported that, these proteins, except for histones, were extensively ubiquitylated on the chromatin. Histone H2A is the most abundant Ub substrate in mammals, and monoubiquitylated H2A (uH2A) has been shown to mark unsynapsed regions of meiotic chromosomes undergoing MSUC (Baarends et al., 2005), yet the Ub pathway mediating the H2A ubiquitylation during meiosis remains unknown. To determine the possible role of UBR2 in histone ubiquitylation, I stained uH2A on control and *UBR2*<sup>-/-</sup> spermatocytes. In control cells uH2A staining was first detected at late-zygotene mainly on unsynapsed axes and as foci-like signals in the chromatin (Fig. 8A). As spermatocytes enter pachytene, uH2A signals surged throughout the entire chromatin, with the highest level in the XY chromatin domain (Fig. 8B, 8C). Notably, uH2A showed striking similarity to UBR2 in temporal and spatial localization on meiotic chromosomes at zygotene and pachytene (Fig. 8 vs. Fig. 2). Moreover, the uH2A staining was drastically diminished in *UBR2*<sup>-/-</sup> spermatocytes (Fig. 8) throughout the entire meiotic stages, which was reproducibly observed in 154 nuclei from P16 testes. The down-regulation of uH2A in mutant spermatocytes prior to the onset of meiotic defects eliminates the possibility that H2A ubiquitylation is nonspecifically affected due to developmental arrest. These results suggest that monoubiquitylation of H2A during male meiosis requires, directly or indirectly, UBR2. Consistent with this finding, immunoblotting of acid-extracted histones revealed a reduced steady state level of uH2A, but not

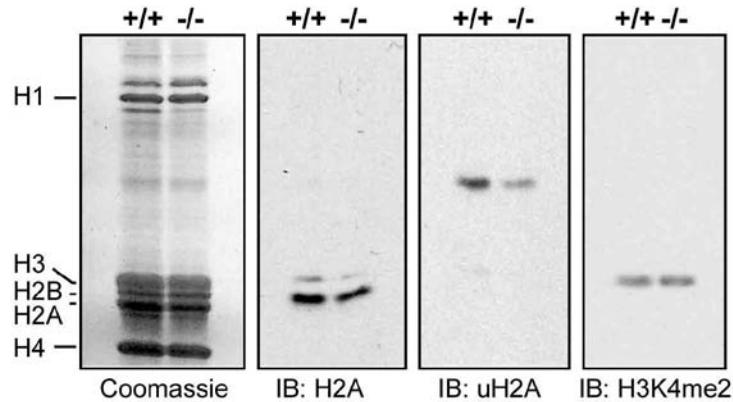


**Figure 9. Ubiquitylation of H2A in control and *UBR2*<sup>-/-</sup> testis.**

Coomassie staining and immunoblotting of acid-extracted histones from P19 wild type and *UBR2*<sup>-/-</sup> testes using antibodies indicated below.

of H2A, in P19 *UBR2*<sup>-/-</sup> testes compared to the littermate controls (Fig. 9). The significant but moderate difference of uH2A levels in two genotypes can be explained by the fact that testes contain a highly heterogeneous cell population. These results identify UBR2 as an E3 that mediates ubiquitylation of histone H2A in male meiosis.

#### 2.4.4 UBR2 and HR6B mediate H2A monoubiquitylation

HR6B (RAD6) facilitates the N-end rule-dependent proteolysis and interacts with recombinant UBR2 stably expressed in NIH3T3 cells (Kwon et al., 2003; Kwon et al., 2001). During spermatogenesis, HR6B localizes to meiotic chromatin and is involved in transcriptional silencing of the X and Y chromosomes (Baarends et al., 2007). *S. cerevisiae* RAD6, the homolog of HR6B, is an E2 of the N-end rule pathway (Dohmen et al., 1991) and mediates ubiquitylation of histone H2B to control chromatin condensation and gene silencing (Robzyk et al., 2000; Wood et al., 2003). To test the functional relationship between endogenous UBR2 and HR6B in the testis, the X-peptide pulldown technique was employed (Tasaki et al., 2005). The 12-mer

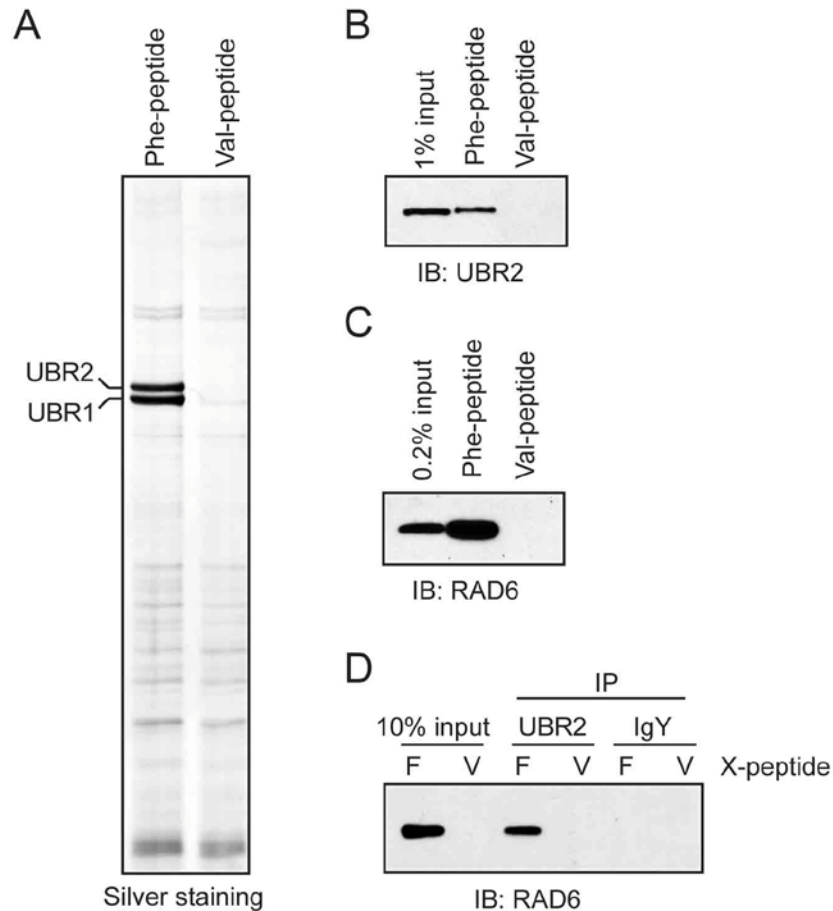


**Figure 10. Interaction of UBR2 and HR6B in testis.**

(A) Partial purification of endogenous UBR2 from rat testes using degron-bearing peptides (see Methods). (B-D) Endogenous UBR2 interacts with RAD6 in the testes. Protein samples prepared by Phe-peptide or Val-peptide were subjected to immunoblotting for UBR2 (B), RAD6 (C), and anti-UBR2 immunoprecipitation and anti-RAD6 immunoblotting (D). F, Phe-peptide; V, Val-peptide.

synthetic peptides bearing either N-terminal Phe (type-2 destabilizing) or Val (stabilizing) were synthesized and conjugated with beads, and bead-conjugated peptides were mixed with extracts from rat testes. Silver staining and immunoblotting analysis revealed the presence of UBR2 (as a mixture with UBR1) in precipitates prepared using Phe-peptide, but not Val-peptide (Fig. 10A, B). As expression analyses indicate that UBR1 and UBR2, respectively, are prominently expressed in spermatogonia and spermatocytes (Kwon et al., 2003) (data not shown), it is UBR2 that plays a major role in meiosis. Anti-RAD6 immunoblotting of precipitates indicated that RAD6 was co-purified by Phe-peptide but not by Val-peptide (Fig. 10C). Immunoprecipitation

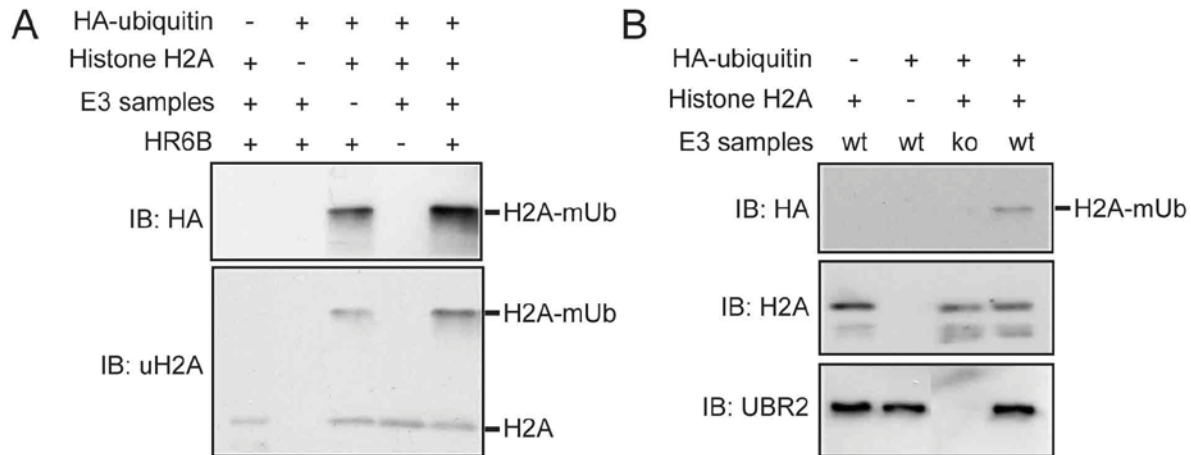


**Figure 11. *in vitro* ubiquitylation of histone H2A by UBR2-HR6B as an E3-E2 complex.**

(A) UBR2 and RAD6 cooperatively mediate monoubiquitylation of H2A. *In vitro* ubiquitylation reactions, containing purified H2A, HA-ubiquitin and HR6B, was performed in the presence or absence of E3 samples prepared from rat testes using Phe-peptide (see Methods). Reactions were subjected to immunoblotting for HA or uH2A. (B) Similar to (A) except that E3 samples were prepared from *+/+* and *UBR2<sup>-/-</sup>* mouse testes. Reactions were subjected to immunoblotting for HA, H2A, or UBR2.

of endogenous UBR2 from captured proteins brought down RAD6 (Fig. 10D). Together with previous findings, these results collectively suggest that UBR2 and HR6B form an E2-E3 complex that mediates histone ubiquitylation and chromatin inactivation during meiosis.

To directly determine the E2 and E3 activities of UBR2 and HR6B in ubiquitylation of histone H2A *in vitro*, affinity-pulldown technique that allows rapid purification of endogenous N-recognins was employed (see Methods). Using this technique, endogenous UBR2 was purified by ~1,000-fold from 5 g rat testes proteins, yielding ~100 µg UBR2 in 20% homogeneity. *In vitro* ubiquitylation assay with purified histone H2A revealed that human HR6B alone has the ability to facilitate monoubiquitylation of histone H2A, making it difficult to determine precisely the E3 activity of UBR2. Nonetheless, the addition of purified UBR2 significantly enhanced HR6B-dependent H2A ubiquitylation (Fig. 11A). To further characterize the E3 activity of UBR2, endogenous UBR2 was purified, in part as a complex with RAD6, from wild type and *UBR2<sup>-/-</sup>* testes using analogous techniques. Purified proteins, containing UBR2, from wild type

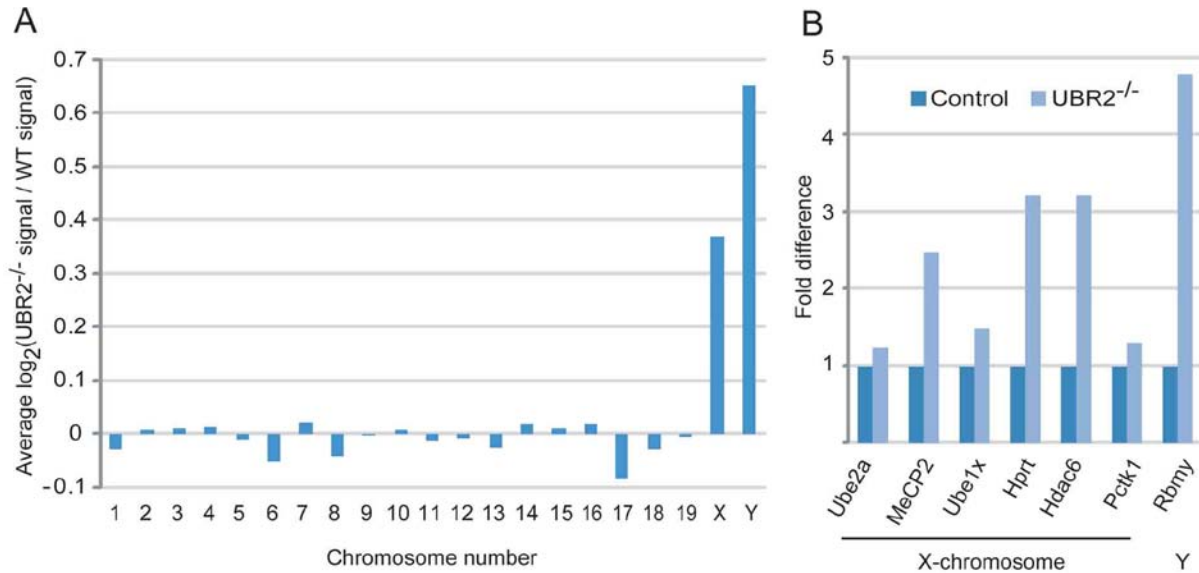


**Figure 12. Defective MSCI in *UBR2*<sup>-/-</sup> spermatocytes.**

(A) Microarray analysis of control and *UBR2*<sup>-/-</sup> testes at 16 dpp. (B) Real-time RT-PCR analysis of X- or Y-linked genes using control and *UBR2*<sup>-/-</sup> testes.

testes mediated monoubiquitylation of H2A and, moreover, this ubiquitylation activity was significantly reduced in reactions with samples from *UBR2*<sup>-/-</sup> testes (Fig. 11B). These results together suggest that UBR2 and HR6B cooperatively mediate the ubiquitylation of histone H2A during meiosis, likely in the context of meiotic chromatin (see Discussion).

#### 2.4.5 Impaired MSCI in *UBR2*<sup>-/-</sup> spermatocytes

It has been reported that ubiquitylation of histone H2A is associated with the repression of transcription in inactive X-chromosome of female, bivalent genes in ES cells, Polycomb, and Hox gene (Cao et al., 2005; de Napoles et al., 2004; Stock et al., 2007; Wang et al., 2004a). During meiotic prophase, uH2A is enriched in the sex body where transcription of genes linked to the XY chromosomes is silenced through a process called meiotic sex chromosome inactivation (MSCI) (Baarends et al., 1999; Turner, 2007). To examine whether MSCI is altered

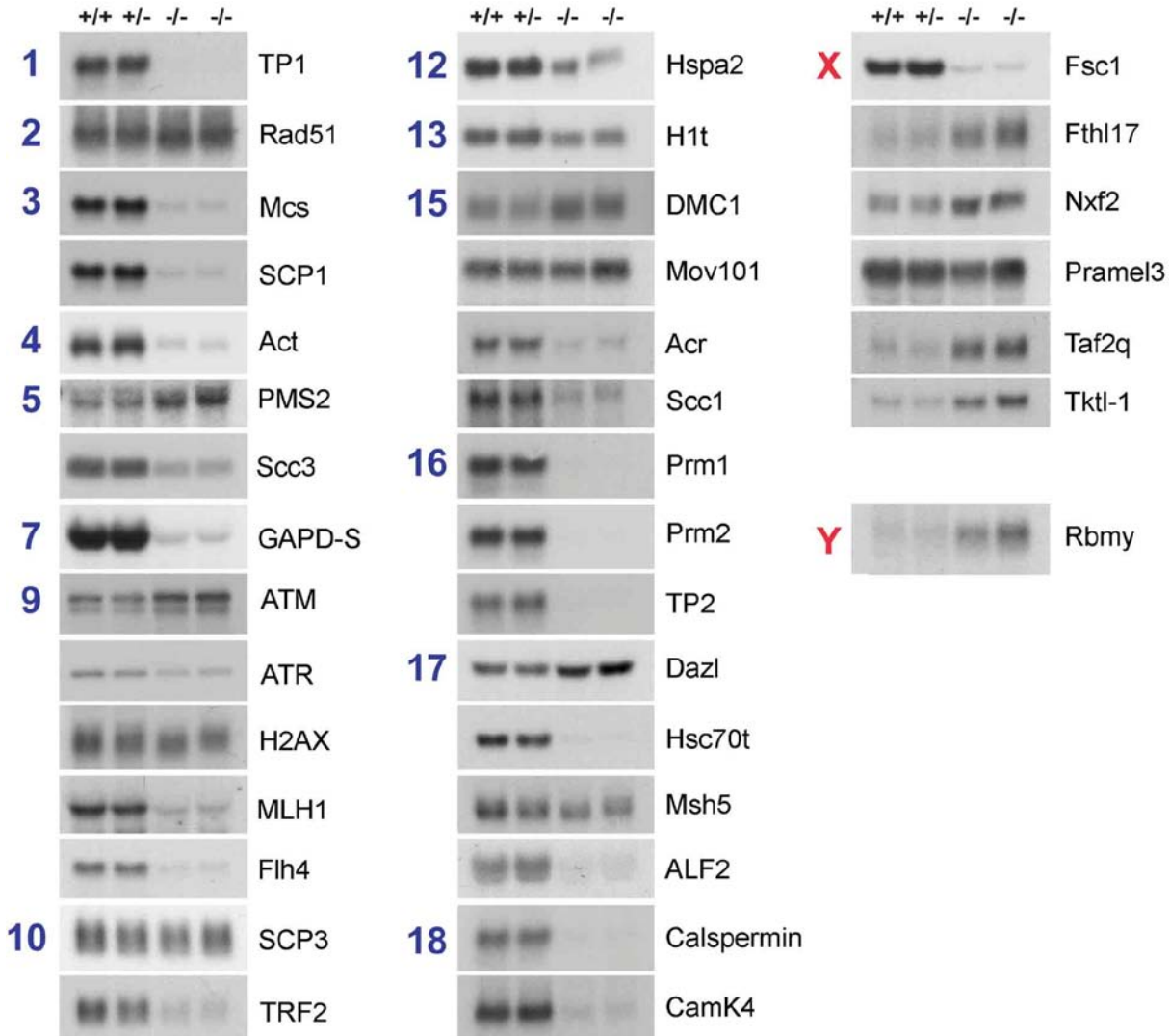


**Figure 13. Northern blot analysis of genes expression during spermatogenesis.**

Chromosome number (left) and gene name (right) are denoted. Probes were generated from 30 autosomal (blue)-, 7 XY (red)-linked genes.

in *UBR2*<sup>-/-</sup> testis, I performed microarray analysis. Since meiotic prophase of juvenile male mice is highly synchronous (Ashley, 2004) and spermatocytes of *UBR2*<sup>-/-</sup> mice were arrested around mid-pachytene stage, RNA was prepared from testis at 16 d.p.p. when most of spermatocytes are at early-pachytene (Goetz et al., 1984). The ratio of mean expression level of *UBR2*<sup>-/-</sup> to wild type in individual chromosome showed that the expression level of XY-linked genes was remarkably increased in *UBR2*<sup>-/-</sup> cells compared to wild type without significant changes in other

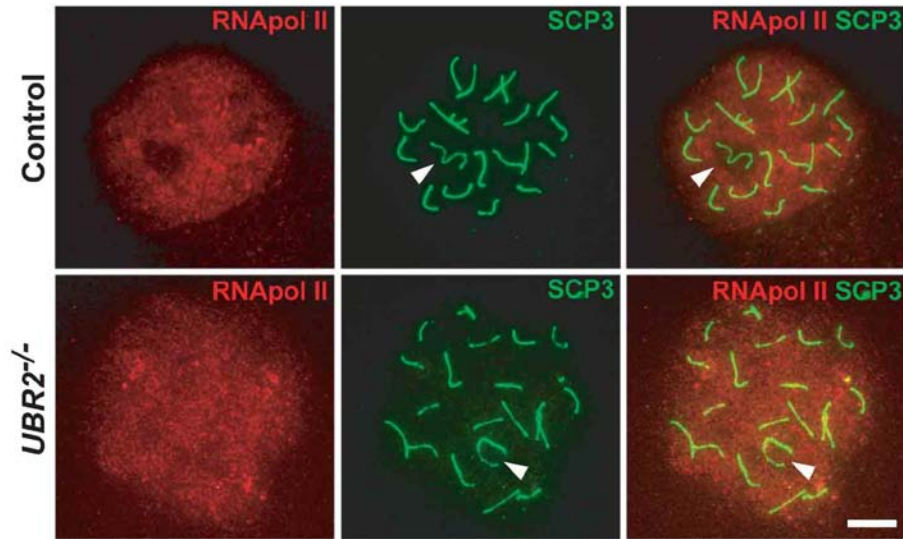


**Figure 14. Defective RNA polymerase II exclusion in *UBR2*<sup>-/-</sup> spermatocytes.**

The staining patterns of RNA polymerase II (red) and SCP3 (green) on spread chromosomes from control and *UBR2*<sup>-/-</sup> spermatocytes. Sex chromosomes are indicated by arrowheads. Scale bar: 10  $\mu$ m

autosomes (Fig. 12A). This result suggests that MSCI is impaired in *UBR2*<sup>-/-</sup> spermatocytes. To confirm defective MSCI in *UBR2*<sup>-/-</sup> testis, real-time RT-PCR was carried out with a set of XY-linked genes. The results consistently showed that the expression level of XY-linked genes was significantly increased in *UBR2*<sup>-/-</sup> cells (Fig. 12B). I further confirmed the MSCI defect in *UBR2*<sup>-/-</sup> testis using Northern analysis with probes generated from 37 genes expressed in testis (Cooke and Saunders, 2002; Dix et al., 1997; Wang et al., 2001; Zhang et al., 2001). Most of sex-linked genes were unregulated in *UBR2*<sup>-/-</sup> testes, however, genes in autosomal chromosomes showed either unchanged or decreased expression in *UBR2*-deficient cells, partly because they are components of cellular structures (e.g., SCP3) or exclusively post-meiotic (e.g., TP2), respectively (Fig. 13). Taken together, these results demonstrate that *UBR2* is required for the MSCI during spermatogenesis.

MSCI in pachytene spermatocytes is manifested by the exclusion of RNA polymerase II from the sex body and defective exclusion is coupled with impaired MSCI (Fernandez-Capetillo

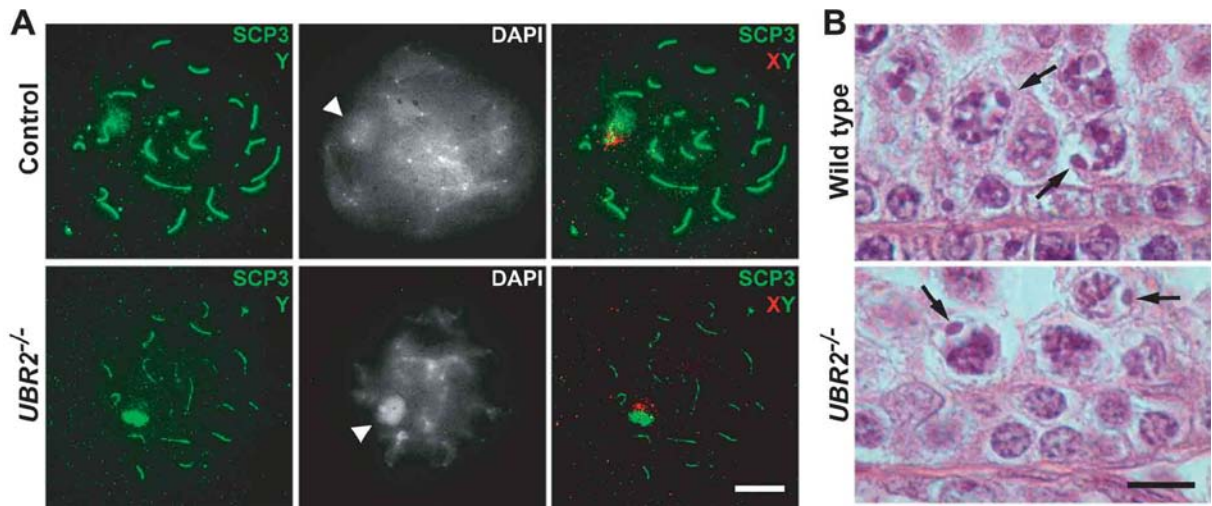


**Figure 15. XY synapsis and sex body formation in control and *UBR2*<sup>-/-</sup> spermatocytes.**

(A) FISH labeling of control and *UBR2*<sup>-/-</sup> spermatocytes with X (red) and Y (green) chromosome-specific probes, with SCP3 costaining (green). Dense peripheral DAPI staining indicates the sex body (arrowhead). (B) H&E staining of sections of seminiferous tubules from control and *UBR2*<sup>-/-</sup> testes. The XY bodies are indicated by arrows. Scale bar: 10  $\mu$ m

et al., 2003). Therefore, I examined whether the localization of RNA polymerase is altered in *UBR2*<sup>-/-</sup> pachytene spermatocytes by immunostaining. RNA polymerase II signal was excluded from the region covering sex chromosomes in control spermatocytes. By contrast, however, uniform distribution of signal was observed throughout *UBR2*<sup>-/-</sup> nucleus including sex chromosomes (Fig. 14). These results suggest that the failure of RNA polymerase II exclusion from sex body is involved in defective MSCI in *UBR2*<sup>-/-</sup> spermatocytes.

Disruption of either *BRCA1* or *H2AX* in mice results in not only impaired MSCI but also defective XY body formation (Fernandez-Capetillo et al., 2003; Turner et al., 2004). In pachytene spermatocytes, X-Y chromosomes, which lacks homologous region, are partially synapsed at pseudoautosomal region (PAR) and secluded from autosomes by forming condensed heterochromatin structure called sex body. To examine if XY synapsis and the formation of the sex body were affected in *UBR2*<sup>-/-</sup> spermatocytes, I applied immunostaining combined with

fluorescence *in situ* hybridization (FISH) using labeled probes recognizing either X or Y chromosome. In wild type and *UBR2*<sup>-/-</sup> pachytene spermatocytes, X and Y chromosomes were localized together in the sex body indicated by a dense DAPI staining (Fig. 15A). Moreover, hematoxylin and eosin (H&E) stained sections of seminiferous tubules from 4 weeks-old wild type and *UBR2*<sup>-/-</sup> mice revealed that the majority of *UBR2*<sup>-/-</sup> spermatocytes contained distinct sex bodies at the nuclear periphery (Fig. 15B). Thus, these results suggest that UBR2 is dispensable for the X-Y synapsis and the formation of sex body.

#### **2.4.6 Co-localization of UBR2 with ATR/BRCA in MSCI**

Transcriptional silencing of the X and Y chromosomes is associated with histone modifications such as phosphorylation and ubiquitylation. Recent studies revealed that MSCI requires a histone phosphorylation pathway comprising the tumor suppressor BRCA1, the PI3-like kinase ATR and the histone H2AX (Turner, 2007). Surprisingly, distinctive localizations of UBR2 signal on AEs of unsynapsed and sex chromosomes show coinciding localizations of BRCA1 and ATR1 in zygotene and pachytene spermatocytes. BRCA1 and ATR are co-localized on AEs of unsynapsed and sex chromosomes, where BRCA1 is required for the localization of ATR (Turner et al., 2004; Turner et al., 2005). I therefore examined whether UBR2 is colocalized with BRCA1 and/or ATR by immunostaining. UBR2 and BRCA1 signals were overlapped on most unsynapsed autosomes and XY chromosomes (Fig. 16A-C). UBR2 and ATR signals were also overlapped in the regions abovementioned besides ATR localization on sex chromatin (Fig. 16D-F). Intriguingly, while UBR2 signal marked most of unsynapsed AEs, however, it wasn't detected near synaptic fork, a junction between synapsed and unsynapsed AEs (Fig. 16B, E). On the contrary, BRCA1 and ATR signals were found on synaptic forks but absent from the distal

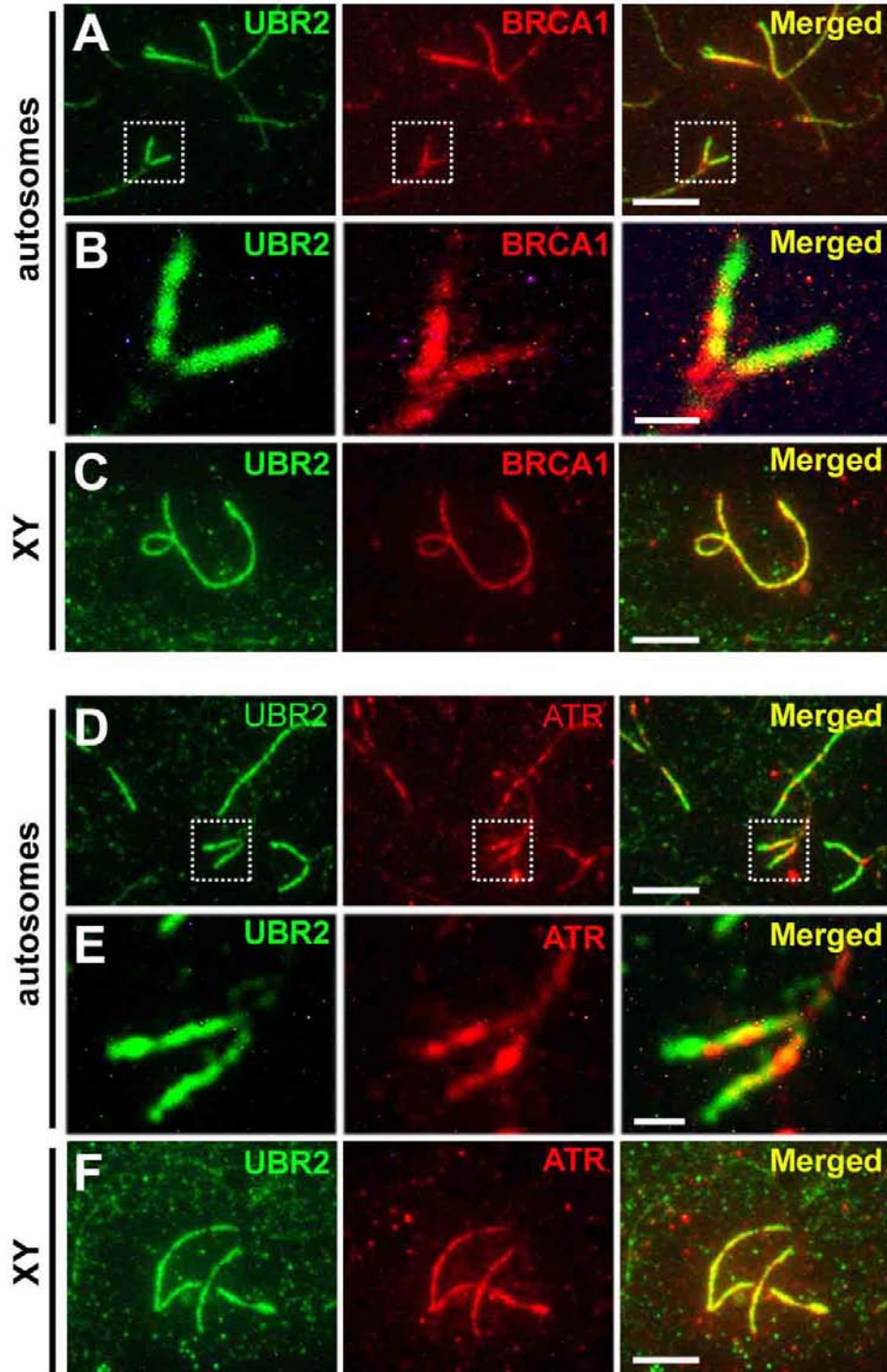


**Figure 16. Co-localization of UBR2 with BRCA1 and ATR on meiotic chromosomes.**

(A, C) Localization of UBR2 (green) and BRCA1 (red) on unsynapsed axes of the autosomes at zygotene (A) and the sex chromosomes at pachytene (C). (B) Enlarged images for chromosomal regions indicated by the insets in (A). (D, F) Localization of UBR2 (green) and ATR (red) on unsynapsed axes of the autosomes at zygotene (D) and the sex chromosomes at pachytene (F). (E) Enlarged images for chromosomal regions indicated by the insets in (A). Scale bars: (A, C, D, F) 5  $\mu\text{m}$ ; (B, E) 1  $\mu\text{m}$

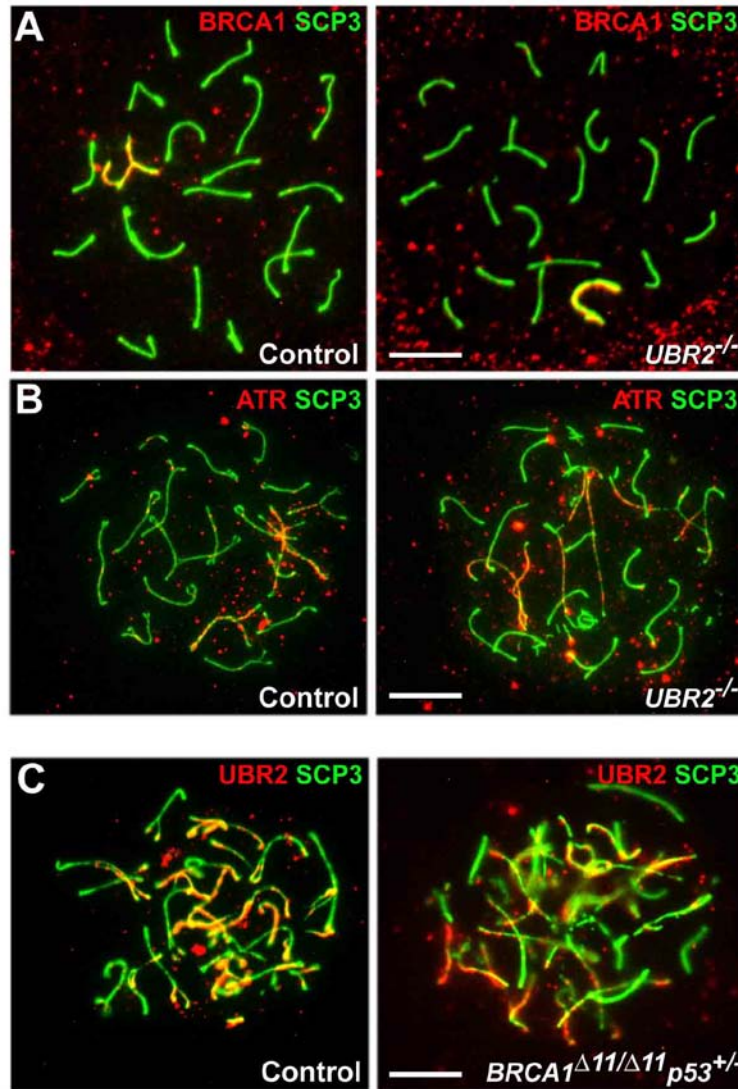


**Figure 17. Mutual independent function between UBR2 and BRCA1/ATR.**

(G, H) BRCA1 (G) and ATR (H) localizations on the meiotic chromosomes are not significantly altered in *UBR2*<sup>-/-</sup> spermatocytes. (I) UBR2 localization on meiotic chromosomes is not significantly altered in *Brca1*<sup>Δ11/Δ11</sup>*p53*<sup>+/-</sup> zygotene spermatocytes. Scale bars: 10 μm

regions of unsynapsed AEs (Fig. 16B, E). This suggests that the repression of transcription in meiosis may be governed by different mechanisms such as phosphorylation and ubiquitylation.

Next, to see if there is a functional implication between these molecules, I examined the localization of BRCA1 and ATR in *UBR2*<sup>-/-</sup> spermatocytes by immunostaining. Neither BRCA1 nor ATR localization was significantly altered in *UBR2*<sup>-/-</sup> pachytene nuclei compared to control

(Fig. 17A, B). Likewise, the localization of UBR2 was not affected in *Brcal<sup>Δ11/Δ11</sup>p53<sup>+/-</sup>* spermatocytes (Fig. 17C). Co-immunoprecipitation using antibodies for UBR2, BRCA1 and ATR, failed to detect the interaction (data not shown). These results collectively indicate that the functions of UBR2 and BRCA1 in transcriptional silencing are largely independent from each other.

## 2.5 DISCUSSION

In this project, I show that UBR2, the recognition E3 component of the N-end rule pathway, marks unsynapsed regions of meiotic chromosomes undergoing transcriptional silencing and that *UBR2<sup>-/-</sup>* spermatocytes are impaired in transcriptional silencing of the XY-linked genes. Similar staining patterns of uH2A and UBR2 correlate to the downregulation of uH2A on UBR2-deficient meiotic chromosomes. UBR2 forms an E2-E3 complex with HR6B and accelerates HR6B-dependent monoubiquitylation of H2A. The spatiotemporal distribution of UBR2 on meiotic chromosomes correlates to that of BRCA1 that marks the unpaired axes to histone phosphorylation and thereby transcriptional silencing; nonetheless, their localizations are mutually independent.

It is increasingly clear that transcriptional silencing of the X and Y chromosomes is part of a more general mechanism, MSUC, where all unpaired meiotic chromosomal segments are silenced as part of a checkpoint that senses inappropriately exposed DNA regions and eliminate germ cells undergoing impaired synapsis (Turner, 2007). In *Neurospora crassa* and *Caenorhabditis elegans* there is a similar but mechanistically distinct chromatin inactivation process called meiotic silencing by unpaired DNA (MSUD) where the presence of an unpaired

DNA segment during meiosis inactivates all homologous DNA segments (reviewed in Turner, 2007). In addition to male germ cells where the X and Y chromosomes are inactivated through MSCI, female somatic cells utilize another mechanism to inactivate one of two X chromosomes. Recent studies revealed that these processes are regulated by significantly overlapping molecular mechanisms. For example, the X-inactive transcript (Xist) is indispensable for female X inactivation (Csankovszki et al., 1999), yet Xist knockout has limited impact on spermatogenesis and XY body formation (McCarrey et al., 2002). On the other hand, BRCA1 and uH2A have been implicated in not only MSCI and MSUC but also female X chromosome inactivation (Baarends et al., 2005; Turner et al., 2005). Thus, it is parsimonious to speculate that UBR2 may participate in MSUC as well as MSCI. Some *UBR2*<sup>-/-</sup> female mice die throughout development without terminal phenotypes, indicative of cellular failure rather than organ defects, yet the mechanism underlying female-specific lethality remains elusive (Kwon et al., 2003). UBR2 localization to the MSCI- and MSUC-specific axial regions raises an intriguing possibility that UBR2-dependent ubiquitylation may participate in X inactivation in female somatic cells at certain developmental stages, a process critical for female development and survival.

The results suggest that UBR2 and HR6B form an E2-E3 complex to cooperatively mediate monoubiquitylation of H2A during meiosis. HR6B accumulates on the XY chromatin domain during pachytene and is required for the maintenance of transcriptional silencing of X- and Y-linked genes (Baarends et al., 2007). Consistent with the chromosomal localization of HR6B, HR6B-deficient male mice are infertile associated with meiotic and postmeiotic defects (Baarends et al., 2003; Roest et al., 1996). *S. cerevisiae* RAD6 participates in the N-end rule pathway, meiosis, and DNA repair (Dohmen et al., 1991; Robzyk et al., 2000). In addition, the yeast E2 mediates monoubiquitylation of histone H2B, with help from the Ub ligase Bre1, to

control gene silencing (Robzyk et al., 2000; Wood et al., 2003). Thus, this E2-E3 system has an evolutionarily conserved function not only in the N-end rule-dependent proteolysis but in nonproteolytic monoubiquitylation of histones. It has been shown that, in certain somatic cells, the Polycomb repressor complexes (PRC) mediate H2A monoubiquitylation (Cao et al., 2005; de Napoles et al., 2004). However, their function may not be generally applicable to the XY body of spermatocytes, as one study reported that the components of this E3 complex are excluded from this subnuclear region during pachytene (Takada et al., 2007). These results together suggest that histone ubiquitylation is controlled by tissue/cell type-specific E3 systems in mammals, and it may be UBR2, rather than the Polycomb E3 complex, that mediates H2A ubiquitylation in male meiosis. Perhaps owing to the presence of the PRC E3 complexes, I was not able to detect UBR2-specific H2A ubiquitylation using H2A overexpressed in +/+ and *UBR2*<sup>-/-</sup> mouse embryonic fibroblasts (MEFs) (data not shown).

UBR2 accumulates on the XY axes but not in the XY chromatin domain (Figure 1D and 1E), whereas RAD6/HR6B and H2A localize to the entire XY chromatin (Baarends et al., 2005). Analogously, BRCA1 is recruited to the XY axes, while ATR spreads throughout the XY chromatin (Turner et al., 2004). This localization pattern is consistent with a model where HR6B on the XY chromatin is activated by long-distance chromatin interaction with UBR2 on the axial elements. Ub ligases with the HECT ubiquitylation domain form thioester intermediates with Ub, which is then transferred to target proteins that are bound to the E3. By contrast, Ub is directly transferred from an E2 to the substrate in E3 ligases with RING-finger. It is after all HR6B that carries and transfers Ub to the substrate. Taken together, it is speculated that UBR2 functions as a scaffolding protein on the axial element where it interacts with HR6B, an essential event for histone ubiquitylation. Proliferating cell nuclear antigen (PCNA) plays an essential role in

chromatin function as a component of the replication and repair machinery through its activity on DNA, which allows rapid moving of the machinery through chromatin. The repair of DNA lesions during replication is initiated in part through damage-induced monoubiquitylation of PCNA by the E2-E3 complex, composed of RAD6 and RAD18, which promotes translesion synthesis (Fu et al., 2008). Perhaps, histone ubiquitylation and phosphorylation during meiosis may utilize an analogous, PCNA-like processivity factor that allows HR6B and ATR to rapidly move through the XY chromatin. Although UBR2 and BRCA1 show several analogies in their functions during meiosis, including co-localization on inactive chromosomal axes, null phenotypes in MSCI and meiotic DNA repair (Ouyang et al., 2006; Xu et al., 2003), the accumulation of UBR2 and BRCA1 on meiotic chromatin is mutually independent (Figure 3). In addition, although  $\gamma$ H2AX formation is known to be essential for MSCI (Fernandez-Capetillo et al., 2003), these data show that it is not sufficient, and UBR2 and H2A ubiquitylation are equally important to achieve silencing. Thus, the two RING-finger proteins may represent two parallel pathways that mediate ubiquitylation and phosphorylation as part of histone modification systems controlling inactivation of unpaired meiotic chromosomes.

UBR2 has been known as the major recognition E3 component of the N-end rule pathway. As such, it is counterintuitive that UBR2 mediates nonproteolytic monoubiquitylation on meiotic chromatin. The physiological meaning of these findings in the context of the N-end rule-dependent proteolysis is yet to be investigated.

### **3.0 THE ROLE OF UBR2 IN DNA DAMAGE RESPONSE THROUGH HISTONE MODIFICATIONS**

#### **3.1 SUMMARY**

DNA damage response (DDR) constitutes cascades of signal transduction and is required for cellular homeostasis and genomic integrity. Ubiquitin plays a crucial role in signal transduction yet its role in DDR just has emerged. In this project, to characterize the role of UBR2, I examined the DDR pathway in germ cells and somatic cells. UBR2 is required for the repair of double strand breaks (DSBs) induced by SPO11, a meiotic topoisomerase, during spermatogenesis. Recruitment of proteins involved in early phase of DSB repair such as Rad51, RPA1 and FANCD2 is normal but significant reduced in *UBR2*<sup>-/-</sup> spermatocytes. UBR2 is also required for the formation of crossover between homologous chromosomes but its recruitment is independent from SPO11-induced DSBs. In somatic cells, UBR2 is exclusively associated with non-heterochromatin throughout nucleus and responds to genotoxic stress via post-translational modification. UBR2 is required for the ubiquitylation induced by DNA damage response (DDR). Moreover, histone modifications involved in DDR pathway are altered in UBR2-deficient cells including impaired ubiquitylation of H2A, methylation of H3 and phosphorylation of H2AX. *UBR2*<sup>-/-</sup> mouse embryonic fibroblasts (MEFs) show increased vulnerability to the genotoxic agents and aberrations of chromosomes compared to wild type. Taken together, it suggests that

UBR2 is involved in histone modifications and is required for the ubiquitylation of DDR pathway presumably for the maintenance of genomic integrity.

### 3.2 BACKGROUND

To maintain genomic integrity, eukaryotic cells are equipped with various mechanisms by which DNA lesion is repaired in efficient manner. Defective repair mechanisms of DNA damage have been associated with various human diseases as well as the initiation of tumorigenesis (Lobrich and Jeggo, 2007; McKinnon and Caldecott, 2007). The cascades of the signal transduction pathways constitute a proper DNA damage response (DDR) to protect the integrity of genome. A set of phosphatidyl inositol 3-kinases (PI-3 kinases), ataxia telangiectasia mutated (ATM) and ataxia telangiectasia and RAD3-related (ATR) play an initiative role in the pathways by activating multiple proteins involved in the signal transduction of checkpoints (Cimprich and Cortez, 2008; Shiloh, 2003). Among the initial steps of DDR pathways, H2AX, one of the histone H2A variants, is phosphorylated on Ser-139 by the PI-3 kinases at the DNA damage sites (Rogakou et al., 1999). Thus,  $\gamma$ H2AX, a phosphorylated H2AX, not only marks DNA damage sites as a molecular beacon but also provides a platform to recruit multiple factors in the repair pathways such as RPA, Rad51, and FANCD2 (Bogliolo et al., 2007; Stucki and Jackson, 2006).

Ubiquitylation has been emerging as a crucial protein post-translational modification in addition to phosphorylation in the signal transduction of DDR pathways. Fanconi Anemia (FA) is an autosomal recessive syndrome characterized by cancer susceptibility and FA cells show increased sensitivity to DNA cross-linking agent. FANCD2 and FANCI, two components of FA complex, are ubiquitylated and localized to chromatin upon DNA damage for the repair (Wang

et al., 2004b; Smogorzewska et al., 2007). Proliferating cell nuclear antigen (PCNA) plays an essential role as a component of the replication and repair machinery. Monoubiquitylation of PCNA by an E2-E3 complex, RAD6 and RAD18, is implicated in the repair of DNA lesions during replication (Fu et al., 2008). Among ubiquitylation induced by DNA damage, various histones are ubiquitylated in DDR pathway, presumably for the chromatin remodeling. Histone H2A is ubiquitylated by E3 ligases, Ring2 and RNF8, upon UV irradiation and ionizing radiation (IR), respectively (Bergink et al., 2006; Mailand et al., 2007). RNF8 also ubiquitylates histone H2AX (Huen et al., 2007; Mailand et al., 2007). Similarly, ubiquitylation of histone H3 and H4 is mediated by E3 ligase complex, CUL4-DDB-ROC1, upon UV irradiation (Wang et al., 2006). Moreover, ubiquitylation and histone H2B is required for the DNA damage checkpoint response (Giannattasio et al., 2005).

Here I show that UBR2 is required for the maintenance of genomic integrity by responding DNA damage through histone modifications.

### **3.3 METHODS**

#### **3.3.1 Immunofluorescence microscopy**

Immunofluorescence staining on surface-spread spermatocytes was carried out as described previously (see METHODS 2.3.2). For the immunostaining of cultured cells, cells grown on cover glasses were briefly washed in PBS, fixed in freshly prepared 2% (or 4%) paraformaldehyde in PBS for 15 min at RT, and then washed in PBS with 0.1% Triton X-100 (PBT). Cells were incubated with antibodies in blocking solution (10% heat-inactivated goat

serum in PBT) and washed in PBT. VECTASHIELD containing DAPI (Vector laboratories) was used for mounting and counterstaining.

### **3.3.2 Cell culture and Genotoxic stress**

Mouse embryonic fibroblasts (MEFs), U2OS cells (human osteosarcoma) and HeLa cells were grown in DMEM (Invitrogen) supplemented with 10% FBS (Hyclone), 2 mM L-glutamine (Invitrogen) and 1% penicillin-streptomycin (Invitrogen). For mitomycin C (MMC) (Sigma) treatment, cells were incubated with final concentration of 0.1 µg/ml in medium for 24 h. Media were replaced with PBS for UV irradiation. Cells were irradiated at 20 J/m<sup>2</sup> with UV crosslinker (Stratagene), incubated in culture media, and processed for immunostaining as described above.

### **3.3.3 Fractionation of cell extracts and immunoblotting**

Cells were resuspended in buffer A (10mM HEPES, pH 7.6, 10 mM KCl, 1.5 mM MgCl<sub>2</sub>, 1 mM DTT) with protease inhibitors mix (Sigma) and disrupted with the Dounce homogenizer (Kontes) on ice, followed by centrifugation at 2000g for 10 min at 4°C. Supernatant was collected as a cytosolic fraction. Pellet was resuspended with buffer B (10mM HEPES, pH 7.6, 400 mM NaCl, 1mM MgCl<sub>2</sub>, 1 mM DTT, 1mM EDTA, 10% Glycerol with protease inhibitors mix (Sigma)), incubated on ice for 30 min, and then centrifuged at max speed for 15 min at 4°C. Supernatant was collected as a nuclear fraction. Pellet was incubated with micrococcal nuclease for 15 min at RT and collected as a chromatin-bound fraction. Proteins were separated by SDS-PAGE and subjected to immunoblotting using antibodies for UBR2 (5-1) and histone H3K79me2 (Abcam).

### 3.3.4 RNA interference and real-time RT-PCR

Pre-designed *Silencer*<sup>®</sup> Select siRNA (Ambion) for UBR2 was used to the following sequences: sense, 5'- CAACUACAGUAGAUCGAGATT-3'; antisense, 5'- UCUCGAUCUACUGUAGUUGCA-3'. 25 nM of siRNA was transfected into U2OS cells using Lipofectamine<sup>™</sup> LTX with Plus<sup>™</sup> reagent (all Invitrogen) according to manufacturer's instruction. siRNA for GAPDH and negative control (Ambion) were used as controls. Real-time RT-PCR was carried out as previously described (METHODS 2.3.5).

### 3.3.5 *in vivo* ubiquitylation assay

Full-length histone H2A tagged with the flag at N-terminal was constructed. Ubiquitin tagged with the HA at N-terminal was co-transfected with H2A into U2OS cells using Lipofectamine<sup>™</sup> 2000 (Invitrogen) in accordance with manufacturer's instruction. Next day, siRNA for either UBR2 or negative control was transfected as described above. On the second day, cells were UV-irradiated as described above, incubated for 2 h, and lysed in IP buffer (50 mM Tris pH 8.0, 150 mM NaCl, 0.1% SDS, 0.5% Sodium deoxycholate, 1% NP-40) with protease inhibitors mix (Sigma). Lysates were sonicated for the fragmentation of chromatin and centrifuged at max speed for 15 min at 4°C. For immunoprecipitation (IP), supernatant were incubated with anti-flag antibody conjugated with agarose beads (Sigma) for O/N at 4°C. Flag immunoprecipitants were separated by SDS-PAGE and analyzed by immunoblotting using antibodies for flag and HA (all Sigma).

### **3.3.6 Cell survivality by MTT assay**

$1-2 \times 10^4$  of wild type and *UBR2*<sup>-/-</sup> MEF cells were plated onto 96-well plates. Next day, cells are treated with various concentrations of doxorubicin, hydroxyurea (HU) and methyl methanesulfonate (MMS) (all Sigma). After 3 days, MTT (3-(4,5-dimethylthiazol-2-yl)2,5-diphenyl tetrazolium bromide, Sigma) was added to a concentration of final 0.5 mg/ml, followed by 5h incubation. Media was removed and 150  $\mu$ L of DMSO was added to each well, followed by incubation at 37°C for 5 min. Absorbance was measured at 550 nm. All samples were triplicated.

### **3.3.7 Metaphase chromosome spread from MEFs**

Exponentially growing MEFs were treated with 1  $\mu$ g/ml Colcemid (Invitorgen) for 1 h and washed in PBS. Cells were incubated in 0.56% KCl for 1 h at 37°C and pelleted at 1,200 rpm for 8 min. Nuclei were resuspended with the fixative (25% glacial acetic acid in methyl ethanol) and centrifuged at 6,800 rpm for 1 min, three times. Pellets were resuspended with fresh fixative and chromosome spreads were prepared as previously described (Henegariu et al., 2001).

## 3.4 RESULTS

### 3.4.1 Unresolved meiotic DSBs in *UBR2*-deficient spermatocytes

During meiosis, intrinsic DSBs are generated by SPO11, a topoisomerase-related protein, which is required for pairing, exchange, and the separation between homologous chromosomes (Romanienko and Camerini-Otero, 2000).  $\gamma$ H2AX, a phosphorylated H2AX, marks DSB sites induced by SPO11 during meiosis as well as by genotoxic stress such as ionizing radiation (IR) in cell culture (Mahadevaiah et al., 2001; Rogakou et al., 1999). In addition,  $\gamma$ H2AX is the earliest known marker of the XY body formation during late zygotene/early pachytene. To determine whether meiotic DSB repair is affected in *UBR2*<sup>-/-</sup> spermatocytes, I immunostained spermatocytes with antibody recognizing  $\gamma$ H2AX. In wild type spermatocytes,  $\gamma$ H2AX signal appeared as distinct foci at leptotene and became gradually prominent in the XY body at late zygotene, resulting in almost exclusive localization to the XY body by mid-pachytene (Fig. 18A, C, E, G). In *UBR2*<sup>-/-</sup> cells, the formation and pattern of  $\gamma$ H2AX foci were normal at leptotene through zygotene (Fig. 18B, D). In pachytene spermatocytes,  $\gamma$ H2AX was increased on the XY body as in controls (Fig. 18F), but, highly disorganized  $\gamma$ H2AX staining remained on various regions of autosomal chromosomes (Fig. 18H). Thus these results indicate that *UBR2* is required for the repair of DSBs during meiotic prophase.

### 3.4.2 The recruitment of proteins in meiotic recombination

Meiotic DSBs induced by SPO11 trigger sequential recruitments of recombination proteins such as RAD51, RPA1 and FANCD2 to the lesions (Garcia-Higuera et al., 2001; Moens et al., 2002;

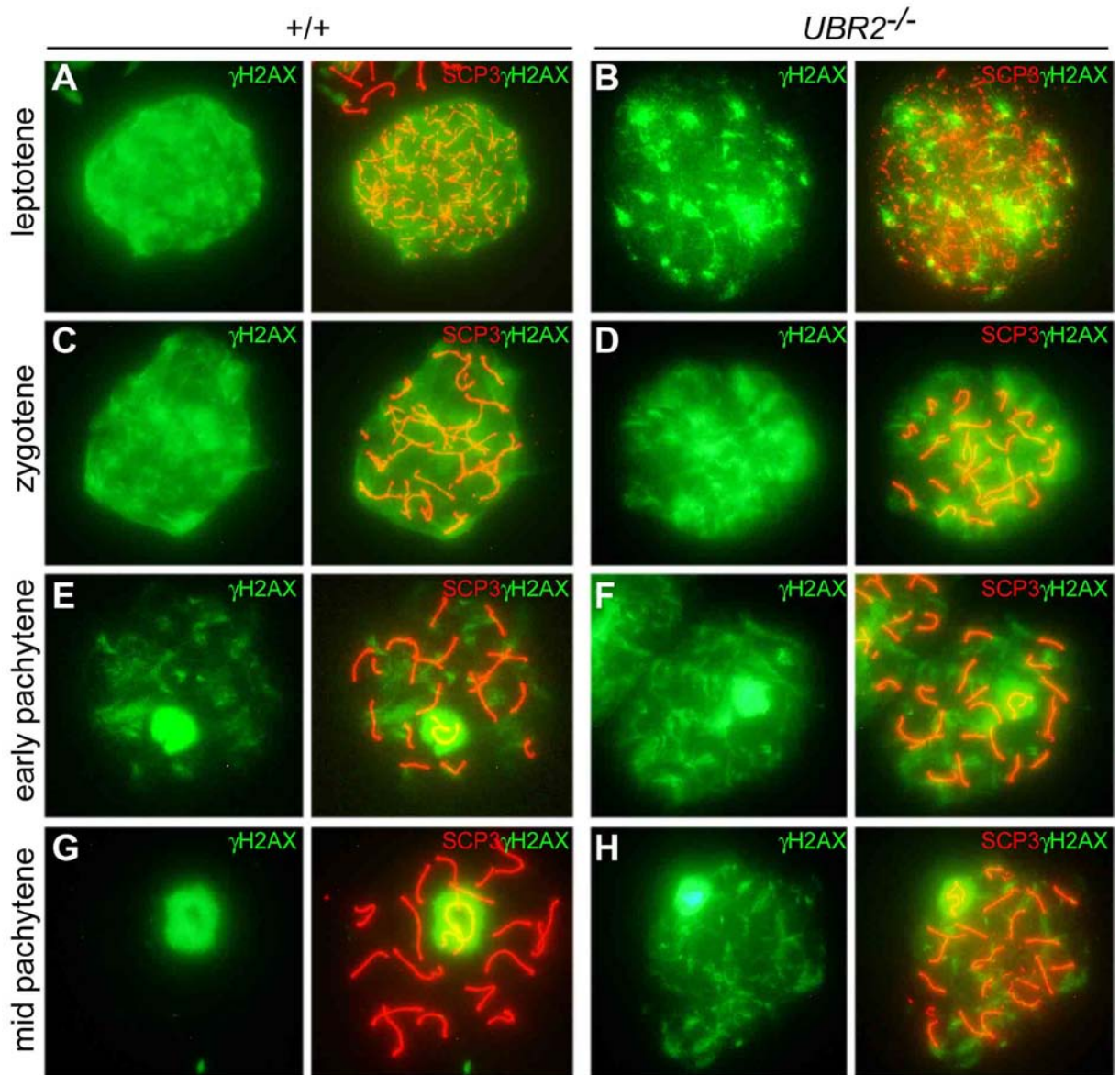


**Figure 18. Defective resolution of meiotic DSBs in *UBR2*<sup>-/-</sup> spermatocytes.**

Wild type (A, C, E, G) and *UBR2*<sup>-/-</sup> (B, D, F, H) spermatocytes were stained with  $\gamma$ H2AX (green) and SCP3 (red). (A, B) Leptotene, (C, D) Zygotene, (E, F) Early pachytene, (G, H) Mid pachytene.

Romanienko and Camerini-Otero, 2000). The number of RAD51 and FANCD2 foci in *UBR2*<sup>-/-</sup> spermatocytes was comparable to that of wild type from leptotene through zygotene, yet showed moderately reduced foci at pachytene (Fig. 19A, B). Likewise, *UBR2*<sup>-/-</sup> spermatocytes at zygotene through early pachytene showed normal recruitment of RPA along the AEs yet with reduced foci (Fig. 19C, D). Thus, UBR2 is dispensable for early events of homologous recombination (HR). Repair of meiotic DSBs by HR is required for the formation of crossover which is marked by MLH1, one of the mismatch repair proteins (Baker et al., 1996). Whereas MLH1 signal formed one or two distinct spots per autosomal axis in wild type spermatocytes at mid-pachytene, this was not observed in most of mid-pachytene-like *UBR2*<sup>-/-</sup> cells (Fig. 20), consistent with the prolonged  $\gamma$ H2AX foci in mutant cells. Collectively, these results indicate that UBR2 is involved in a meiotic HR pathway to resolve DSBs.

Recruitment of proteins involved in early recombination and repair proteins such as RAD51 is disrupted in *SPO11*<sup>-/-</sup> spermatocytes (Romanienko and Camerini-Otero, 2000). To determine whether UBR2 localization on AEs is DSB-dependent, I immunostained UBR2 on spread chromosomes of *SPO11*<sup>-/-</sup> spermatocytes. UBR2 localization on AEs was not significantly affected in early *SPO11*<sup>-/-</sup> spermatocytes (Fig. 21), which suggests that UBR2 has another role in early spermatocytes. Given that incomplete synapsis between homologous chromosomes was increased in *UBR2*<sup>-/-</sup> pachytene spermatocytes (data not shown), DSB-independent UBR2 localization on AEs may suggest a role of UBR2 in the synapsis of homologous chromosomes.

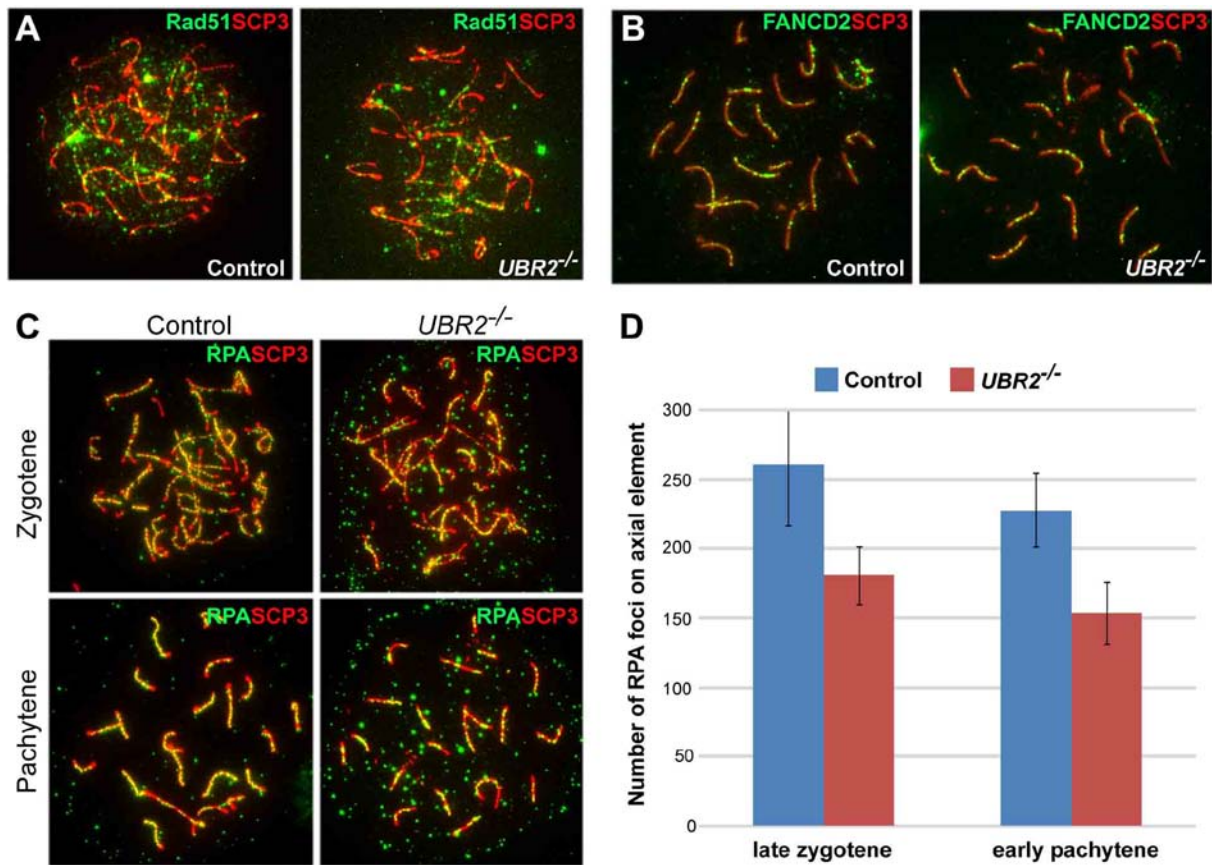


**Figure 19. Recruitment of recombination proteins in control and *UBR2*<sup>-/-</sup> spermatocytes.** SCP3 (red) was co-stained. (A) Rad51 (green) in pachytene, (B) FANCD2 (green) in pachytene, (C) RPA1 (green) in zygotene and pachytene spermatocytes. (D) Comparison of number of RPA foci on axial elements in control and *UBR2*<sup>-/-</sup> nuclei.

### 3.4.3 Intracellular localization of UBR2 in somatic cells

Proteins involved in meiotic recombination during spermatogenesis were also found in common DDR pathway such as homologous recombination (HR) upon DNA damage by ionizing radiation (IR) (Burgoyne et al., 2007). Hence, it is conceivable that UBR2 is also implicated in the DDR pathways in somatic cells. To understand the role of UBR2 in somatic DDR pathway, I examined the intracellular localization of UBR2 in MEFs by immunofluorescence analysis.

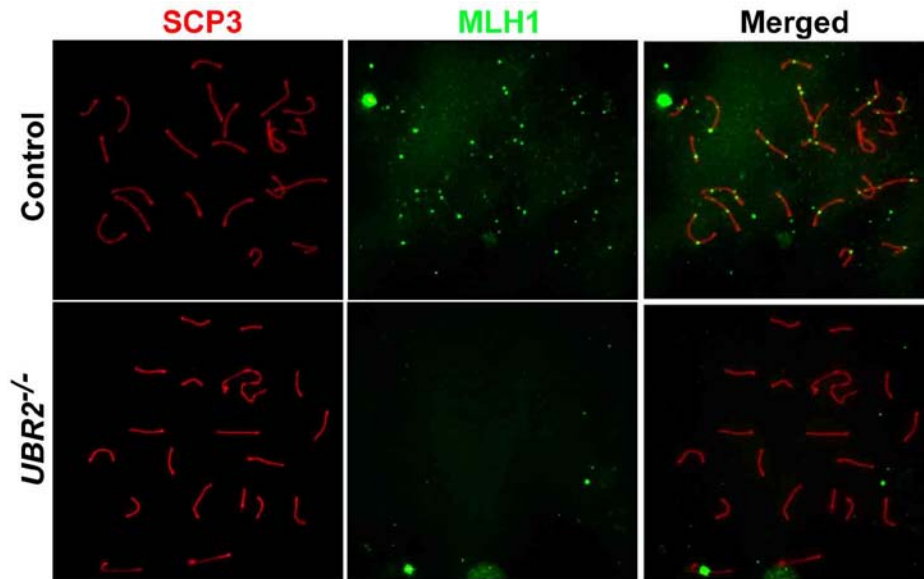


**Figure 20. Impaired crossover formation in *UBR2*<sup>-/-</sup> spermatocytes.**  
Mid pachytene spermatocytes from control and *UBR2*<sup>-/-</sup> were stained with MLH1 (green) and SCP3 (red).

Consistent with the meiotic chromatin localization, widely dispersed UBR2 staining was detected throughout nucleus with sporadic exclusions (Fig. 22A). The regions devoid of UBR2 were co-localized with heterochromatin, indicated by dense DAPI staining, which was often implicated in transcriptional inactivation. In addition to nuclear localization, scattered UBR2 signals were observed in the cytoplasm yet with reduced intensity compared nucleus. To exclude the possibility that intracellular localization of signal may be due to non-specific binding of UBR2 antibody, peptides which had been used to raise antibody earlier were co-incubated with antibody. Disappearance of the signal upon co-incubation with peptides verified that UBR2 localizes on both non-heterochromatin of nucleus and cytoplasm in somatic cells.

To further investigate the nature of UBR2 localization, MEF lysates were biochemically separated into cytoplasmic, soluble nuclear and chromatin-bound fractions and UBR2 was detected by immunoblotting. Consistent with immunostaining results, UBR2 was detected both in cytoplasm and nucleus. Intriguingly, nuclear UBR2 was almost exclusively chromatin-bound

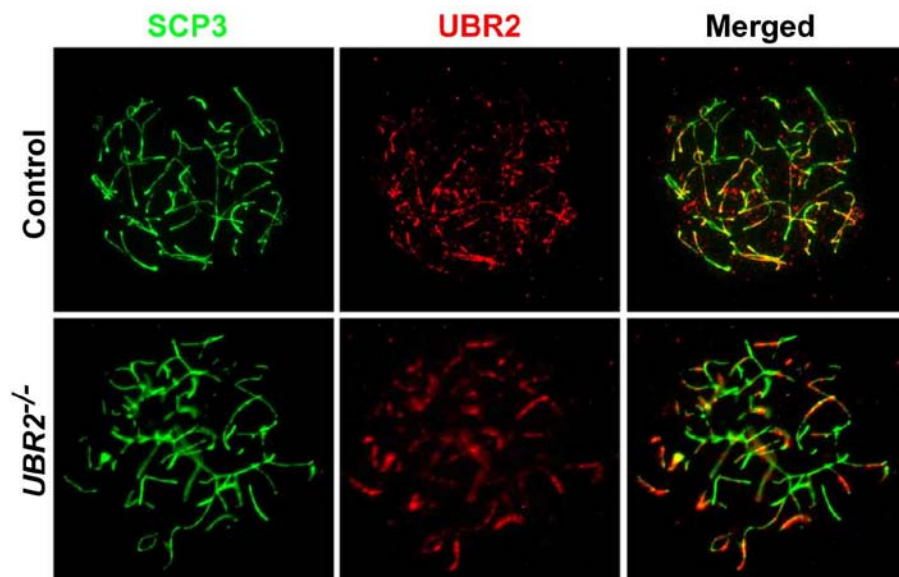


**Figure 21. UBR2 localization in control and *SPO11*<sup>-/-</sup> spermatocytes.** Zygotene spermatocytes from control and *SPO11*<sup>-/-</sup> were stained with UBR2 (red) and SCP3 (green).

form, which comprised ~20% of whole cellular UBR2 (Fig. 22B). Together, these results suggest the role of UBR2 on active chromatin in somatic cells.

#### 3.4.4 Upregulation of UBR2 signal upon DNA damage

Proteins involved in repair mechanisms are recruited to the sites of DNA damage, which appear as foci in fluorescence microscopy. To examine the localization of UBR2 in DNA damage response, DNA damage was induced by treating MMC, a potent DNA cross-linker, to MEFs, U2OS and HeLa cells. Unexpectedly, scattered UBR2 signal was dramatically increased in overall nucleus and cytoplasm instead of foci formation upon DNA damage (Fig. 23A, B). To exclude the possibility that the upregulation of UBR2 signal is MMC-dependent, UV was irradiated to induce DNA damage and same results were observed as in MMC treatment (Fig. 23A). Next, to determine if upregulation of UBR2 signal in DDR is associated with the change

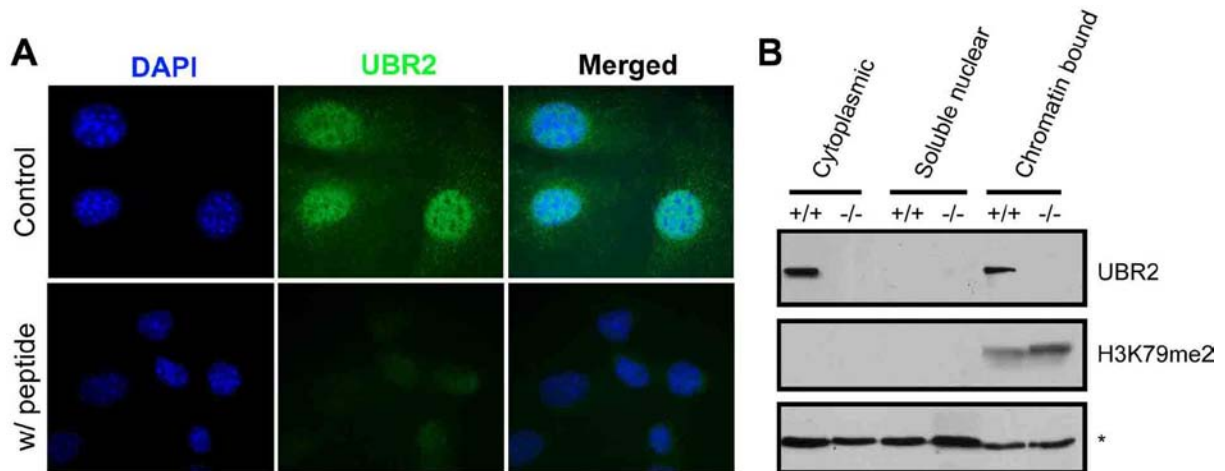


**Figure 22. Chromatin associated UBR2 localization in somatic cells.**

(A) Immunofluorescence staining of UBR2 in MEFs. Peptide used for raising antibody was incubated together to confirm the specificity of antibody. (B) Biochemical fractionation of MEF extracts. Immunoblotting using the antibody of dimethylated histone H3-lysine 79 (H3K79me2) indicates the integrity of fractionation of extracts. Asterisk indicates non-specific bands for a loading control.

of transcription, I measured the level of transcription using quantitative real-time RT-PCR. The level of UBR2 mRNA upon DNA damage was comparable to the control (Fig. 24B). These results suggest that the upregulation of UBR2 upon DNA damage is presumably due to the post-translational modification.

### 3.4.5 Impaired ubiquitylation upon DNA damage in UBR2-deficient cells

It was shown that both mono- and polyubiquitylation were defective during meiotic prophase in *UBR2*<sup>-/-</sup> spermatocytes (See Chapter 2). To assess whether ubiquitylation in somatic cells is affected by UBR2 deficiency, endogenous UBR2 was depleted by siRNA and stained with FK2 antibody which detects all ubiquitin-conjugates not ubiquitin itself, in U2OS cells. Steady state level of ubiquitylation in UBR2-deficient cells was comparable to that of control (Fig. 25C, upper panel). Consistent with previous studies showing accumulation of ubiquitin-conjugate



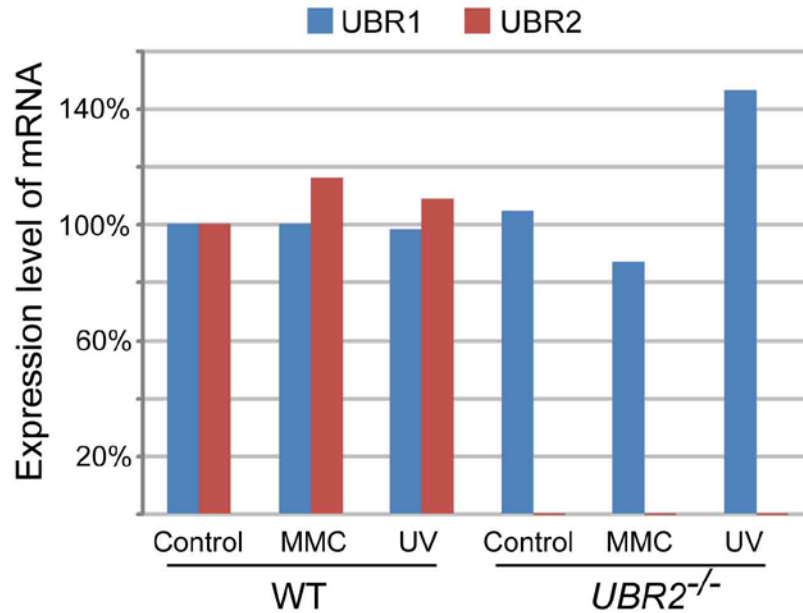


**Figure 24. The level of UBR2 mRNA in DDR**

The level of UBR2 mRNA (red) was measured in wild type and *UBR2*<sup>-/-</sup> MEFs. The level of UBR1 mRNA (blue) was also measured as a control by real-time RT-PCR. GAPDH was used for normalization.

upon DNA damage (Mailand, 2007), increased level of ubiquitylation was observed throughout nucleus upon DNA damage by MMC treatment in control cells. UBR2-knockdown cells, on the other hand, still showed slight increase of ubiquitylation by MMC treatment, but degree of increment was far less compared to the control (Fig. 25C, lower panel). Taken together, these data suggest that UBR2 mediates the ubiquitylation induced by DNA damage.

### 3.4.6 Altered histone modification in UBR2-deficient cells

It was shown that UBR2 mediates the ubiquitylation of histone H2A to repress transcription with HR6B (RAD6), an E2 Ub-conjugating enzyme of the N-end rule pathway, as an E2-E3 complex (see Chapter 2). To determine if ubiquitylation of histone H2A is also affected by the UBR2-deficiency in somatic cells, I carried out *in vivo* ubiquitylation assay. A construct of histone H2A

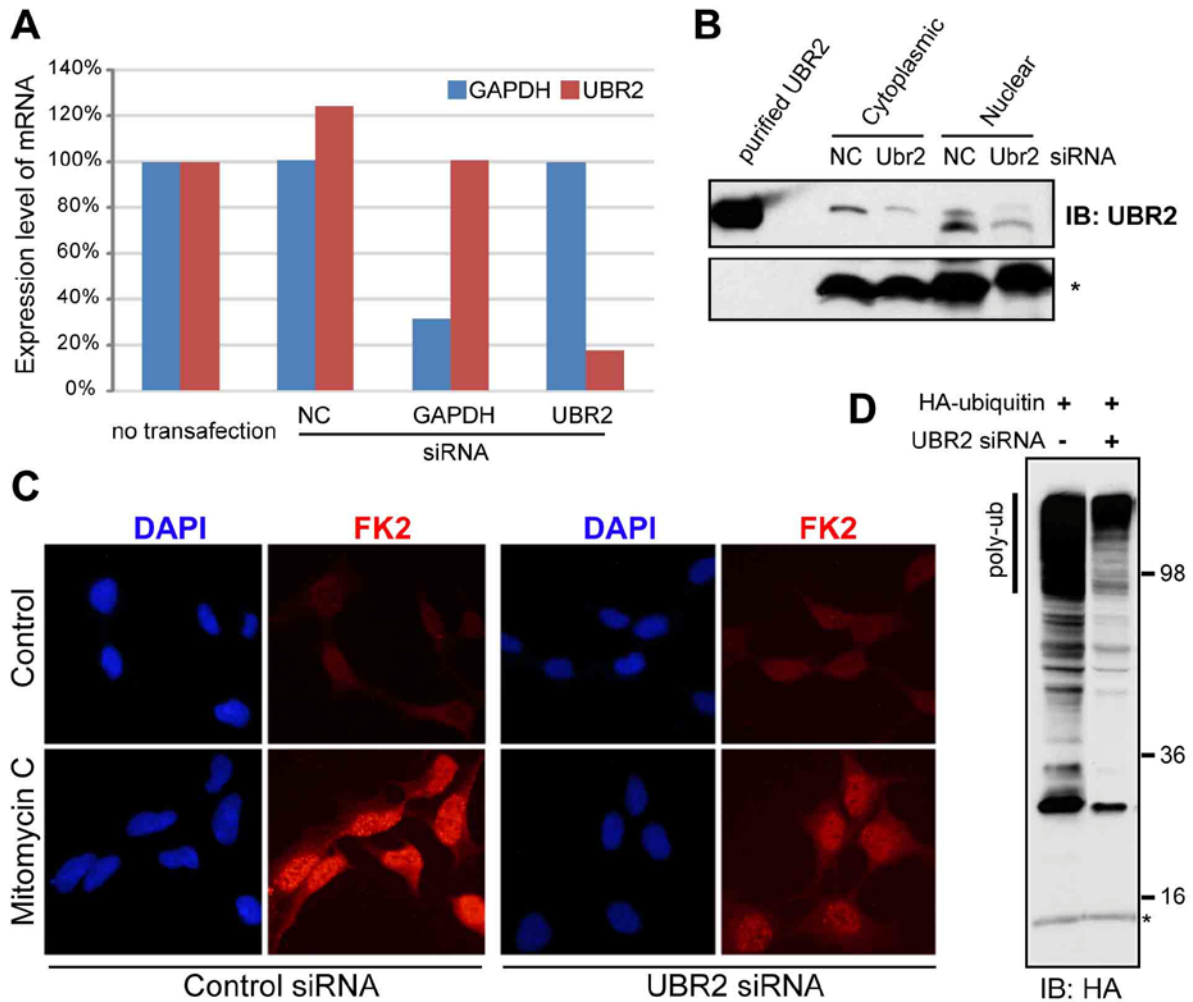


**Figure 25. Impaired DDR-related ubiquitylation in UBR2-deficient cells.**

(A) Depletion of UBR2 mRNA by siRNA in U2OS cells. NC and GAPDH siRNA were used as a negative and positive control, respectively. (B) Knock-down of UBR2 protein by siRNA in U2OS cells. Purified UBR2 protein by Phe-peptide pull-down (see methods in chapter 2) was used as a positive control. (C) U2OS cells were transfected with siRNA indicated below and treated with MMC for DNA damage. Overall ubiquitylation was detected by immunohistochemistry using FK2 antibody. (D) Ubiquitylation was detected by immunoblotting using anti-HA antibody. Asterisk indicates non-specific bands as a loading control (B, D).

with N-terminal flag was co-expressed with HA-ubiquitin in U2OS cells. Not surprisingly, ubiquitylation of H2A was significantly impaired in UBR2-knockdown cells (Fig. 26A). Moreover, impaired H2A ubiquitylation appeared to be more affected in genotoxic condition (i.e. UV irradiation). These results demonstrates that UBR2 is involved in the ubiquitylation of histone H2A at steady state level and facilitates its activity as an E3 ubiquitin ligase upon DDR pathway.

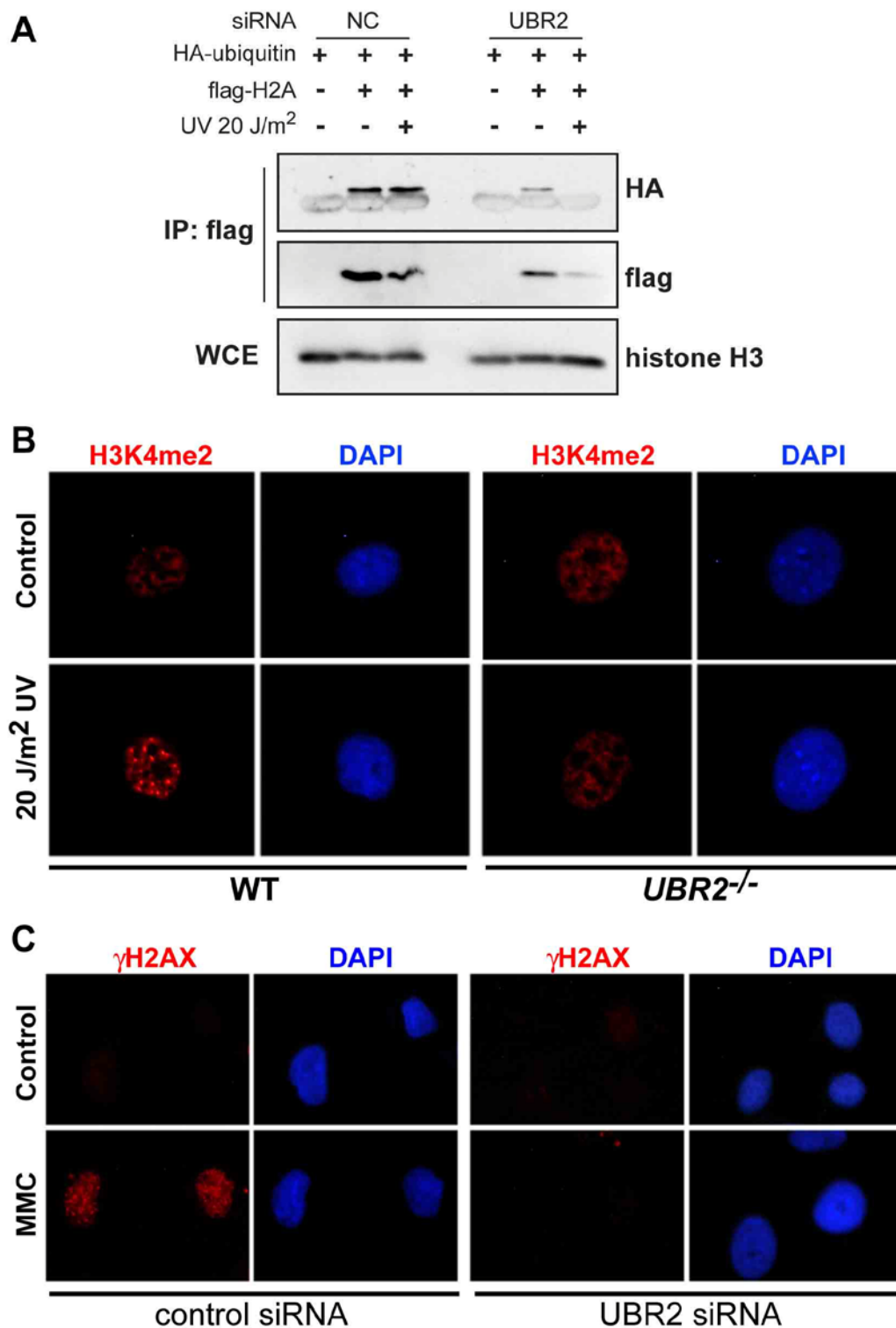


**Figure 26. Altered histone modifications in UBR2-deficient cells.**

(A) *in vivo* ubiquitylation assay of histone H2A in U2OS cells. Antibodies used in immunoblotting are denoted (right). Histone H3 in whole cell lysates (WCE) is used as a control for IP. (B) Immunostaining in MEFs using antibody recognizing dimethylated histone H3 at Lys 4 (H3K4me2). (C)  $\gamma$ H2AX staining in U2OS cells transfected with siRNA.

RAD6 is also required for the ubiquitylation of histone H2B with Bre1, a RING-finger E3 Ub-ligase (Wood et al., 2003). Here, I hypothesized that substrates of RAD6 can be ubiquitylated, at least in part, by these RING-finger E3s, in that substrate ubiquitylation by other E3 is affected in UBR2-deficient cells because it is RAD6 that transfer an ubiquitin to the targets after all. To test if the ubiquitylation of histone H2B is impaired in UBR2-deficient cells, I immunostained cells with an antibody recognizing the di-methylation of histone H3 at Lys 4 (H3K4me2), for which the ubiquitylation of H2B at Lys 123 is prerequisite (Dover et al., 2002; Sun and Allis, 2002; Wood et al., 2003). H3K4me2 signal was detected in wild type and *UBR2*<sup>-/-</sup> MEFs indistinguishably (Fig. 26B, upper panel). Upon UV irradiation, however, wild type cells showed several H3K4me2 foci while *UBR2*<sup>-/-</sup> MEFs didn't show any discernable change (Fig. 26B, lower panel). These results suggest that UBR2 is involved in the ubiquitylation of H2B in DDR pathway induced by UV irradiation.

One of the conspicuous and prevailing events in histone modifications is the phosphorylation of histone H2AX upon DNA damage (Fernandez-Capetillo et al., 2004; van Attikum and Gasser, 2005). Unexpectedly, the number of cells showing  $\gamma$ H2AX (phosphorylated H2AX) foci upon DNA damage was significantly reduced with UBR2 knock-down by siRNA (Fig. 26C). These results indicate that UBR2 is required for the retention of  $\gamma$ H2AX foci upon DNA damage and collectively suggest that UBR2 play multiple roles in the early phase of DDR pathway likely through the ubiquitylation of histones.

### **3.4.7 Genomic instability in UBR-deficient MEFs**

Cells with defective DDR pathway can result in genomic instability such as increased sensitivity to the agents that can induce DNA damage or chromosomal aberrations. To assess the

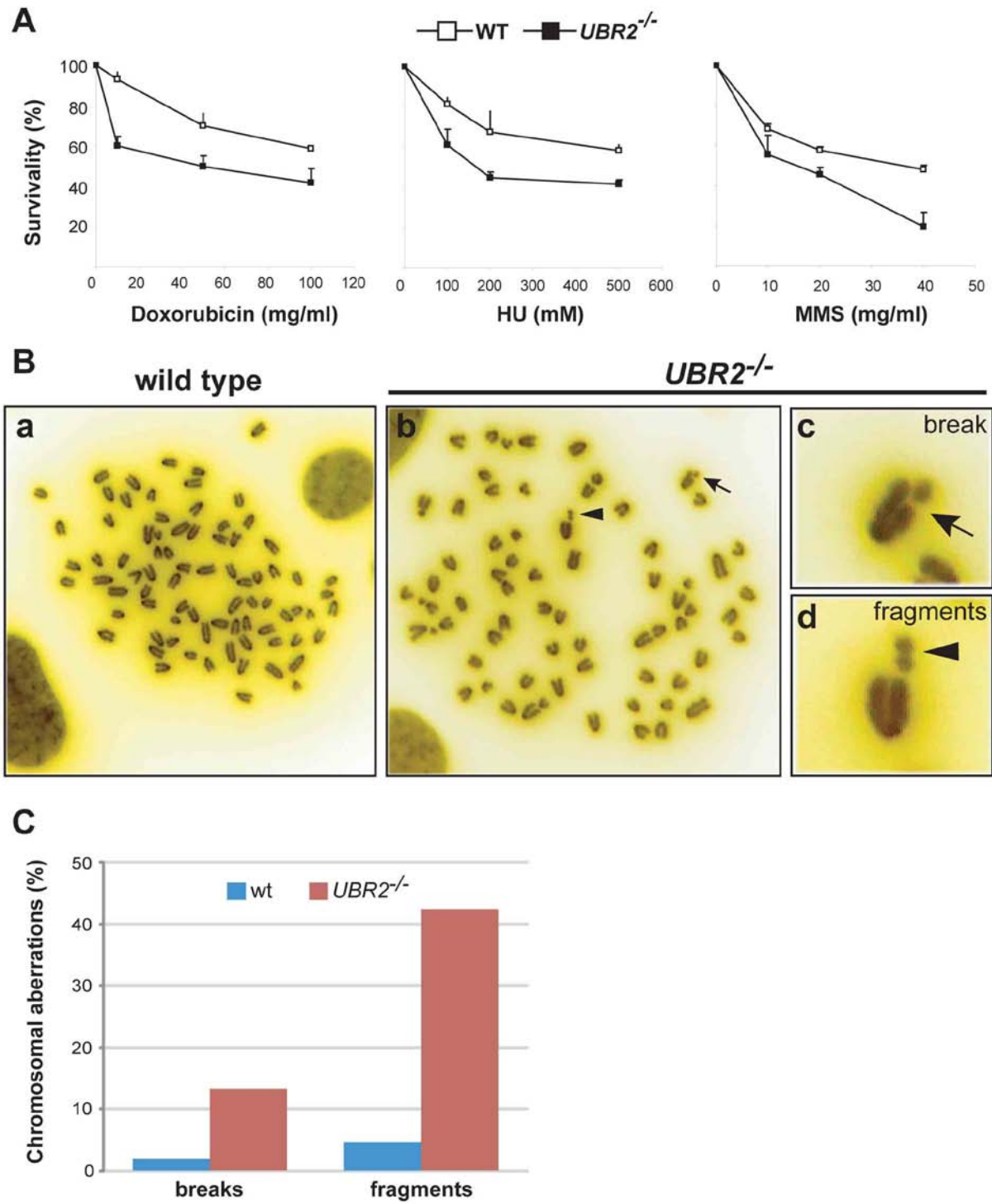


**Figure 27. Genomic instability in  $UBR2^{-/-}$  MEFs.**

(A) Survival rates of wild type and  $UBR2^{-/-}$  MEFs were measured by MTT assay in different concentrations of genotoxins denoted below. (B) Metaphase chromosome spreads from wild type (a) and  $UBR2^{-/-}$  (b) MEFs. Chromosomal aberrations such as break (c) and fragments (d) are indicated by arrows and arrowheads, respectively. (C) The frequencies of chromosomal aberrations in wild type and  $UBR2^{-/-}$  MEFs.

susceptibility to those agents, I treated wild type and *UBR2*<sup>-/-</sup> MEFs with different doses of doxorubicin, hydroxyurea (HU) and methyl methanesulfonate (MMS) and measured cell survival by MTT assay. *UBR2*-null MEFs showed increased sensitivity to these agents (Fig. 27A). To examine chromosomal integrity, metaphase spreads were prepared from wild type and *UBR2*<sup>-/-</sup> cells. The number of chromosomes was largely comparable between wild type and *UBR2*-null nuclei (75.3 and 77.5, respectively). However, the number of abnormal chromosomes such as breaks and fragmentations was significantly increased in *UBR2*<sup>-/-</sup> MEFs (15 and 48 out of 109 nuclei, respectively) compared to wild type (2 and 5 out of 113 nuclei, respectively) (Fig. 27B, C). Taken together, these results suggest that *UBR2* is required for the maintenance of genomic integrity.

### 3.5 DISCUSSION

In his project, I show that *UBR2*, the recognition E3 component of the N-end rule pathway, is required for the resolution of DSBs induced by Spo11 in germ cells. Proteins required for DSBs repair such as Rad51, RPA1 and FANCD2 normally form foci, but show reduced number in *UBR2*<sup>-/-</sup> spermatocytes. Impaired formation of crossover, one of the results from meiotic DSB repair by HR, is associated with *UBR2* deficiency. In somatic cells, nuclear *UBR2* is exclusively associated with chromatin and responds to DNA damage. *UBR2* is involved in ubiquitylation induced by DNA damage and modifications of histones. *UBR2*<sup>-/-</sup> cells shows vulnerability to genotoxic agents and increased chromosomal aberrations.

DSBs, induced by genotoxic agents, are highly detrimental lesions that can lead to mutation, cancer or cell death if not properly repaired. During meiosis, DSBs can be generated

intrinsically by SPO11 to form a crossover which is crucial for proper exchange and separation between homologous chromosomes. DSBs are detected, mediated and resolved through the cascades of signal transduction by many proteins. It has been shown that mutant mice with defective DNA damage repair are infertile due to defective gametogenesis (Cooke and Saunders, 2002). Thus it can be inferred that molecular mechanisms underlying DSB repair are shared in meiosis. Pachytene arrest of *UBR2*<sup>-/-</sup> spermatocytes correlates with defects in the repair of SPO11-induced DSBs. In wild type spermatocytes,  $\gamma$ H2AX foci at DSB sites disappear from autosomes by mid-pachytene; however, in *UBR2*<sup>-/-</sup> spermatocytes the foci remain as disorganized staining on various chromosomal regions, associated with the reduced foci of repair proteins and near absence of crossovers. Thus, it may be defective DSBs repair that trigger pachytene arrest and subsequent germ cell death and infertility.

Diffused localization of UBR2 signal on non-heterochromatin throughout nucleus and its increment upon DNA damage without change of mRNA level is likely due to the change of configuration by post-translational modifications such as phosphorylation. Mammalian UBR1/UBR2 proteins are a homologue for yeast UBR1 whose phosphorylation cascade is mediated by several kinases to regulate the N-end rule pathway. During past years, it has been shown that proteins involved in DNA damage response (DDR) are regulated by phosphatidylinositol 3-kinases (PI-3 kinases), ataxia telangiectasia mutated (ATM) and ataxia telangiectasia and RAD3-related (ATR) (Dornan et al., 2006; Mu et al., 2007). ATM and ATR, which share substrates in DDR pathway, are recruited to DNA damage sites by a sensor complex and phosphorylate targets to activate the signal transduction of DDR pathways. The global response of UBR2 throughout nucleus upon DNA damage doesn't seem to be in the same context with the focal activation of substrates by PI-3 kinases at DNA damage sites. Despite spatial discrepancy,

the study of Chk2, one of the substrates, still opens a possibility that UBR2 is one of the substrate of the kinases in response to genotoxic stress. Chk2, a cell cycle checkpoint protein, is activated by ATM at DSB sites, but spreads throughout the entire nucleus with high mobility, presumably as a messenger of damage alert to whole nucleus (Lukas et al., 2003). Whether UBR2 is deemed to change its conformation with chromatin upon DNA damage is another intriguing question that should be addressed by biochemical fractionation and immunofluorescence analyses.

The impaired ubiquitylation of UBR2-deficient cells in response to DNA damage demonstrates that UBR2 is involved in DDR pathway via ubiquitylation of target proteins as an E3 ligase. Similar reports have recently been shown that a ring finger E3 ubiquitin ligase, RNF8, is recruited to DSB sites and mediates the ubiquitylation of histone H2A and H2AX, upon DNA damage by ionizing radiation (IR) (Huen et al., 2007; Mailand et al., 2007). Overall ubiquitylation induced by IR is drastically impaired with the depletion of RNF8 by siRNA, which shows a remarkable resemblance in UBR2-deficient cells (Mailand et al., 2007). Is the response of UBR2 upon DNA damage in the same context with that of RNF8? Pieces of following results suggest that they may be involved in different mechanisms: 1) UBR2 is tightly associated with overall chromatin at steady state while RNF8 accumulates on DNA damage sites (Huen et al., 2007), and 2) RNF8 is recruited to DSB sites by MDC1 bound to  $\gamma$ H2AX. Therefore, knockdown of RNF8 doesn't interfere with upstream events of DDR pathway like  $\gamma$ H2AX formation and retention at DSB sites (Mailand et al., 2007). However, the number of cells showing  $\gamma$ H2AX foci upon DNA damage was significantly reduced by UBR2 knock-down, which indicates the role of UBR2 in either formation or retention of  $\gamma$ H2AX (i.e. phosphorylation of H2AX or inhibition of  $\gamma$ H2AX dephosphorylation, respectively). Thus,

UBR2 is more likely involved in the early steps of DDR pathway as a sensor of damage, owing to its global distribution.

RING-finger E3 Ub-ligases such as UBR1 (homologue of mouse UBR1 and UBR2), UBR2 (homologue of mouse UBR3), BRE1 and Rad18 were co-purified with tagged-RAD6, a E2-Ub conjugating enzyme, in yeast (Wood et al., 2003). RAD6 interacts with Bre1 and Rad18 to mediate ubiquitylation of histone H2B and PCNA, respectively (Wood et al., 2003; Fu et al., 2008). Hence it is conceivable that diverse selection of substrates by E2 enzymes can be conducted by eclectic interactions with specific E3 enzymes. These data suggest that UBR2 is required for the H2B ubiquitylation, which is not consistent with the model that E3s determine substrate selectivity. This subtle discrepancy can be explained, at least in part, by RING-finger E3s, in that it is E2 enzymes that transfer an ubiquitin to substrate after all. Here I propose a model that RAD6 is recruited and transfer an ubiquitin to histone H2B in the context of UBR2 which was bound to chromatin and activated by post-translational modification upon DNA damage. In this model, ubiquitylation of histones by UBR2 presumably alter chromatin configuration and may provide a platform for the efficient cascades of signal transduction in DDR pathway (i.g. phosphorylation of  $\gamma$ H2AX by ATM/ATR at DSB sites).

MEFs derived from *UBR2*<sup>-/-</sup> mice show increased chromosomal abnormality with defective homologous recombination (Ouyang et al., 2006) as well as susceptibility to genotoxic agents. Collectively, these data suggests that UBR2 is required for the maintenance of genomic integrity presumably by facilitating damage alert through ubiquitylation.

## 4.0 THE ROLE OF UBR1 AND UBR2 IN THE NEUROGENESIS AND CARDIOVASCULAR DEVELOPMENT

### 4.1 SUMMARY

The N-end rule relates the *in vivo* half-life of a protein to the identity of its N-terminal residue. A subset of degradation signals recognized by the N-end rule pathway comprises the signals, called N-degrons, whose determinants include destabilizing N-terminal residues. Previous work identified a family of mammalian E3 ubiquitin ligases, including UBR1 and UBR2, which share the UBR box and recognize N-degrons. These E3 enzymes mediate the multifunctional N-end rule pathway, but their individual roles are just beginning to emerge. Mutations of *UBR1* in humans are the cause of the Johanson-Blizzard syndrome (JBS). UBR1 and UBR2 are 46% identical, and appear to be indistinguishable in their recognition of N-degrons. *UBR1*<sup>-/-</sup> mice are viable but have defects that include pancreatic insufficiency, similarly to *UBR1*<sup>-/-</sup> human patients with JBS. *UBR2*<sup>-/-</sup> mice are inviable in some strain backgrounds, and are defective in male meiosis. To examine functional relationships between UBR1 and UBR2, I constructed mouse strains lacking both of these E3s. *UBR1*<sup>-/-</sup>*UBR2*<sup>-/-</sup> embryos die at midgestation, with defects in neurogenesis and cardiovascular development. These defects included reduced proliferation as well as precocious migration and differentiation of neural progenitor cells. The expression of regulators such as D-type cyclins and Notch1 was also altered in *UBR1*<sup>-/-</sup>*UBR2*<sup>-/-</sup> embryos.

These results suggest that the functions of UBR1 and UBR2 are significantly divergent, in part because of differences in their expression patterns, and possibly also because of differences in their recognition of protein substrates that contain degradation signals other than N-degrons.

## 4.2 BACKGROUND

Little is known about how the ubiquitylation by UBR box proteins controls biological processes. Previously, 200 kDa-UBR1 has been characterized as a founding N-recognin that can bind to certain N-degrons (Kwon et al., 1998; Kwon et al., 2001). *UBR1*<sup>-/-</sup> mice showed growth retardation associated with reduced fat deposition and hypoglycemia, indicating a state of mild malnutrition (Kwon et al., 2001). Johanson-Blizzard syndrome, an autosomal recessive disorder with exocrine pancreatic insufficiency and other multiple malformations, is caused by mutations in *UBR1* (Zenker et al., 2005). Consistent with *UBR1* being Johanson-Blizzard gene, *UBR1*<sup>-/-</sup> mice show an exocrine pancreatic insufficiency with impaired stimulus-secretion coupling and increased susceptibility to pancreatic injury (Zenker et al., 2005). UBR2 is similar to UBR1 in size (200 kDa), sequence (46% identity), and specificities to N-degrons (Kwon et al., 2003). *UBR2*<sup>-/-</sup> male mice are infertile due to defects in homologous chromosome pairing during meiotic prophase I, whereas bulk of *UBR2*<sup>-/-</sup> female mice are lethal without specific terminal phenotypes (Kwon et al., 2003). Therefore, UBR1 and UBR2 are biochemically similar but have distinctive physiological functions. The only known mammalian proteins whose proteolysis depends on N-degrons are a set of closely related RGS proteins (RGS4, RGS5, and RGS16) that counter regulate specific G protein-coupled receptor (GPCR) signaling pathways in the cardiovascular and nervous systems (Hu et al., 2005; Lee et al., 2005). Proteolysis of these RGS

proteins is fine regulated through the ATE1-UBR1/UBR2 circuit in a manner that also requires NO and O<sub>2</sub> (Hu et al., 2005; Lee et al., 2005). Therefore, one molecular function of UBR1 and UBR2 is to control cell growth (proliferation, differentiation, and death) in response to extracellular stimuli (e.g., mitogen, anti-mitogen, O<sub>2</sub>, and stress) through regulated proteolysis of RGS proteins.

As part of long-term efforts to understand the function of the N-end rule pathway, I hypothesized that UBR1 and UBR2 cooperate each other *in vivo* to control specific physiological processes. *UBR1*<sup>-/-</sup>*UBR2*<sup>-/-</sup> embryos die at midgestation associated with defects in neurogenesis and cardiovascular development. These results indicate that UBR1 and UBR2 are important for homeostasis in proliferation and differentiation of neural precursors during mouse embryogenesis.

## 4.3 METHODS

### 4.3.1 *UBR1*<sup>-/-</sup>*UBR2*<sup>-/-</sup> mice

Construction and characterization of *UBR1*<sup>-/-</sup> and *UBR2*<sup>-/-</sup> mice were described (Kwon et al., 2001; Kwon et al., 2003). *UBR1*<sup>-/-</sup>*UBR2*<sup>-/-</sup> mice were produced by interbreeding *UBR1*<sup>+/-</sup>*UBR2*<sup>+/-</sup> mice in the 129SvImJ and C57BL/6 genetic background (Tasaki et al., 2005). For timed pregnancies, E0.5 was defined as the morning on which a vaginal plug was present, and fetal stage was confirmed by comparing the morphology to characterized embryonic structures. The gender and genotype of mice (embryos) were determined by PCR as described (Kwon et al., 2001; Kwon et al., 2003).

### **4.3.2 Histology and immunohistochemistry**

Embryos were fixed with freshly prepared 4% paraformaldehyde in PBS for 2h at RT or for overnight at 4°C with gentle rocking. Samples were washed in PBS, dehydrated in serial ethanol, cleared in histosol (National Diagnostics) and embedded in paraffin. Paraffin-embedded embryos were serially sectioned and stained with hematoxylin-eosin (H&E) for histology. For immunohistochemistry on sectioned embryos, samples were deparaffinated in histosol, rehydrated in serial ethanol, and boiled in antigen retrieval buffer (10 mM sodium citrate, pH 6.0) for 10 min. After cooling down, slides were subjected to blocking, incubation with antibodies, and counterstaining with DAPI as previously described (see METHODS 2.3.2). Antibodies used for immunostaining are listed in Table 3.

### **4.3.3 Measurements of cell proliferation and death**

For proliferation assay, pregnant females were injected intraperitoneally with BrdU (Sigma) (50 µg/g body weight) and killed 1-5 hr later. Embryos were harvested, fixed and processed for paraffin section. Incorporated BrdU was visualized by immunostaining as described above. To detect apoptotic nuclei, transverse sections of embryos were subjected to terminal transferase-mediated dUTP-biotin nick end labeling (TUNEL) assay using In situ Cell Death Detection Kit (Roche), followed by counterstaining with DAPI.

**Table 3. Antibodies used in immunohistochemistry and immunoblotting**

Antibody	Species	Dilution	Reference
Neurofilament	mouse	1:50	Developmental Studies Hybridoma Bank
Tropomyosin	mouse	1:100	Developmental Studies Hybridoma Bank
Nestin	mouse	1:50	Developmental Studies Hybridoma Bank
Cyclin D1	mouse	1:100	SantaCruz, sc-450
Cyclin D2	rabbit	1:250	SantaCruz, M-20
Cyclin D3	rabbit	1:250	SantaCruz, C-16
Cyclin E	rabbit	1:250	SantaCruz, sc-481
Cyclin A	rabbit	1:250	SantaCruz, sc-596
Cyclin B	rabbit	1:250	SantaCruz, sc-752
p38	rabbit	1:1000	Cell Signaling
phospho-p38	rabbit	1:100	Cell Signaling, 4631
Notch1 (ICD)	rabbit	1:1000	Cell Signaling, 2421
Notch1	mouse	1:1000	Sigma, N6780
tubulin $\beta$ III	mouse	1:100	Sigma, T8660
GABA	rabbit	1:1000	Sigma, A2052
actin	rabbit	1:2500	Sigma, A5060
MAP2	rabbit	1:200	Chemicon, AB5622
BrdU	rat	1:20	Accurate Chemical
phosphor-H3	rabbit	1:200	upstate, 06-570
PECAM	rat	1:100	Pharmlingen, 557355
Anti-mouse IgG FITC	goat	1:250	Jackson Immunoresearch
Anti-mouse IgG Cy3	goat	1:250	Jackson Immunoresearch, 115-165-146
Anti-rabbit IgG FITC	goat	1:250	Jackson Immunoresearch
Anti-rat IgG Cy3	goat	1:250	Jackson Immunoresearch
Anti-rabbit IgG Alexa Fluor® 555	goat	1:400	Molecular Probes, A21429
Anti-mouse IgG HRP	goat	1:10,000	SantaCruz
Anti-rabbit IgG HRP	goat	1:250	SantaCruz
Anti-rat IgG HRP	goat	1:10,000	SantaCruz

#### 4.3.4 Whole mount PECAM staining

E10.5 yolk sacs and embryos were harvested, fixed in fresh fixative for overnight at 4°C, and stored in 70% ethanol at 4°C. Samples were rehydrated by serial methanol diluted in PBS with 0.2% Tx-100 for 10 min, followed by washing in PBS with 0.2% Tx-100 for 10 min. Bleaching with 0.3% H<sub>2</sub>O<sub>2</sub> in PBS for 10 min and permeabilization with 10 µg/ml proteinase K (Roche) in 10 mM Tris pH 8.0 for 10 min were applied before blocking and antibody incubation. For chromogenic immunostaining, samples were developed in Acetate-Imidazole buffer (0.17M sodium acetate, 10 mM imidazole) containing DAB, NiSO<sub>4</sub>, and H<sub>2</sub>O<sub>2</sub> at 4°C.

#### 4.3.5 Immunoblotting

Different litters of E10.5 embryos were harvested and homogenated in lysis buffer (50 mM Tris pH 8.0, 150 mM NaCl, 0.1% SDS, 0.5% Sodium deoxycholate, 1% NP-40) with protease inhibitors mix (Sigma). Proteins were separated by SDS-PAGE and subjected to immunoblotting. Antibodies used for immunoblotting are listed in Table 3.

## 4.4 RESULTS

#### 4.4.1 Embryonic lethality of *UBR1*<sup>-/-</sup>*UBR2*<sup>-/-</sup> double mutant

To determine the function of UBR1 and UBR2, *UBR1*<sup>+/-</sup> and *UBR2*<sup>+/-</sup> mice were intercrossed, yielding *UBR1*<sup>+/-</sup>*UBR2*<sup>+/-</sup> mice on the C57BL6/129 background. *UBR1*<sup>+/-</sup>*UBR2*<sup>+/-</sup> mice grew

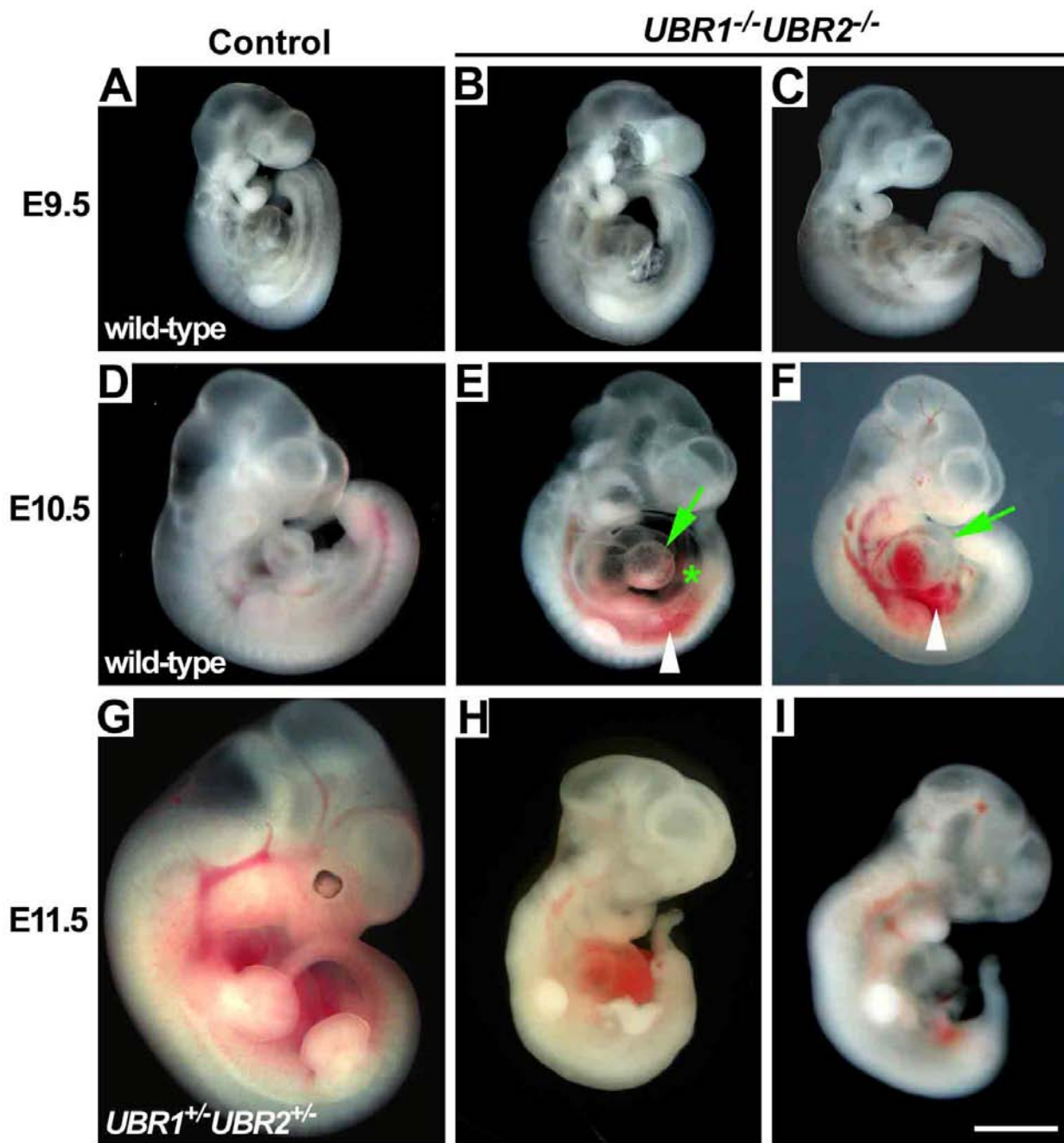


**Figure 28. Gross morphology of *UBR1<sup>-/-</sup>UBR2<sup>-/-</sup>* mouse embryos.**

(A-I) The appearance of control and *UBR1<sup>-/-</sup>UBR2<sup>-/-</sup>* embryos at E9.5 (A-C), E10.5 (D-F), and E11.5 (G-I). Arrow, the heart; asterisk, swollen pericardial sac; arrowhead, a hemorrhage. Scale bar: 1 mm.

normally and were fertile, although subtle morphological or physiological abnormalities could not be ruled out. No  $UBR1^{-/-}UBR2^{-/-}$  adult mice were retrieved from heterozygous intercrosses, suggesting functional interplay between UBR1 and UBR2. To ascertain the timing and nature of the lethality, I examined the morphology of more than 1,000 embryos at various stages (mainly E7.5-E13.5) produced from timed intercrosses between  $UBR1^{+/-}UBR2^{+/-}$  and/or  $UBR1^{-/-}UBR2^{+/-}$  mice.

E9.5  $UBR1^{-/-}UBR2^{-/-}$  embryos were comparably recovered and were indistinguishable on gross inspection from their littermates (Fig. 28B, C), suggesting that loss of UBR1 and UBR2 does not affect significantly embryonic development up to this time. E10.5  $UBR1^{-/-}UBR2^{-/-}$  embryos were also comparably recovered and were apparently normal in neural tube closure,

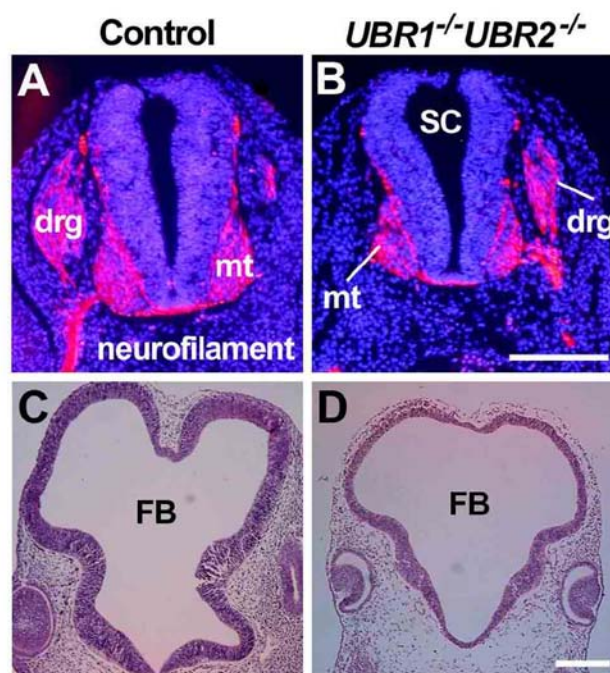


**Figure 29. Abnormal development of the central nervous system in  $UBR1^{-/-}UBR2^{-/-}$  embryos**

(A, B) Transverse sections of E10.5  $UBR1^{-/-}UBR2^{-/-}$  (B) and littermate  $UBR1^{+/-}UBR2^{+/-}$  control (A) embryos stained for neurofilaments. (C, D) H&E-stained transverse sections of  $UBR1^{-/-}UBR2^{-/-}$  (D) and littermate control embryos (C); drg, dorsal root ganglia; mt, motor neuron; SC, spinal cord; FB, forebrain; Scale bars, 200  $\mu$ m.

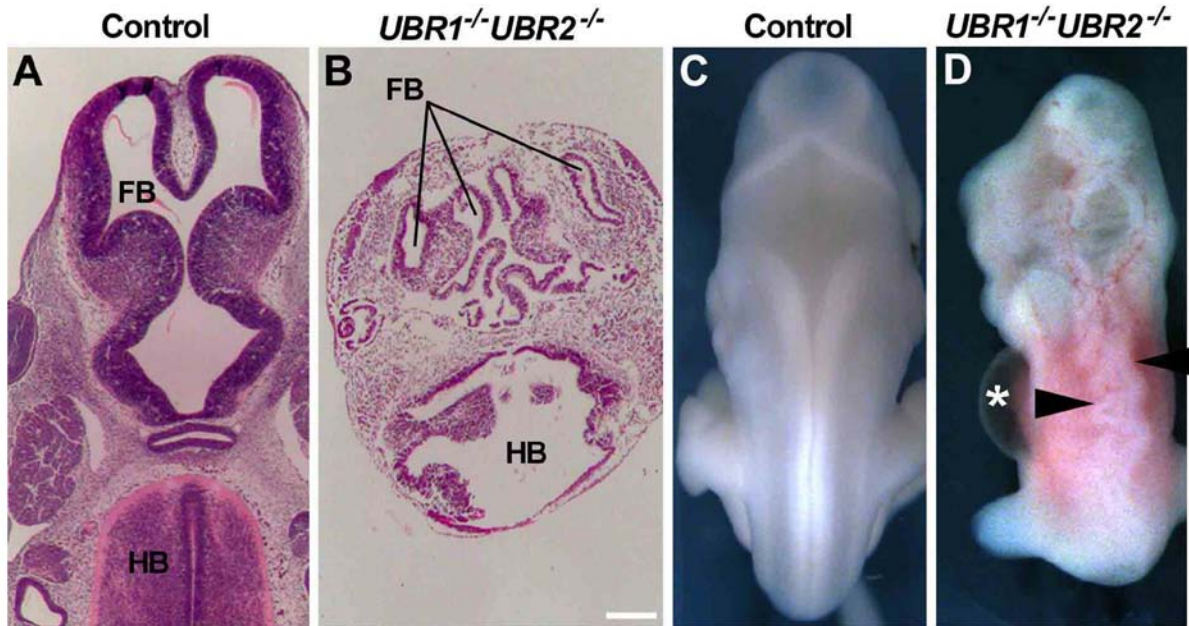


**Figure 30. Abnormal development of the neural tube in *UBR1*<sup>-/-</sup>*UBR2*<sup>-/-</sup> embryos**

(A, B) H&E-stained transverse sections of *UBR1*<sup>-/-</sup>*UBR2*<sup>-/-</sup> (B) and littermate control embryos (A) at E11.5. (C, D) Dorsal views of E11.5 *UBR1*<sup>-/-</sup>*UBR2*<sup>-/-</sup> (D) and control embryos (C). FB, forebrain; HB, hindbrain; the asterisk and arrowheads in D: swollen pericardial sac and kinked neural tube, respectively. Scale bars, 200  $\mu$ m.

axial rotation, normal branchial arch, and anterior limb bud development. However, the mutants at E10.5 were slightly smaller (by ~10-15%) compared to littermate controls (Fig. 28E, F), partly because of defects in nervous and cardiovascular development (see below). E11.5 *UBR1*<sup>-/-</sup>*UBR2*<sup>-/-</sup> mutants were either found dead or appeared to be arrested in sizes at ~E10.5 (Fig. 28H, I). No live *UBR1*<sup>-/-</sup>*UBR2*<sup>-/-</sup> mutants were observed at E12.5, suggesting that they die before this time. These results indicate that loss of UBR1 and UBR2 disrupts physiological processes that are indispensable for embryonic development between E10.0 and E11.5.

#### 4.4.2 Impaired Neurogenesis in Embryos Lacking UBR1 and UBR2

The neural tubes of *UBR1<sup>-/-</sup>UBR2<sup>-/-</sup>* embryos at E10.5 were apparently normal in external morphology, but they became all severely kinked by E11.5 (Fig. 30D, arrowhead). Upon histological examination of embryonic sections, the neuroepithelium of E10.5 *UBR1<sup>-/-</sup>UBR2<sup>-/-</sup>* embryos showed moderate thinning, which was severer in the forebrain than in the spinal cord (Fig. 29B, D). Various central nervous tissues at E10.5 did not gain thickness significantly by E11.5 (Fig. 30B), suggesting that neural proliferation has been disrupted at E10.25-E10.5. Nonetheless, they comparably expressed neurofilament, a marker of mature neurons (Fig. 29B), suggesting that development of the spinal cord is normal until ~E10.25. Notably, the forebrain of E11.5 *UBR1<sup>-/-</sup>UBR2<sup>-/-</sup>* embryos became highly distorted in morphology in that its neuroepithelium was highly serpentine and thin, and broken into fragments with irregular thicknesses (Fig. 30B). These results indicate that the forebrain of *UBR1<sup>-/-</sup>UBR2<sup>-/-</sup>* embryos at this stage may normally undergo developmental programs (e.g., differentiation and migration) without proper neural proliferation.

Mammalian neurogenesis begins with a stem cell-like self-renewal of neural progenitor cells, thereby providing neurons in correct numbers and diverse types (McConnell, 1995). During neurogenesis, neural precursor cells undergo several rounds of the cell cycle at the

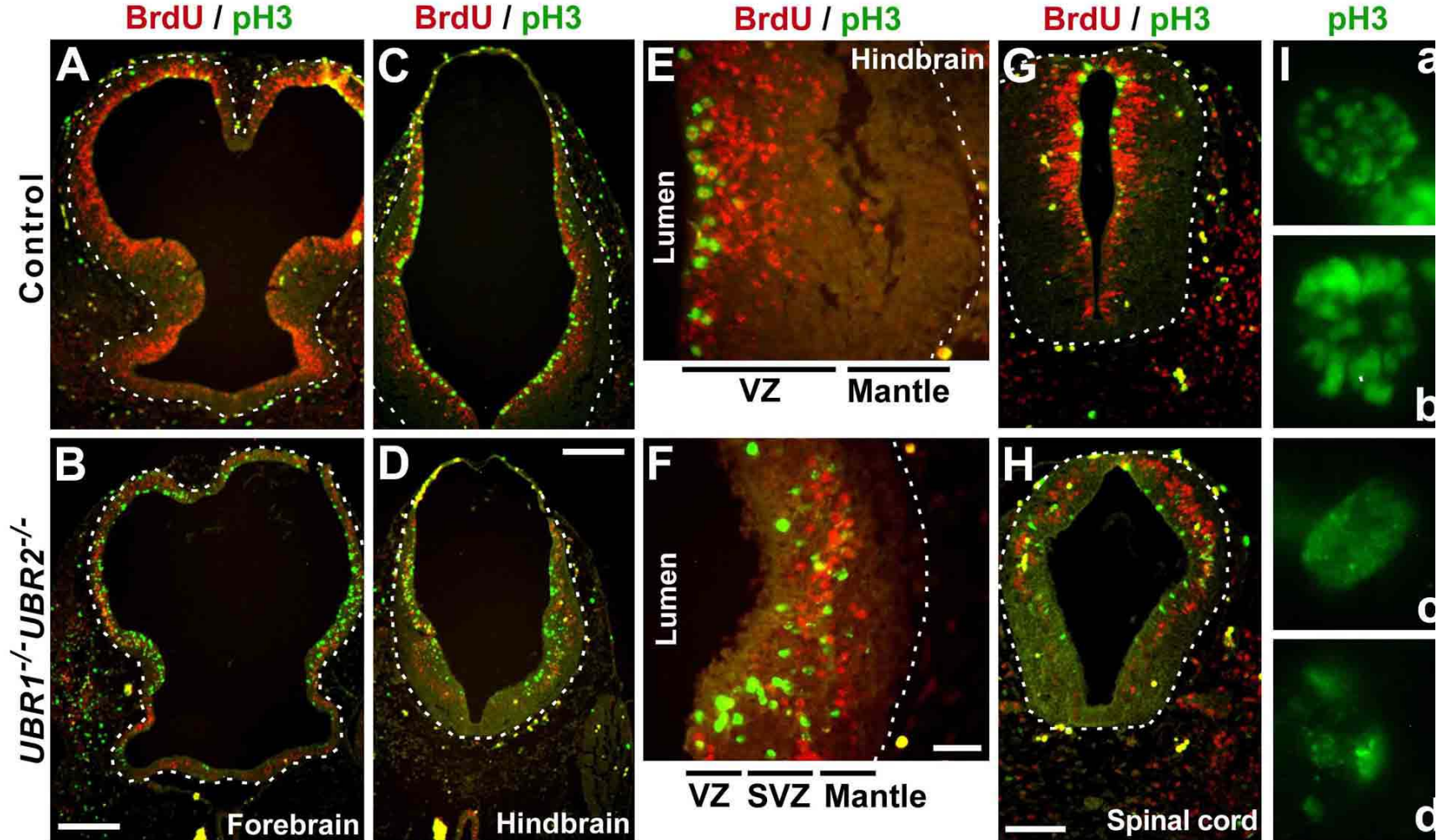


**Figure 31. Abnormal proliferation patterns in  $UBR1^{-/-}UBR2^{-/-}$  neural tubes**

Transverse sections of E10.5  $UBR1^{-/-}UBR2^{-/-}$  embryos (B, D, F, H, Ic, Id) and littermate controls (A, C, E, G, Ia, Ib) that were stained for BrdU (red), pH3 (green), as indicated above the panels. (E, F) Enlarged views of hindbrain regions indicated by squares in C and D. (Ia-Id) Representative morphologies of pH3-positive nuclei of cells in E10.5  $UBR1^{-/-}UBR2^{-/-}$  (Ic, Id) and control (Ia, Ib) hindbrains. Scale bars, 200  $\mu$ m (A-D); 40  $\mu$ m (E, F); and 100  $\mu$ m (G, H).

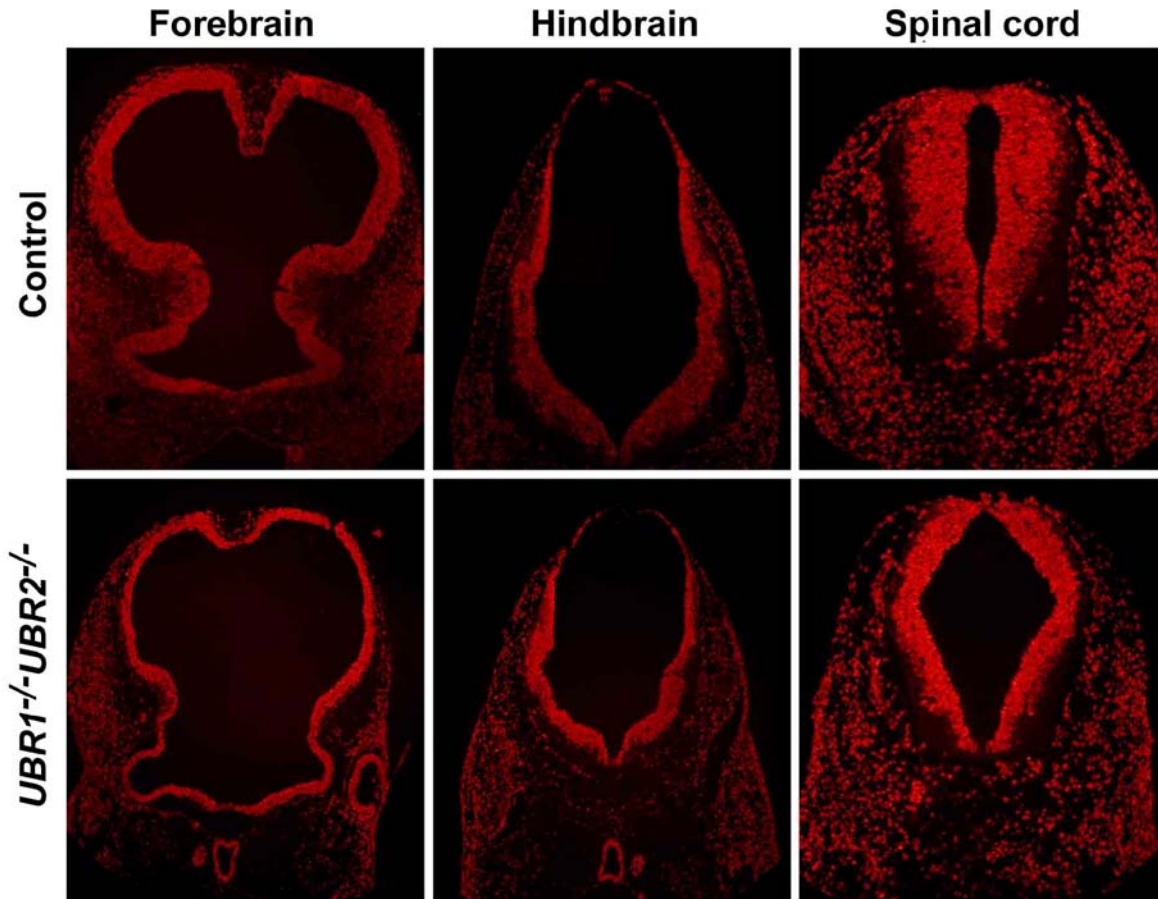


**Figure 32. Active phase of cell cycle in neural tube of  $UBR1^{-/-}UBR2^{-/-}$  embryos**

Different regions of neural tubes are indicated above. Sections from control and double mutant embryos were stained for Ki67 (red), a marker for cells in active cell cycle.

ventricular zone (VZ; see Fig. 31E), before they exit the cell cycle. They subsequently migrate laterally from the VZ to the differentiation zone (mantle), which is composed of post-mitotic, differentiating neurons and glia, and differentiate therein, resulting in radially arranged layers of neurons, with the last-born neurons in the outermost layer (McConnell, 1995). The proper control of proliferation and differentiation is crucial for the size, shape and properties of the central nervous system. However, the underlying molecular mechanisms, like those governing stem-cell self-renewal in general, remain poorly understood.

To examine the nature of neural tissue deformation, I injected BrdU into pregnant female mice, harvested embryos, and determined the number of BrdU-positive cells on the transverse sections of E10.5 embryos. In control embryos, BrdU was prominently incorporated into the VZ of various neural tissues (Fig. 31E). Importantly, the number of BrdU-positive neural cells (in S phase) was substantially reduced throughout the entire anterior-posterior axis of E10.5 *UBR1*<sup>-/-</sup>*UBR2*<sup>-/-</sup> embryos compared to control embryos (Fig. 31B, D, F, H), suggesting that proliferation of neural precursors is impaired in the absence of UBR1 and UBR2. The reduced BrdU index should not be due to nonspecific growth retardation, given that the level of neural cells expressing Ki67, a marker for all cells active in the cell cycle, was comparable in neural tube of mutants (Fig. 32). To test whether knockout of *UBR1* and *UBR2* would also perturb mitosis, I evaluated mitotic cells in the neural tube by staining phospho-histone H3 (pH3), a marker for mitotic cells. In control embryos, pH3-positive mitotic cells were observed in the apical surface of VZ, a single-cell layer facing the lumen (Fig. 31A, C, E, G). However, a strikingly increased number of pH3-positive neural precursors were found in the forebrain of E10.5 *UBR1*<sup>-/-</sup>*UBR2*<sup>-/-</sup> embryos compared to control embryos (Fig. 31B). Further, the spatial distribution of mutant mitotic cells was highly disorganized in that they were also found throughout the layer lateral to the VZ (Fig. 31F; see below). The pH3 index in double mutants was similar in the hindbrain and even somewhat lower in the spinal cord (Fig. 31D, H). These results suggest that the control of mitotic activities has been impaired in the mutant neural precursors in a manner depending on the anterior-posterior axis. Further, while mitotic cells in control embryos were mainly at prophase or prometaphase (Fig. 31Ia, Ib), many pH3-positive mitotic neural cells in *UBR1*<sup>-/-</sup>*UBR2*<sup>-/-</sup> embryos appeared to be at the stage between interface and prophase (Fig. 31Ic, Id), indicating an apparent arrest at the G2-M transition. I also determined whether cell death is

involved in neural tube deformation by using TUNEL assay on the transverse sections of embryos. Significantly increased number of TUNEL-positive cells was observed throughout the entire neural tube regions of E10.5 *UBR1*<sup>-/-</sup>*UBR2*<sup>-/-</sup> embryos, with a heightened effect in the forebrain (Fig. 33). These results demonstrate that the decreased BrdU index (for S phase) associated with perturbed mitotic activities and increased cell death mainly account for morphological defects in neurogenesis.

The neuroepithelium of normally developing E10.5 embryos can be divided into two layers: 1) the VZ containing proliferative neural precursors that undergo interkinetic nuclear migration, and 2) the mantle containing postmeiotic neurons. In contrast, the neuroepithelium of

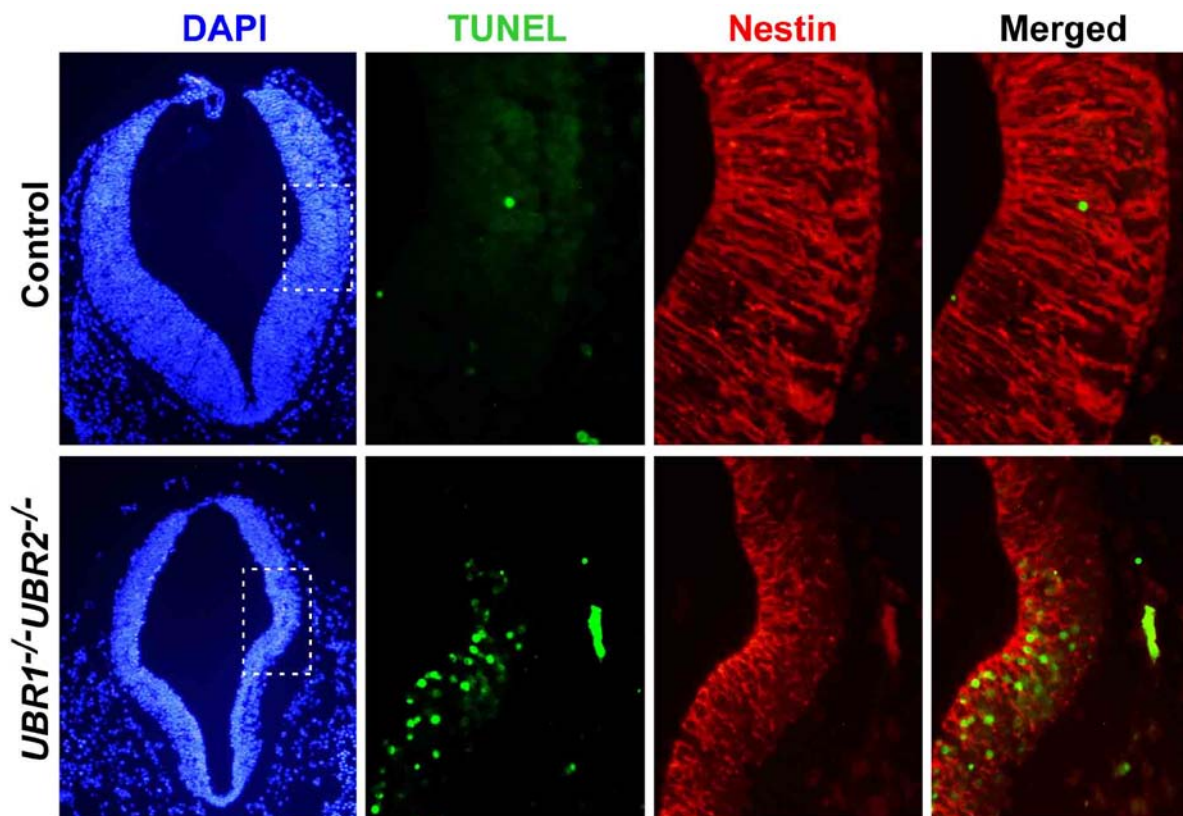


**Figure 33. Increased apoptosis in *UBR1*<sup>-/-</sup>*UBR2*<sup>-/-</sup> neural precursors**

Transverse sections of neural tube at E10.5 control and *UBR1*<sup>-/-</sup>*UBR2*<sup>-/-</sup> embryos. Staining for nestin (red) and TUNEL (green) represent neural precursors and apoptotic cells, respectively. Stained regions are magnified as indicated by insets in DAPI.

E10.5 *UBR1*<sup>-/-</sup>*UBR2*<sup>-/-</sup> embryos could be divided into three distinctive layers, BrdU<sup>-</sup>pH3<sup>+</sup>, BrdU<sup>+</sup>pH3<sup>+</sup>, and BrdU<sup>-</sup>pH3<sup>-</sup> (Fig. 31F). When progenitor cells in the VZ become postmeiotic, they usually migrate to the mantle. However, at the later stage of neurogenesis, some precursors that leave the VZ remain mitotically active and enter a secondary proliferative zone called the subventricular zone (SVZ) that lies between the VZ and mantle (Takahashi et al., 1995). The nuclei of VZ cells migrate up and down the apical-basal axis during the cell cycle (interkinetic nuclear migration), while SVZ cells do not undergo this nuclear migration. Therefore, the most parsimonious interpretation for the three layers (Fig. 31F) in the mutants are that they are the VZ (BrdU<sup>-</sup>pH3<sup>+</sup>), SVZ (BrdU<sup>+</sup>pH3<sup>+</sup>), and mantle (BrdU<sup>-</sup>pH3<sup>-</sup>), among which BrdU<sup>+</sup>pH3<sup>+</sup> SVZ has been generated due to premature migration of mitotically active neural precursors from the VZ. Consistent with this interpretation, the BrdU<sup>+</sup>pH3<sup>+</sup> SVZ-like zone indeed lied between nestin signals (specific for neural precursors in the VZ, Fig. 34F) and MAP2 signals (for the dendrites of post-meiotic neurons in the mantle, Fig. 34H) or tubulin  $\beta$ III signals (for the tubulin-rich processes of post-meiotic neurons in the mantle, Fig. 34J). GABA is produced in specific neurons of the forebrain derived from the SVZ (Anderson et al., 1997). I therefore asked whether GABAergic neurons would be precociously generated in E10.5 *UBR1*<sup>-/-</sup>*UBR2*<sup>-/-</sup> forebrain, which was indeed confirmed by staining for GABA (Fig. 34L).

Neural progenitor cells within the neural tube normally undergo S phase when their nuclei are in the outer half of the VZ. The nuclei then translocate towards the ventricular surface where cells undergo mitosis. Therefore, in *UBR1*<sup>-/-</sup>*UBR2*<sup>-/-</sup> embryos, the proliferation through G1-S transition or S phase is eliminated almost completely in the VZ (the primary proliferative zone) but less severely in the SVZ (the secondary proliferative zone), indicating that ubiquitylation by UBR1 and UBR2 may be more important for cell proliferation in early

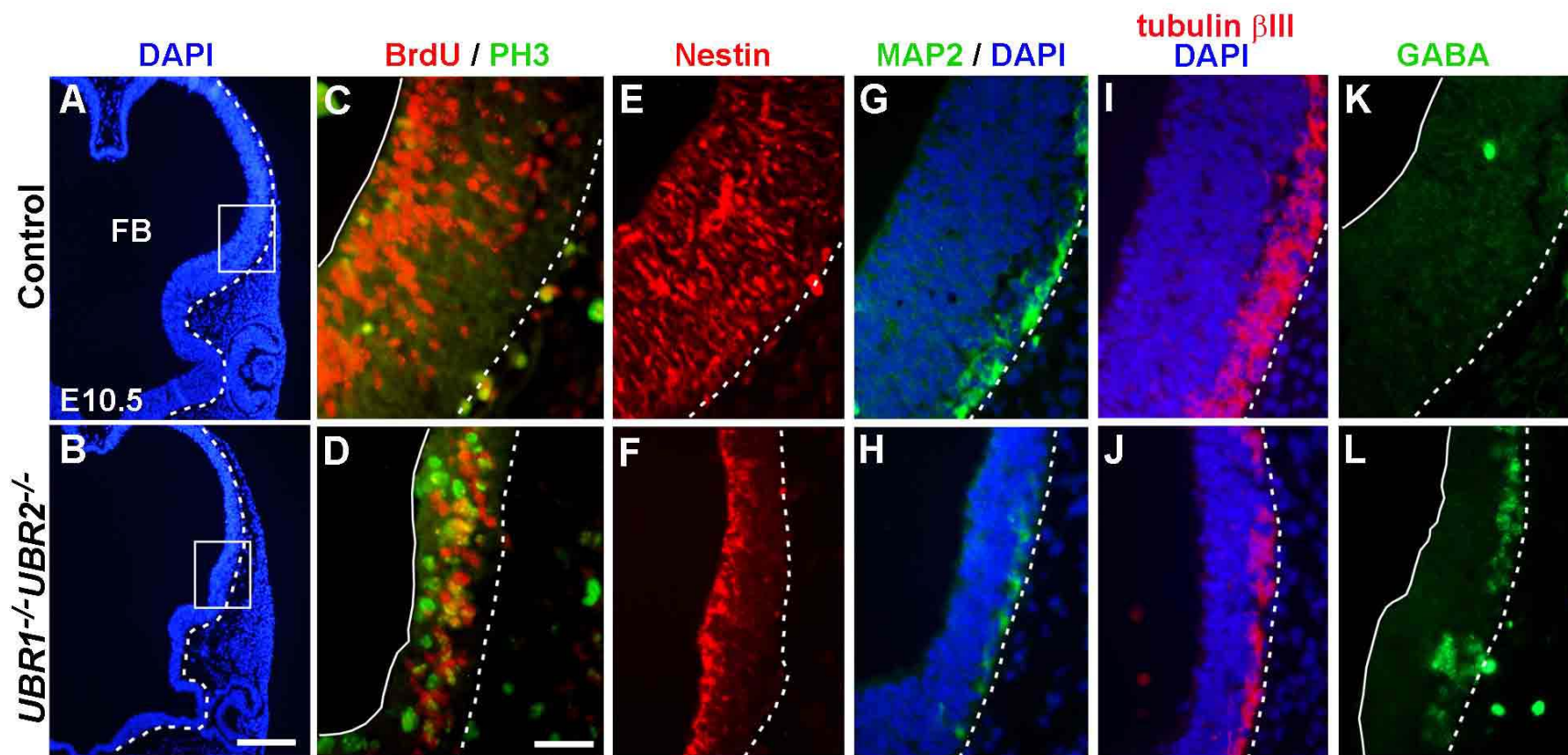


**Figure 34. Abnormal differentiation patterns of  $UBR1^{-/-}UBR2^{-/-}$  neural precursors.**

Transverse sections of forebrain regions (indicated by squares in *A* and *B*) in E10.5  $UBR1^{-/-}UBR2^{-/-}$  (*B*, *D*, *F*, *H*, *J*, *L*) and  $UBR1^{+/+}UBR2^{+/-}$  control embryos (*A*, *C*, *E*, *G*, *I*, *K*) were stained for DNA (blue), BrdU (red), p3 (green), nestin (red), MAP2 (green), tubulin  $\beta$ III (red), and/or GABA (green), as indicated above the panels. Scale bars: 200  $\mu$ m (*A*, *B*) and 40  $\mu$ m (*C*-*L*).

neurogenesis than in late neurogenesis. These results together suggest that neural precursors in *UBR1<sup>-/-</sup>UBR2<sup>-/-</sup>* embryos prematurely migrate from the VZ into the SVZ, indicative of accelerated differentiation of neural precursors. If reduced proliferation of neural precursors is coupled with their accelerated differentiation, neural precursors should be gradually depleted as neurogenesis progresses. Depletion of nestin-positive, neural precursors was indeed observed in E10.5 *UBR1<sup>-/-</sup>UBR2<sup>-/-</sup>* embryos (Fig. 32, 34F), which was more severe by E11.5 (data not shown). These results collectively indicate that ubiquitin ligases UBR1 and UBR2 are crucial for the control of proliferation and differentiation of neural precursor cells during mouse embryogenesis.

#### **4.4.3 Impaired cardiovascular development in mutant embryos**

In addition to defects in neurogenesis, *UBR1<sup>-/-</sup>UBR2<sup>-/-</sup>* embryos also displayed cardiovascular defects. The hearts of E9.5 double mutants showed a normal looping of the linear heart tube and appropriate cardiac morphology (data not shown). By contrast, most E10.5 double mutants developed local hemorrhages, swollen pericardial sac, and/or pericardial effusion (Fig. 28E, F, 35B), indicating blood leakage into the abdominal cavity and other hemodynamic insufficiency. A large space between the heart and pericardium in the mutants was evident, consistent with pericardial fluid accumulation (Fig. 35D, asterisk). Development of their atria and ventricle was arrested at ~E10.5. Disorganization of the myocardial wall was observed with variable degrees of ventricular atrophy, and the thickness of the ventricular wall was reduced compared to littermate controls (Fig. 36D, arrowhead). Although the control heart at this stage had abundant and thick trabeculae, *UBR1<sup>-/-</sup>UBR2<sup>-/-</sup>* embryos had thinner and less-abundant trabeculations. Interatrial

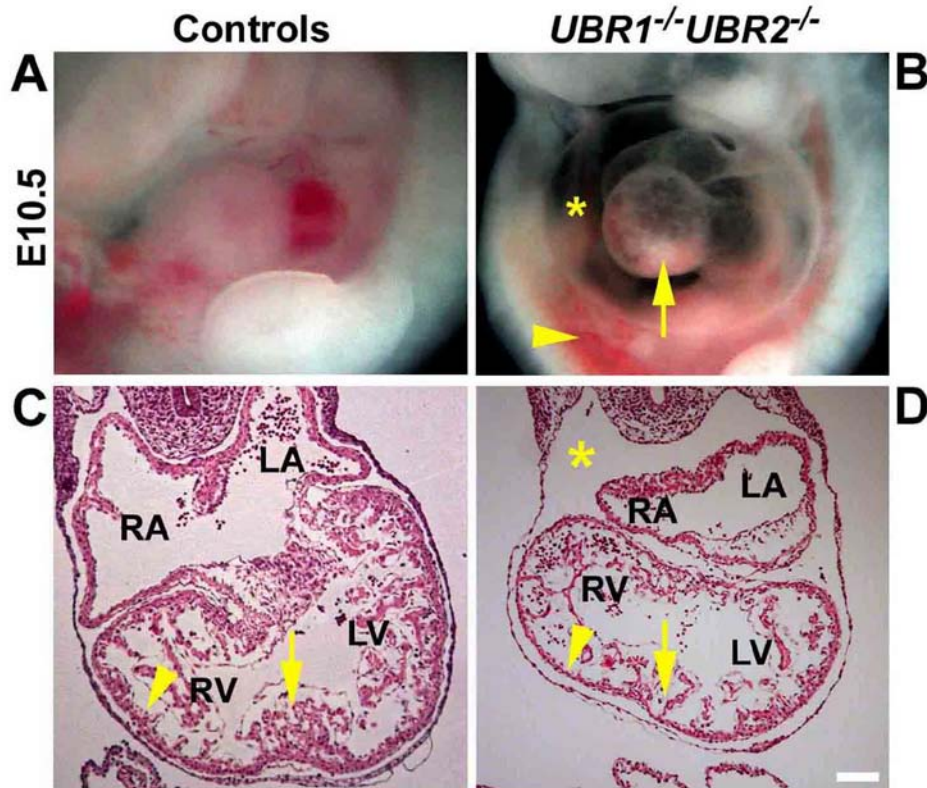


**Figure 35. Impaired cardiac development in *UBR1*<sup>-/-</sup>*UBR2*<sup>-/-</sup> embryos.**

(A, B) Lateral views of E10.5 *UBR1*<sup>-/-</sup>*UBR2*<sup>-/-</sup> (B) and littermate *UBR1*<sup>+/+</sup>*UBR2*<sup>+/-</sup> control embryos (A). Arrow, abnormal heart morphology; asterisk, swollen pericardial sac; arrowhead, hemorrhage. (C, D) H&E-stained transverse sections of E10.5 *UBR1*<sup>-/-</sup>*UBR2*<sup>-/-</sup> (D) and littermate wild-type control hearts (C). Asterisk, swollen pericardial space; arrowhead, ventricular wall. Arrows, sites of septum formation in wild-type (but not in *UBR1*<sup>-/-</sup>*UBR2*<sup>-/-</sup>) embryos. RA, right atrium; LA, left atrium; RV; right ventricle; LV, left ventricle. Scale bars, 100  $\mu$ m.

and interventricular septa began to form in control embryos (Fig. 35C, arrow), which was not observed in the mutants. In the control hearts, tropomyosin signals (for cardiomyocytes) were cytoplasmic and revealed well organized cardiomyocyte-based cardiac structures including the ventricular wall and trabeculae (Fig. 36 A-D). However, tropomyosin signals in the mutant hearts were often disorganized and localized both in the cytoplasm and nucleus (Fig. 36E-F). These results together indicate that the proliferation of *UBR1*<sup>-/-</sup>*UBR2*<sup>-/-</sup> cardiac cells is impaired around ~E10.5, resulting in abnormal cardiac morphogenesis.

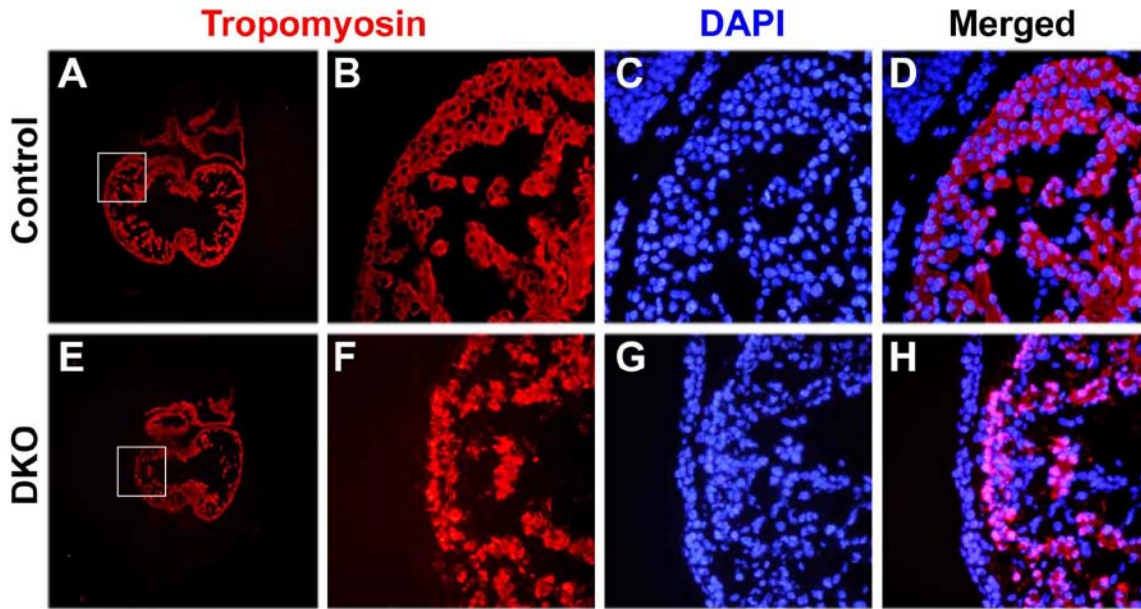


**Figure 36. Impaired development of cardiac cells in  $UBR1^{-/-}UBR2^{-/-}$  embryos.**

Transverse sections of E10.5 embryonic heart from control (A-D) and double mutant (E-H) are immunostained with Tropomyosin (red). The region indicated by squares in A and B, respectively, are magnified in B-D and F-H.

I also examined vascular development in  $UBR1^{-/-}UBR2^{-/-}$  embryos. Whole mount staining of PECAM-1 (platelet endothelial cell adhesion molecule-1), a marker for blood vessels, showed that the honeycomb-like network of primary vascular plexus form normally in E9.5  $UBR1^{-/-}UBR2^{-/-}$  yolk sacs and embryos proper (data not shown).  $UBR1^{-/-}UBR2^{-/-}$  yolk sacs had typical endothelial cells and blood islands that contained fetal nucleated erythrocyte, suggesting that the formation of primary vasculature is not affected in E9.5  $UBR1^{-/-}UBR2^{-/-}$  embryos. However, by E10.5,  $UBR1^{-/-}UBR2^{-/-}$  yolk sacs appeared pale, and the yolk sac blood vessels were thinner and less branched (Fig. 37B). Staining with anti-PECAM-1 antibody showed that growth, remodeling, and branching of both small and large vessels were impaired, resulting in the poorly organized vascular network (Fig. 37D, arrowhead). Similarly, large vessels such as intracranial artery (Fig. 37F, arrowhead) in E10.5  $UBR1^{-/-}UBR2^{-/-}$  embryos were thin and poorly

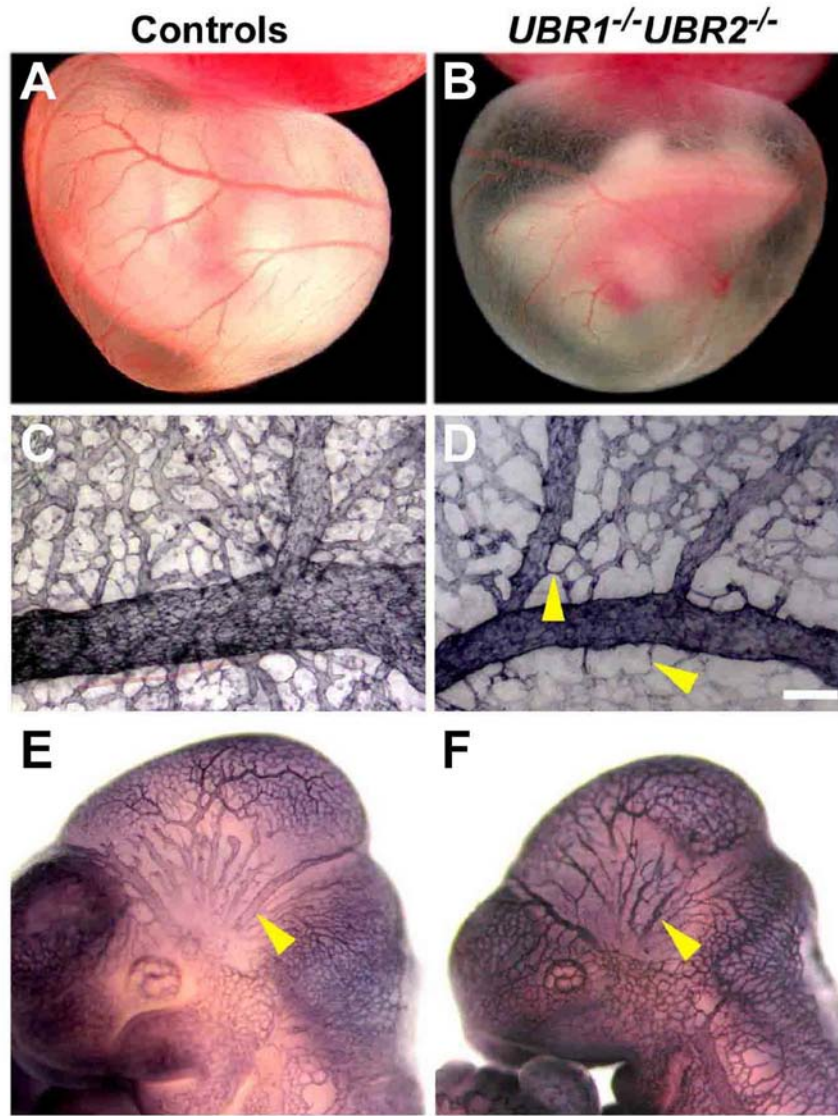


**Figure 37. Impaired vascular development in *UBR1*<sup>-/-</sup>*UBR2*<sup>-/-</sup> embryos**

(A, B) The appearance of yolk sac attached to placenta at E10.5 control (A) and double mutant (B) embryos. (C, D) PECAM-stained E10.5 *UBR1*<sup>-/-</sup>*UBR2*<sup>-/-</sup> (D) and *UBR1*<sup>+/+</sup>*UBR2*<sup>+/+</sup> (C) yolk sacs. Arrowheads in D indicate some of the differences in the branching patterns, relative to wild-type embryos. (E, F) PECAM-stained E10.5 *UBR1*<sup>-/-</sup>*UBR2*<sup>-/-</sup> (F) and *UBR1*<sup>+/+</sup>*UBR2*<sup>+/+</sup> (E) whole embryos. Arrowhead, the intracranial artery. Scale bar, 100  $\mu$ m.

developed, perhaps due to insufficient growth and remodeling. These results together suggest that ubiquitylation by UBR1 and UBR2 is required for normal cardiovascular development.

#### 4.4.4 Molecular Analysis of Mouse Embryos Lacking UBR1 and UBR2

As an attempt to identify molecular circuits underlying impaired neurogenesis and cardiovascular development, I examined some molecules known to be associated with proliferation and differentiation by immunoblotting from control and double mutant embryos. Decreased BrdU index in the VZ of *UBR1*<sup>-/-</sup>*UBR2*<sup>-/-</sup> embryos indicates a likely arrest at G1-S transition. Various regulatory mechanisms modulate cell growth through the core cell cycle machinery that contains cyclins and their associated cyclin-dependent kinases (CDKs). These cyclin-CDK complexes phosphorylate critical cellular substrates, thereby allowing cell cycle progression (Sherr and Roberts, 1999). Hence, the levels of various cyclins in E10.5 *UBR1*<sup>-/-</sup>*UBR2*<sup>-/-</sup> embryos and littermate controls were determined. Blots from whole embryo lysates showed a substantial decrease in the amount of cyclin D3 in *UBR1*<sup>-/-</sup>*UBR2*<sup>-/-</sup> embryos compared to littermate controls (Fig. 38B). The amount of cyclins D1 and D2 were also moderately decreased in the mutants. In contrast, the levels of other cyclins such as type A, B, and E cyclins were not affected (Fig. 38B). Semi-quantitative RT-PCR and Northern blot analysis indicated that the differences for cyclin D3 was not due to lower *Ccnd3* mRNA which was indistinguishable between the mutants and controls (data not shown). Thus, down-regulation of D-type cyclins is likely to be due to post-transcriptional modification. Given that D-type cyclins are critical for transformation of the pre-replication complex into an active replication fork during the G1-to-S phase transition (Sherr and Roberts, 1999), deficiency of D-type cyclins at least in part explains the decreased BrdU index.

I next asked whether *UBR1*<sup>-/-</sup>*UBR2*<sup>-/-</sup> embryos would phenocopy any of known mutant mice. Mice lacking components of the Notch signaling pathway showed kinked neural tube

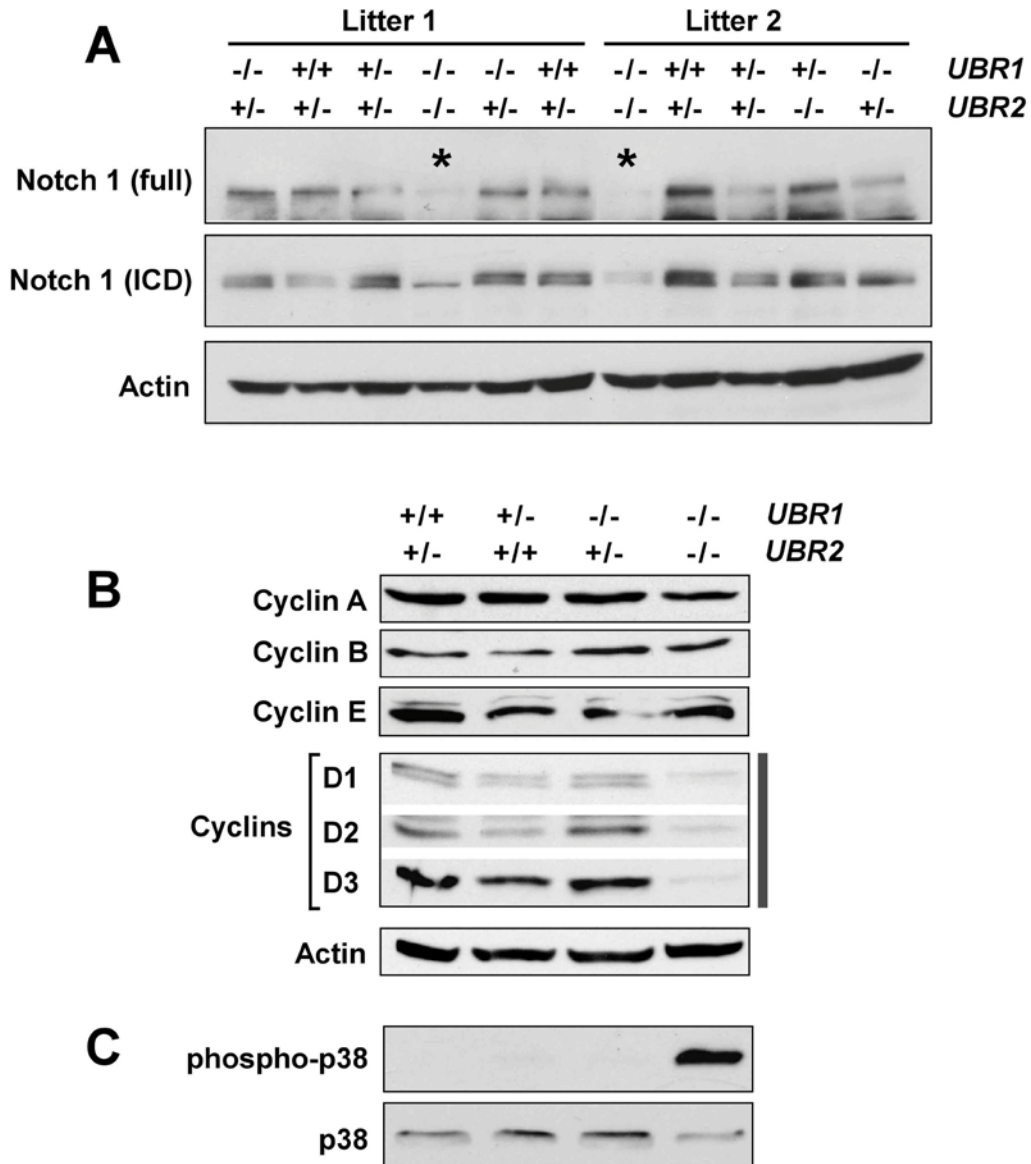


**Figure 38. Immunoblot analysis of *UBR1*<sup>-/-</sup>*UBR2*<sup>-/-</sup> embryos.**

Whole-embryo extracts from E10.5 *UBR1*<sup>-/-</sup>*UBR2*<sup>-/-</sup> and littermate control embryos were immunoblotted for proteins indicated on the left.

associated with impairment in neurogenesis and cardiovascular development: Notch 1 (de la Pompa et al., 1997), PBR-Jκ (Oka et al., 1995), Mib1 (Koo et al., 2005), protein O-fucosylase 1 (Shi and Stanley, 2003), or presenilins 1 and 2 (Donoviel et al., 1999). The Notch pathway is important for inhibiting neuronal differentiation and thereby reserves cell-type diversity (de la

Pompa et al., 1997). When Notch 1 is activated by its ligand, the intracellular domain (ICD) of Notch 1 is cleaved by the  $\gamma$ -secretase complex containing presenilin 1 and 2 (Koo et al., 2005). The released ICD translocates to the nucleus to form a complex with RBP-J $\kappa$ , and thereby to activate Notch target genes (Koo et al., 2005). E10.5 *UBR1*<sup>-/-</sup>*UBR2*<sup>-/-</sup> embryos contained a significantly reduced amount of Notch 1 compared to littermate controls (Fig. 38A), while the level of Notch 1 mRNA is not significantly affected when determined by semi-quantitative RT-PCR (data not shown). Therefore, Notch insufficiency may be part of circuits underlying impaired neurogenesis and cardiovascular development in these mutants.

A set of RGS proteins (RGS4, RGS5, and RGS16) has recently been identified as the first *in vivo* substrates of the mammalian N-end rule pathway (Lee et al., 2005). RGS proteins are negative regulators of the GPCR signaling pathway that controls cell growth (proliferation, differentiation, and death) in part through the mitogen-activated protein kinase (MAPK) pathway. I asked whether knockout of *UBR1* and *UBR2* would affect the function of the MAPK pathway known to be regulated by RGS proteins. The level of phospho-p38 (active) was substantially increased in E10.5 *UBR1*<sup>-/-</sup>*UBR2*<sup>-/-</sup> embryos (Fig. 38C), while those of unphosphorylated p38 (inactive) and ERK MAPKs were not affected (data not shown). The level of p38 mRNA was not affected (data not shown). The p38 MAPK induces cell cycle exit and differentiation of many cell types (Engel et al., 2005). These results suggest that abnormalities in D-type cyclins, Notch 1, and p38 MAPK collectively contributes to reduced proliferation and increased differentiation of neural precursors in *UBR1*<sup>-/-</sup>*UBR2*<sup>-/-</sup> embryos (see Discussion).

## 4.5 DISCUSSION

These results suggest functional interplay between ubiquitin ligases UBR1 and UBR2 of the N-end rule pathway during mouse embryogenesis. Consistent are previous findings that UBR1 and UBR2 are similar each other in protein sequence (46% overall identity), size (200 kDa), and the enzymatic specificities to N-terminal destabilizing residues of model substrates (Kwon et al., 1998; Kwon et al., 2001; Kwon et al., 2003). *UBR1<sup>-/-</sup>UBR2<sup>-/-</sup>* embryos die at midgestation (before ~E12.0) associated with defects in neurogenesis and cardiovascular development, implicating UBR1 and UBR2 as novel players in these processes. These findings suggest that substantially decreased BrdU index (for S phase) associated with abnormal pH3 index (for M phase) and increased TUNEL index (for cell death) collectively underlies abnormal morphogenesis of the central nervous system. Although it is unclear whether a single molecular circuit underlies these abnormalities, these results indicate that ubiquitylation by UBR1 and UBR2 may be crucial for cell proliferation through G1-to-S transition, which is in part supported by the result that D-type cyclins, critical for progression through G1 phase, are post-transcriptionally down-regulated in *UBR1<sup>-/-</sup>UBR2<sup>-/-</sup>* embryos, while other examined cyclins are not affected. Another line of evidence relevant with this speculation is the previous finding (Yin et al., 2004) that UBR1 and UBR2 form a stable complex with RECQL4 helicase without RECQL4 ubiquitylation. RECQL4 is a member of the RecQ helicase family whose mutations are found in the Werner and Bloom syndrome (Thompson and Schild, 2002) and has been recently implicated as an essential component of the pre-replication complex for the G1-S transition (Sangrithi et al., 2005).

In contrast to normal E10.5 neuroepithelium that is composed of the VZ and the mantle, E10.5 *UBR1*<sup>-/-</sup>*UBR2*<sup>-/-</sup> neuroepithelium contains the SVZ-like zone in which BrdU-positive cells and pH3-positive cells are mixed each other, perhaps due to lack of interkinetic nuclear migration. The premature appearance of the SVZ is likely due to uncontrolled early migration of mitotically active neural precursors from the VZ, and therefore indicates that knockout of *UBR1* and *UBR2* accelerates certain aspects, if not all, of differentiation of neural precursor cells. Consistent with this speculation are the findings that the mantle of E10.5 *UBR1*<sup>-/-</sup>*UBR2*<sup>-/-</sup> forebrain precociously produces GABA, a neurotransmitter that is synthesized from the SVZ-derived neurons (Anderson et al., 1997), and that *UBR1*<sup>-/-</sup>*UBR2*<sup>-/-</sup> embryos contain a reduced level of Notch 1, a key inhibitor of neuronal differentiation. Notably, many mutant mice deficient in components of the Notch pathway show remarkable similarity to *UBR1*<sup>-/-</sup>*UBR2*<sup>-/-</sup> embryos in that they display the kinked neural tube associated with impairment in neurogenesis and cardiovascular development. However, the lethality of *UBR1*<sup>-/-</sup>*UBR2*<sup>-/-</sup> embryos before E12.0 precludes the detailed analysis of neuron differentiation at the later embryogenesis, like many Notch-deficient mutants. Therefore, definitive answer will require construction and characterization of tissue-specific knockout of *UBR2* in the background of *UBR1* null mutation.

The causative molecular mechanism underlying impaired neurogenesis remains to be further elucidated. One feasible model is that UBR1 and UBR2 may ubiquitylate multiple short-lived proteins that sense extracellular stimuli for homeostasis in cell proliferation, differentiation, and death. I have recently found that a set of RGS proteins (RGS4, RGS5, and RGS16), negative regulators of the GPCR signaling, are *in vivo* substrates of UBR1 and UBR2 (Lee et al., 2005). *In vivo* degradation of these RGS proteins are perturbed in *UBR1*<sup>-/-</sup>*UBR2*<sup>-/-</sup> cells, suggesting that failure to properly degrade these RGS proteins may contribute to phenotypes observed in this

study. Indeed, these RGS proteins have been functionally implicated in nervous and cardiovascular homeostasis (Lee et al., 2005 and references therein). The possible involvement of the N-end rule pathway in sensing extracellular stimuli is also supported by the fact that Notch 1, p38, and D-type cyclins commonly sense extracellular stimuli for the control of cell proliferation, differentiation, and/or death.

In addition to defects in neurogenesis, *UBR1*<sup>-/-</sup>*UBR2*<sup>-/-</sup> embryos are impaired in cardiovascular development. These results indicate that myocardial growth in *UBR1*<sup>-/-</sup>*UBR2*<sup>-/-</sup> embryos is arrested at ~E10.5, resulting in thinning of ventricular wall and poorly developed trabeculae, and occasionally disorganized expression of tropomyosin (a marker for cardiomyocytes). Similarly, growth and remodeling of both small and large vessels are impaired in the yolk sacs and embryos proper of E10.5 *UBR1*<sup>-/-</sup>*UBR2*<sup>-/-</sup> embryos. Given that normal central nervous development does not appear to be critical for embryonic survival, death of *UBR1*<sup>-/-</sup>*UBR2*<sup>-/-</sup> embryos at ~E12.0 is likely the result of vascular defects. Cardiovascular defects in *UBR1*<sup>-/-</sup>*UBR2*<sup>-/-</sup> embryos are consistent with the previous finding that mouse embryos lacking ATE1 Arg-transferase (Kwon et al., 2002), an upstream component of UBR1 and UBR2, die during embryogenesis associated with various cardiovascular defects (Kwon et al., 2002). ATE1 conjugates Arg to a set of acidic N-terminal residues (Asp, Glu, and Cys), yielding N-terminal Arg, a primary destabilizing residue, for the recognition by UBR1 and UBR2 (Hu et al., 2005; Lee et al., 2005). *ATE1*<sup>-/-</sup> embryonic hearts show poorly developed trabeculae and thin ventricular wall, suggesting that cardiac phenotypes of two mutant strains may be in part due to the same molecular circuit. However, although ATE1 and UBR proteins function in the same pathway, *ATE1*<sup>-/-</sup> embryos did not develop severe defects in neurogenesis, suggesting that the molecular circuit underlying disrupted neurogenesis in *UBR1*<sup>-/-</sup>*UBR2*<sup>-/-</sup> embryos is independent

from ATE1. These results with *ATE1*<sup>-/-</sup> and *UBR1*<sup>-/-</sup>*UBR2*<sup>-/-</sup> embryos implicate the N-end rule pathway as a major Ub system important for cardiovascular development. It is to be determined whether defects in neurogenesis and cardiovascular defects are primary or secondary. To current knowledge, cardiovascular defects in mutant animals usually do not affect the morphology of neural tissues in a manner shown in this study. Thus, the defects in neurogenesis are most likely primary rather than secondary to cardiovascular or other defects. However, it is to be determined whether the cardiovascular defects are primary or secondary to neurogenesis defects or other nutritional stress and whether a single molecular circuit underlies defects in neurogenesis and cardiovascular development.

## 5.0 PERSPECTIVES

The research goal of this dissertation is to elucidate the physiological functions of E3 ubiquitin ligases of the N-end rule pathway in spermatogenesis, DNA damage response (DDR) and embryogenesis. Through dissertational research, I found that UBR2, an E3 component of the N-end rule pathway, mediates meiotic transcriptional inactivation and DDR pathway via histone ubiquitylation. Furthermore, I show that Wdivergent and cooperative functions of UBR1 and UBR2 in neurogenesis and cardiovascular development.

Among many proteins that have been reported as targets of ubiquitylation, histones are the first discovered. Several E3 ubiquitin ligases has been shown to ubiquitylate histone H2A including UBR2. How does UBR2 recognize histone H2A in specific physiological conditions such as spermatogenesis and DDR pathway compared to other E3 ligases? Is it related with the UBR domain of E3 ligases of the N-end rule pathway, which recognize destabilizing N-terminal residues? To address these questions, future study is to investigate the interaction between histone H2A and various fragments of UBR2 in the presence of dipeptides, the inhibitors of the N-end rule pathway.

Intriguingly, UBR2 signal dramatically surges throughout the nucleus after completion of synapsis and DNA damage in spermatogenesis and DDR pathway, respectively. Coincidentally, polyubiquitylation is remarkably increased at the same time, which suggests that dramatic surge of UBR2 is associated with polyubiquitylation. Transcriptional level in MEFs indicates that

either post-translation modification of UBR2 or chromatin remodeling is associated. These results collectively suggest that UBR2 is involved with polyubiquitylation of proteins which are localized throughout nucleus. Is the mechanism underlying the surge of UBR2 signal in the same context? To address this question, correlation in these physiological conditions should be further investigated.

The functional interplay between UBR1 and UBR2, which are biochemically indistinguishable, is required for the neurogenesis and cardiovascular development during embryogenesis. However, these studies is hampered by the availability of embryos and, moreover, embryonic lethality at midgestation. To elucidate the collaborative functions between UBR1 and UBR2 further, one of the approaches may be the generation of organ-specific conditional mutant mice to circumvent the early embryonic lethality.

## BIBLIOGRAPHY

- Anderson, S.A., Eisenstat, D.D., Shi, L., and Rubenstein, J.L. (1997). Interneuron migration from basal forebrain to neocortex: dependence on *Dlx* genes. *Science* 278, 474-476.
- Ardley, H.C., and Robinson, P.A. (2005). E3 ubiquitin ligases. *Essays Biochem* 41, 15-30.
- Ashley, T. (2004). The mouse "tool box" for meiotic studies. *Cytogenet Genome Res* 105, 166-171.
- Baarends, W.M., Hoogerbrugge, J.W., Roest, H.P., Ooms, M., Vreeburg, J., Hoeijmakers, J.H., and Grootegoed, J.A. (1999). Histone ubiquitination and chromatin remodeling in mouse spermatogenesis. *Dev Biol* 207, 322-333.
- Baarends, W.M., Wassenaar, E., Hoogerbrugge, J.W., Schoenmakers, S., Sun, Z.W., and Grootegoed, J.A. (2007). Increased phosphorylation and dimethylation of XY body histones in the Hr6b-knockout mouse is associated with derepression of the X chromosome. *J Cell Sci* 120, 1841-1851.
- Baarends, W.M., Wassenaar, E., Hoogerbrugge, J.W., van Cappellen, G., Roest, H.P., Vreeburg, J., Ooms, M., Hoeijmakers, J.H., and Grootegoed, J.A. (2003). Loss of HR6B ubiquitin-conjugating activity results in damaged synaptonemal complex structure and increased crossing-over frequency during the male meiotic prophase. *Mol Cell Biol* 23, 1151-1162.
- Baarends, W.M., Wassenaar, E., van der Laan, R., Hoogerbrugge, J., Sleddens-Linkels, E., Hoeijmakers, J.H., de Boer, P., and Grootegoed, J.A. (2005). Silencing of unpaired chromatin and histone H2A ubiquitination in mammalian meiosis. *Mol Cell Biol* 25, 1041-1053.
- Bachmair, A., Finley, D., and Varshavsky, A. (1986). In vivo half-life of a protein is a function of its amino-terminal residue. *Science* 234, 179-186.
- Bachmair, A., and Varshavsky, A. (1989). The degradation signal in a short-lived protein. *Cell* 56, 1019-1032.
- Bar-Peled, M., and Raikhel, N.V. (1996). A method for isolation and purification of specific antibodies to a protein fused to the GST. *Anal Biochem* 241, 140-142.

- Bergink, S., Salomons, F.A., Hoogstraten, D., Groothuis, T.A., de Waard, H., Wu, J., Yuan, L., Citterio, E., Houtsmuller, A.B., Neefjes, J., *et al.* (2006). DNA damage triggers nucleotide excision repair-dependent monoubiquitylation of histone H2A. *Genes Dev* 20, 1343-1352.
- Bogliolo, M., Lyakhovich, A., Callen, E., Castella, M., Cappelli, E., Ramirez, M.J., Creus, A., Marcos, R., Kalb, R., Neveling, K., *et al.* (2007). Histone H2AX and Fanconi anemia FANCD2 function in the same pathway to maintain chromosome stability. *EMBO J* 26, 1340-1351.
- Burgoyne, P.S., Mahadevaiah, S.K., and Turner, J.M. (2007). The management of DNA double-strand breaks in mitotic G2, and in mammalian meiosis viewed from a mitotic G2 perspective. *Bioessays* 29, 974-986.
- Cao, R., Tsukada, Y., and Zhang, Y. (2005). Role of Bmi-1 and Ring1A in H2A ubiquitylation and Hox gene silencing. *Mol Cell* 20, 845-854.
- Chen, H.Y., Sun, J.M., Zhang, Y., Davie, J.R., and Meistrich, M.L. (1998). Ubiquitination of histone H3 in elongating spermatids of rat testes. *J Biol Chem* 273, 13165-13169.
- Cimprich, K.A., and Cortez, D. (2008). ATR: an essential regulator of genome integrity. *Nat Rev Mol Cell Biol* 9, 616-627.
- Cooke, H.J., and Saunders, P.T. (2002). Mouse models of male infertility. *Nat Rev Genet* 3, 790-801.
- Csankovszki, G., Panning, B., Bates, B., Pehrson, J.R., and Jaenisch, R. (1999). Conditional deletion of Xist disrupts histone macroH2A localization but not maintenance of X inactivation. *Nat Genet* 22, 323-324.
- de la Pompa, J.L., Wakeham, A., Correia, K.M., Samper, E., Brown, S., Aguilera, R.J., Nakano, T., Honjo, T., Mak, T.W., Rossant, J., *et al.* (1997). Conservation of the Notch signalling pathway in mammalian neurogenesis. *Development* 124, 1139-1148.
- de Napoles, M., Mermoud, J.E., Wakao, R., Tang, Y.A., Endoh, M., Appanah, R., Nesterova, T.B., Silva, J., Otte, A.P., Vidal, M., *et al.* (2004). Polycomb group proteins Ring1A/B link ubiquitylation of histone H2A to heritable gene silencing and X inactivation. *Dev Cell* 7, 663-676.
- Dickins, R.A., Frew, I.J., House, C.M., O'Bryan, M.K., Holloway, A.J., Haviv, I., Traficante, N., de Kretser, D.M., and Bowtell, D.D. (2002). The ubiquitin ligase component Siah1a is required for completion of meiosis I in male mice. *Mol Cell Biol* 22, 2294-2303.
- Dix, D.J., Allen, J.W., Collins, B.W., Poorman-Allen, P., Mori, C., Blizard, D.R., Brown, P.R., Goulding, E.H., Strong, B.D., and Eddy, E.M. (1997). HSP70-2 is required for desynapsis of synaptonemal complexes during meiotic prophase in juvenile and adult mouse spermatocytes. *Development* 124, 4595-4603.

- Dohmen, R.J., Madura, K., Bartel, B., and Varshavsky, A. (1991). The N-end rule is mediated by the UBC2(RAD6) ubiquitin-conjugating enzyme. *Proc Natl Acad Sci U S A* 88, 7351-7355.
- Donoviel, D.B., Hadjantonakis, A.K., Ikeda, M., Zheng, H., Hyslop, P.S., and Bernstein, A. (1999). Mice lacking both presenilin genes exhibit early embryonic patterning defects. *Genes Dev* 13, 2801-2810.
- Dornan, D., Shimizu, H., Mah, A., Dudhela, T., Eby, M., O'Rmyke, K., Seshagiri, S., and Dixit, V.M. (2006). ATM engages autodegradation of the E3 ubiquitin ligase COP1 after DNA damage. *Science* 313, 1122-1126.
- Dover, J., Schneider, J., Tawiah-Boateng, M.A., Wood, A., Dean, K., Johnston, M., and Shilatifard, A. (2002). Methylation of histone H3 by COMPASS requires ubiquitination of histone H2B by Rad6. *J Biol Chem* 277, 28368-28371.
- Engel, F.B., Schebesta, M., Duong, M.T., Lu, G., Ren, S., MadId, J.B., Jiang, H., Wang, Y., and Keating, M.T. (2005). p38 MAP kinase inhibition enables proliferation of adult mammalian cardiomyocytes. *Genes Dev* 19, 1175-1187.
- Fang, J., Chen, T., Chadwick, B., Li, E., and Zhang, Y. (2004). Ring1b-mediated H2A ubiquitination associates with inactive X chromosomes and is involved in initiation of X inactivation. *J Biol Chem* 279, 52812-52815.
- Fernandez-Capetillo, O., Mahadevaiah, S.K., Celeste, A., Romanienko, P.J., Camerini-Otero, R.D., Bonner, W.M., Manova, K., Burgoyne, P., and Nussenzlig, A. (2003). H2AX is required for chromatin remodeling and inactivation of sex chromosomes in male mouse meiosis. *Dev Cell* 4, 497-508.
- Fernandez-Capetillo, O., Lee, A., Nussenzlig, M., and Nussenzlig, A. (2004). H2AX: the histone guardian of the genome. *DNA Repair (Amst)* 3, 959-967.
- Frangioni, J.V., and Neel, B.G. (1993). Solubilization and purification of enzymatically active glutathione S-transferase (pGEX) fusion proteins. *Anal Biochem* 210, 179-187.
- Fu, Y., Zhu, Y., Zhang, K., Yeung, M., Durocher, D., and Xiao, W. (2008). Rad6-Rad18 mediates a eukaryotic SOS response by ubiquitinating the 9-1-1 checkpoint clamp. *Cell* 133, 601-611.
- Fujimuro, M., Sawada, H., and Yokosawa, H. (1994). Production and characterization of monoclonal antibodies specific to multi-ubiquitin chains of polyubiquitinated proteins. *FEBS Lett* 349, 173-180.
- Garcia-Higuera, I., Taniguchi, T., Ganesan, S., Meyn, M.S., Timmers, C., Hejna, J., Grompe, M., and D'Andrea, A.D. (2001). Interaction of the Fanconi anemia proteins and BRCA1 in a common pathway. *Mol Cell* 7, 249-262.

- Giannattasio, M., Lazzaro, F., Plevani, P., and Muzi-Falconi, M. (2005). The DNA damage checkpoint response requires histone H2B ubiquitination by Rad6-Bre1 and H3 methylation by Dot1. *J Biol Chem* 280, 9879-9886.
- Goetz, P., Chandley, A.C., and Speed, R.M. (1984). Morphological and temporal sequence of meiotic prophase development at puberty in the male mouse. *J Cell Sci* 65, 249-263.
- Henegariu, O., Heerema, N.A., LoI Wright, L., Bray-Ward, P., Ward, D.C., and Vance, G.H. (2001). Improvements in cytogenetic slide preparation: controlled chromosome spreading, chemical aging and gradual denaturing. *Cytometry* 43, 101-109.
- Hershko, A., Ciechanover, A., and Varshavsky, A. (2000). Basic Medical Research Award. The ubiquitin system. *Nat Med* 6, 1073-1081.
- Hochstrasser, M. (2006). Lingering mysteries of ubiquitin-chain assembly. *Cell* 124, 27-34.
- Hu, R.G., Sheng, J., Qi, X., Xu, Z., Takahashi, T.T., and Varshavsky, A. (2005). The N-end rule pathway as a nitric oxide sensor controlling the levels of multiple regulators. *Nature* 437, 981-986.
- Huen, M.S., Grant, R., Manke, I., Minn, K., Yu, X., Yaffe, M.B., and Chen, J. (2007). RNF8 transduces the DNA-damage signal via histone ubiquitylation and checkpoint protein assembly. *Cell* 131, 901-914.
- Koo, B.K., Lim, H.S., Song, R., Yoon, M.J., Yoon, K.J., Moon, J.S., Kim, Y.W., Kwon, M.C., Yoo, K.W., Kong, M.P., *et al.* (2005). Mind bomb 1 is essential for generating functional Notch ligands to activate Notch. *Development* 132, 3459-3470.
- Kwon, Y.T., Balogh, S.A., Davydov, I.V., Kashina, A.S., Yoon, J.K., Xie, Y., Gaur, A., Hyde, L., Denenberg, V.H., and Varshavsky, A. (2000). Altered activity, social behavior, and spatial memory in mice lacking the NTAN1p amidase and the asparagine branch of the N-end rule pathway. *Mol Cell Biol* 20, 4135-4148.
- Kwon, Y.T., Kashina, A.S., Davydov, I.V., Hu, R.G., An, J.Y., Seo, J.W., Du, F., and Varshavsky, A. (2002). An essential role of N-terminal arginylation in cardiovascular development. *Science* 297, 96-99.
- Kwon, Y.T., Kashina, A.S., and Varshavsky, A. (1999a). Alternative splicing results in differential expression, activity, and localization of the two forms of arginyl-tRNA-protein transferase, a component of the N-end rule pathway. *Mol Cell Biol* 19, 182-193.
- Kwon, Y.T., Levy, F., and Varshavsky, A. (1999b). Bivalent inhibitor of the N-end rule pathway. *J Biol Chem* 274, 18135-18139.
- Kwon, Y.T., Reiss, Y., Fried, V.A., Hershko, A., Yoon, J.K., Gonda, D.K., Sangan, P., Copeland, N.G., Jenkins, N.A., and Varshavsky, A. (1998). The mouse and human genes encoding the recognition component of the N-end rule pathway. *Proc Natl Acad Sci U S A* 95, 7898-7903.

- Kwon, Y.T., Xia, Z., An, J.Y., Tasaki, T., Davydov, I.V., Seo, J.W., Sheng, J., Xie, Y., and Varshavsky, A. (2003). Female lethality and apoptosis of spermatocytes in mice lacking the UBR2 ubiquitin ligase of the N-end rule pathway. *Mol Cell Biol* 23, 8255-8271.
- Kwon, Y.T., Xia, Z., Davydov, I.V., Lecker, S.H., and Varshavsky, A. (2001). Construction and analysis of mouse strains lacking the ubiquitin ligase UBR1 (E3alpha) of the N-end rule pathway. *Mol Cell Biol* 21, 8007-8021.
- Lee, M.J., Tasaki, T., Moroi, K., An, J.Y., Kimura, S., Davydov, I.V., and Kwon, Y.T. (2005). RGS4 and RGS5 are in vivo substrates of the N-end rule pathway. *Proc Natl Acad Sci U S A* 102, 15030-15035.
- Lobrich, M., and Jeggo, P.A. (2007). The impact of a negligent G2/M checkpoint on genomic instability and cancer induction. *Nat Rev Cancer* 7, 861-869.
- Lukas, C., Falck, J., Bartkova, J., Bartek, J., and Lukas, J. (2003). Distinct spatiotemporal dynamics of mammalian checkpoint regulators induced by DNA damage. *Nat Cell Biol* 5, 255-260.
- Mahadevaiah, S.K., Turner, J.M., Baudat, F., Rogakou, E.P., de Boer, P., Blanco-Rodriguez, J., Jasin, M., Keeney, S., Bonner, W.M., and Burgoyne, P.S. (2001). Recombinational DNA double-strand breaks in mice precede synapsis. *Nat Genet* 27, 271-276.
- Mailand, N., Bekker-Jensen, S., Faustrup, H., Melander, F., Bartek, J., Lukas, C., and Lukas, J. (2007). RNF8 ubiquitylates histones at DNA double-strand breaks and promotes assembly of repair proteins. *Cell* 131, 887-900.
- McCarrey, J.R., Watson, C., Atencio, J., Ostermeier, G.C., Marahrens, Y., Jaenisch, R., and Kraitz, S.A. (2002). X-chromosome inactivation during spermatogenesis is regulated by an Xist/Tsix-independent mechanism in the mouse. *Genesis* 34, 257-266.
- McConnell, S.K. (1995). Constructing the cerebral cortex: neurogenesis and fate determination. *Neuron* 15, 761-768.
- McKinnon, P.J., and Caldecott, K.W. (2007). DNA strand break repair and human genetic disease. *Annu Rev Genomics Hum Genet* 8, 37-55.
- Moens, P.B., Kolas, N.K., Tarsounas, M., Marcon, E., Cohen, P.E., and Spyropoulos, B. (2002). The time course and chromosomal localization of recombination-related proteins at meiosis in the mouse are compatible with models that can resolve the early DNA-DNA interactions without reciprocal recombination. *J Cell Sci* 115, 1611-1622.
- Mu, J.J., Wang, Y., Luo, H., Leng, M., Zhang, J., Yang, T., Besusso, D., Jung, S.Y., and Qin, J. (2007). A proteomic analysis of ataxia telangiectasia-mutated (ATM)/ATM-Rad3-related (ATR) substrates identifies the ubiquitin-proteasome system as a regulator for DNA damage checkpoints. *J Biol Chem* 282, 17330-17334.

- Oka, C., Nakano, T., Wakeham, A., de la Pompa, J.L., Mori, C., Sakai, T., Okazaki, S., Kawaichi, M., Shiota, K., Mak, T.W., *et al.* (1995). Disruption of the mouse RBP-J kappa gene results in early embryonic death. *Development* *121*, 3291-3301.
- Ouyang, Y., Kwon, Y.T., An, J.Y., Eller, D., Tsai, S.C., Diaz-Perez, S., Troke, J.J., Teitell, M.A., and Marahrens, Y. (2006). Loss of Ubr2, an E3 ubiquitin ligase, leads to chromosome fragility and impaired homologous recombinational repair. *Mutat Res* *596*, 64-75.
- Peters, A.H., Plug, A.W., van Vugt, M.J., and de Boer, P. (1997). A drying-down technique for the spreading of mammalian meiocytes from the male and female germline. *Chromosome Res* *5*, 66-68.
- Pickart, C.M. (2004). Back to the future with ubiquitin. *Cell* *116*, 181-190.
- Robzyk, K., Recht, J., and Osley, M.A. (2000). Rad6-dependent ubiquitination of histone H2B in yeast. *Science* *287*, 501-504.
- Roest, H.P., van Klaveren, J., de Wit, J., van Gurp, C.G., Koken, M.H., Vermey, M., van Roijen, J.H., Hoogerbrugge, J.W., Vreeburg, J.T., Baarends, W.M., *et al.* (1996). Inactivation of the HR6B ubiquitin-conjugating DNA repair enzyme in mice causes male sterility associated with chromatin modification. *Cell* *86*, 799-810.
- Rogakou, E.P., Boon, C., Redon, C., and Bonner, W.M. (1999). Megabase chromatin domains involved in DNA double-strand breaks in vivo. *J Cell Biol* *146*, 905-916.
- Romanienko, P.J., and Camerini-Otero, R.D. (2000). The mouse Spo11 gene is required for meiotic chromosome synapsis. *Mol Cell* *6*, 975-987.
- Sangrithi, M.N., Bernal, J.A., Madine, M., Philpott, A., Lee, J., Dunphy, W.G., and Venkitaraman, A.R. (2005). Initiation of DNA replication requires the RECQL4 protein mutated in Rothmund-Thomson syndrome. *Cell* *121*, 887-898.
- Schimenti, J. (2005). Synapsis or silence. *Nat Genet* *37*, 11-13.
- Sherr, C.J., and Roberts, J.M. (1999). CDK inhibitors: positive and negative regulators of G1-phase progression. *Genes Dev* *13*, 1501-1512.
- Shi, S., and Stanley, P. (2003). Protein O-fucosyltransferase 1 is an essential component of Notch signaling pathways. *Proc Natl Acad Sci U S A* *100*, 5234-5239.
- Shiloh, Y. (2003). ATM and related protein kinases: safeguarding genome integrity. *Nat Rev Cancer* *3*, 155-168.
- Smogorzewska, A., Matsuoka, S., Vinciguerra, P., McDonald, E.R., 3rd, Hurov, K.E., Luo, J., Ballif, B.A., Gygi, S.P., Hofmann, K., D'Andrea, A.D., *et al.* (2007). Identification of the FANCI protein, a monoubiquitinated FANCD2 paralog required for DNA repair. *Cell* *129*, 289-301.

- Stock, J.K., Giadrossi, S., Casanova, M., Brookes, E., Vidal, M., Koseki, H., Brockdorff, N., Fisher, A.G., and Pombo, A. (2007). Ring1-mediated ubiquitination of H2A restrains poised RNA polymerase II at bivalent genes in mouse ES cells. *Nat Cell Biol* 9, 1428-1435.
- Stucki, M., and Jackson, S.P. (2006). gammaH2AX and MDC1: anchoring the DNA-damage-response machinery to broken chromosomes. *DNA Repair (Amst)* 5, 534-543.
- Suzuki, T., and Varshavsky, A. (1999). Degradation signals in the lysine-asparagine sequence space. *EMBO J* 18, 6017-6026.
- Sun, Z.W., and Allis, C.D. (2002). Ubiquitination of histone H2B regulates H3 methylation and gene silencing in yeast. *Nature* 418, 104-108.
- Takada, Y., Isono, K., Shinga, J., Turner, J.M., Kitamura, H., Ohara, O., Watanabe, G., Singh, P.B., Kamijo, T., JenuLin, T., *et al.* (2007). Mammalian Polycomb Scmh1 mediates exclusion of Polycomb complexes from the XY body in the pachytene spermatocytes. *Development* 134, 579-590.
- Takahashi, T., Nowakowski, R.S., and Caviness, V.S., Jr. (1995). The cell cycle of the pseudostratified ventricular epithelium of the embryonic murine cerebral wall. *J Neurosci* 15, 6046-6057.
- Tasaki, T., and Kwon, Y.T. (2007). The mammalian N-end rule pathway: new insights into its components and physiological roles. *Trends Biochem Sci* 32, 520-528.
- Tasaki, T., Mulder, L.C., Iwamatsu, A., Lee, M.J., Davydov, I.V., Varshavsky, A., Muesing, M., and Kwon, Y.T. (2005). A family of mammalian E3 ubiquitin ligases that contain the UBR box motif and recognize N-degrons. *Mol Cell Biol* 25, 7120-7136.
- Thompson, L.H., and Schild, D. (2002). Recombinational DNA repair and human disease. *Mutat Res* 509, 49-78.
- Turner, J.M. (2007). Meiotic sex chromosome inactivation. *Development* 134, 1823-1831.
- Turner, J.M., Aprelikova, O., Xu, X., Wang, R., Kim, S., Chandramouli, G.V., Barrett, J.C., Burgoyne, P.S., and Deng, C.X. (2004). BRCA1, histone H2AX phosphorylation, and male meiotic sex chromosome inactivation. *Curr Biol* 14, 2135-2142.
- Turner, J.M., Mahadevaiah, S.K., Fernandez-Capetillo, O., NussenzIig, A., Xu, X., Deng, C.X., and Burgoyne, P.S. (2005). Silencing of unsynapsed meiotic chromosomes in the mouse. *Nat Genet* 37, 41-47.
- Varshavsky, A. (1996). The N-end rule: functions, mysteries, uses. *Proc Natl Acad Sci U S A* 93, 12142-12149.
- Varshavsky, A. (2006). The early history of the ubiquitin field. *Protein Sci* 15, 647-654.

- van Attikum, H., and Gasser, S.M. (2005). The histone code at DNA breaks: a guide to repair? *Nat Rev Mol Cell Biol* 6, 757-765.
- Wang, H., Wang, L., Erdjument-Bromage, H., Vidal, M., Tempst, P., Jones, R.S., and Zhang, Y. (2004a). Role of histone H2A ubiquitination in Polycomb silencing. *Nature* 431, 873-878.
- Wang, H., Zhai, L., Xu, J., Joo, H.Y., Jackson, S., Erdjument-Bromage, H., Tempst, P., Xiong, Y., and Zhang, Y. (2006). Histone H3 and H4 ubiquitylation by the CUL4-DDB-ROC1 ubiquitin ligase facilitates cellular response to DNA damage. *Mol Cell* 22, 383-394.
- Wang, P.J., McCarrey, J.R., Yang, F., and Page, D.C. (2001). An abundance of X-linked genes expressed in spermatogonia. *Nat Genet* 27, 422-426.
- Wang, X., Andreassen, P.R., and D'Andrea, A.D. (2004b). Functional interaction of monoubiquitinated FANCD2 and BRCA2/FANCD1 in chromatin. *Mol Cell Biol* 24, 5850-5862.
- Wood, A., Krogan, N.J., Dover, J., Schneider, J., Heidt, J., Boateng, M.A., Dean, K., Golshani, A., Zhang, Y., Greenblatt, J.F., *et al.* (2003). Bre1, an E3 ubiquitin ligase required for recruitment and substrate selection of Rad6 at a promoter. *Mol Cell* 11, 267-274.
- Xu, X., Aprelikova, O., Moens, P., Deng, C.X., and Furth, P.A. (2003). Impaired meiotic DNA-damage repair and lack of crossing-over during spermatogenesis in BRCA1 full-length isoform deficient mice. *Development* 130, 2001-2012.
- Yin, J., Kwon, Y.T., Varshavsky, A., and Wang, W. (2004). RECQL4, mutated in the Rothmund-Thomson and RAPADILINO syndromes, interacts with ubiquitin ligases UBR1 and UBR2 of the N-end rule pathway. *Hum Mol Genet* 13, 2421-2430.
- Zenker, M., Mayerle, J., Lerch, M.M., Tagariello, A., Zerres, K., Durie, P.R., Beier, M., Hulskamp, G., Guzman, C., Rehder, H., *et al.* (2005). Deficiency of UBR1, a ubiquitin ligase of the N-end rule pathway, causes pancreatic dysfunction, malformations and mental retardation (Johanson-Blizzard syndrome). *Nat Genet* 37, 1345-1350.
- Zhang, D., Penttila, T.L., Morris, P.L., Teichmann, M., and Roeder, R.G. (2001). Spermiogenesis deficiency in mice lacking the Trf2 gene. *Science* 292, 1153-1155.